

**THERMAL DECOMPOSITION STUDY OF HYDROXYLAMINE NITRATE  
DURING STORAGE AND HANDLING**

A Thesis

by

CHUANJI ZHANG

Submitted to the Office of Graduate Studies of  
Texas A&M University  
in partial fulfillment of the requirements for the degree of

MASTER OF SCIENCE

May 2006

Major Subject: Chemical Engineering

**THERMAL DECOMPOSITION STUDY OF HYDROXYLAMINE NITRATE  
DURING STORAGE AND HANDLING**

A Thesis

by

CHUANJI ZHANG

Submitted to the Office of Graduate Studies of  
Texas A&M University  
in partial fulfillment of the requirements for the degree of

MASTER OF SCIENCE

Approved by:

Chair of Committee,	M. Sam Mannan
Committee Members,	Kenneth R. Hall Debjyoti Banerjee
Head of Department,	Kenneth R. Hall

May 2006

Major Subject: Chemical Engineering

## ABSTRACT

Thermal Decomposition Study of Hydroxylamine Nitrate  
During Storage and Handling. (May 2006)

Chuanji Zhang, B.S., Anhui Normal University, China

Chair of Advisory Committee: Dr. M. Sam Mannan

Hydroxylamine nitrate (HAN), an important agent for the nuclear industry and the U.S. Army, has been involved in several costly incidents. To prevent similar incidents, the study of HAN safe storage and handling boundary has become extremely important for industries. However, HAN decomposition involves complicated reaction pathways due to its autocatalytic behavior and therefore presents a challenge for definition of safe boundaries of HAN storage and handling. This research focused on HAN decomposition behavior under various conditions and proposed isothermal aging testing and kinetic-based simulation to determine safety boundaries for HAN storage and handling.

Specifically, HAN decomposition in the presence of glass, titanium, stainless steel with titanium, or stainless steel was examined in an Automatic Pressure Tracking Adiabatic Calorimeter (APTAC).  $n$ -th order kinetics was used for initial reaction rate estimation. Because stainless steel is a commonly used material for HAN containers, isothermal aging tests were conducted in a stainless steel cell to

determine the maximum safe storage time of HAN. Moreover, by changing thermal inertia, data for HAN decomposition in the stainless steel cell were examined and the experimental results were simulated by the Thermal Safety Software package.

This work offers useful guidance for industries that manufacture, handle, and store HAN. The experimental data acquired not only can help with aspects of process safety design, including emergency relief systems, process control, and process equipment selection, but also is a useful reference for the associated theoretical study of autocatalytic decomposition behavior.

To my husband Huachun Xu  
and  
all my family members in China

## ACKNOWLEDGMENTS

I would like to express my appreciation to my advisor, Dr. M. Sam Mannan, for the opportunity of working in the Reactive Chemicals Research Laboratory and working on this industrial project. Over the past two years of my master's study, his guidance and encouragement have supported me in completing this work. I would like to thank Dr. Kenneth R. Hall and Dr. Debjyoti Banerjee for their dedication to serving as my committee members. I also thank Dr. William J. Rogers for his communications with the industrial company that provided HAN samples for testing and for his advice on laboratory techniques. I am full of gratitude to Dr. Arcady Kossoy for his instructions in kinetics modeling with CISP software.

Many thanks go to my colleagues for their assistance in learning and maintaining the APTAC and for their friendly help during graduate study and life, especially to Peter Ralbovsky for his technical advice on the troubleshooting of the APTAC, to Chunyang Wei for the APTAC training and helpful discussion, and to Susan Mitchell for English correction of the entire thesis. I also express my gratitude to Towanna Hubacek for help with graduating document work, and to all the staff at the Mary Kay O'Connor Process Safety Center for help with literature searches and workshop training during my master's program.

Last but not least, I am deeply grateful to my husband, Huachun Xu, for his understanding of my study and career. Without his total and unwavering support, I

would not be able to study chemical engineering and to pursue this master's degree.

## TABLE OF CONTENTS

	Page
ABSTRACT .....	iii
DEDICATION .....	v
ACKNOWLEDGMENTS .....	vi
TABLE OF CONTENTS .....	viii
LIST OF TABLES .....	xi
LIST OF FIGURES .....	xii
 CHAPTER	
I INTRODUCTION .....	1
II CALORIMETRY APPROACH FOR THE STUDY OF THERMAL HAZARDS .....	6
2.1. Introduction .....	6
2.2. Screening Level Calorimetry .....	7
2.2.1. Differential Thermal Analysis (DTA) .....	8
2.2.2. Differential Scanning Calorimetry (DSC) .....	9
2.2.3. Reactive System Screening Tool (RSST) .....	10
2.2.4. Thermogravimetric Analysis (TGA) .....	11
2.2.5. Isoperibolic Calorimetry .....	12
2.3. Advanced Calorimetry .....	13
2.3.1. Accelerating Rate Calorimeter (ARC) .....	14
2.3.2. Automatic Pressure Tracking Adiabatic Calorimeter (APTAC) .....	16
2.4. Comparison of Calorimeters .....	19
2.5. Miniature Calorimetry .....	23
2.6. APTAC Details .....	24
2.6.1. Operation Modes .....	25
2.6.2. Data Acquired .....	26
2.6.3. General Principles of Operation .....	28
III EXPERIMENTAL DETAILS .....	33
3.1. Introduction .....	33

CHAPTER	Page
3.2. Background .....	35
3.2.1. Mechanism of HAN Reacting with Nitrous Acid .....	35
3.2.2. Mechanism of HAN Thermal Decomposition .....	35
3.2.3. Mechanism of Iron Catalyzed HAN Decomposition .....	36
3.2.4. Autocatalytic Decomposition Hazards .....	37
3.3. Experimental Details .....	38
3.3.1. Samples .....	38
3.3.2. Equipment .....	39
3.3.3. Methods .....	40
3.3.4. Thermocouple Calibration .....	41
3.3.4.1. Relative Calibration .....	42
3.3.4.2. Absolute Calibration .....	46
IV EXPERIMENTAL RESULTS AND DISCUSSION .....	47
4.1. HAN Decomposition in Glass Cell with SS316Ti or SS316 .....	47
4.1.1. Objective .....	47
4.1.2. Results .....	48
4.1.3. Discussion .....	51
4.2. HAN Decomposition in Glass, Titanium, and Stainless Steel Cells ...	56
4.2.1. Objective .....	56
4.2.2. Results .....	57
4.2.3. Discussion .....	60
4.3. Searching for Safe Boundary Conditions During HAN Storage and Handling .....	65
4.3.1. Isothermal Aging Testing of the Industrial HAN Sample in a Stainless Steel Cell .....	66
4.3.1.1. Objective .....	66
4.3.1.2. Results .....	66
4.3.1.3. Discussion .....	69
4.3.2. HAN Decomposition in a Stainless Steel Cell with Various Thermal Inertias .....	72
4.3.2.1. Objective .....	72
4.3.2.2. Results .....	72
4.3.2.3. Discussion .....	76
V CONCLUSIONS AND FUTURE WORK .....	80
5.1. Conclusions .....	80
5.2. Future Work .....	81

	Page
REFERENCES.....	82
APPENDIX A .....	86
VITA.....	106

**LIST OF TABLES**

	Page
Table 1.1. Comparison of commonly used calorimeters.....	20
Table 4.1. HWS of HAN decomposition (24mass%) in a glass cell with/without catalyst bar.....	51
Table 4.2. Summary of kinetic parameters of HAN (24mass%) in a glass cell with/without catalysts.....	56
Table 4.3. HWS of the industrial HAN (17mass%) decomposition in different cells.....	57
Table 4.4. Summary of kinetic parameters of the industrial HAN sample (17mass%) in different cells.....	64
Table 4.5. Iso-aging results of the industrial HAN decomposition in a stainless steel cell.....	68
Table 4.6. HWS results of thermal decomposition for different masses of the industrial HAN sample in a stainless steel cell .....	73
Table 4.7. Parameters of initiation stage (A→B) during HAN decomposition .....	77
Table 4.8. Parameters of autocatalytic stage (A→C) during HAN decomposition .....	77

## LIST OF FIGURES

	Page
Figure 2.1. DTA from Orton Instruments .....	9
Figure 2.2. DSC-404C Pegasus® .....	10
Figure 2.3. RSST including a pressure vessel and control unit .....	11
Figure 2.4. TGA.....	12
Figure 2.5. RADEX cell (left), SEDEX cell (middle), and SIKAREX cell (right)..	13
Figure 2.6. Close-up view of ARC .....	16
Figure 2.7. Overall view of the APTAC™ system .....	17
Figure 2.8. Schematic of the APTAC pressure vessel .....	18
Figure 3.1. Gas phase structure of HAN.....	34
Figure 3.2. Mechanism of HAN decomposition proposed by Wei et al. (2004) .....	36
Figure 3.3. Temperature vs. time for the calibration test with initial pressure at 300 psia .....	44
Figure 3.4. Pressure vs. time for the calibration test with initial pressure at 300 psia.....	44
Figure 3.5. Thermocouple offset vs. temperature profile .....	45
Figure 3.6. Default Tabs 6 and 7.....	45
Figure 4.1. Temperature-time profiles of HAN (24mass%) decomposition in a glass cell with/without catalyst .....	49
Figure 4.2. Pressure-time profiles of HAN (24mass%) decomposition in a glass cell with/without catalyst .....	49
Figure 4.3. Self-heating rate-temperature profiles of HAN (24mass%) decomposition in a glass cell with/without catalyst.....	50
Figure 4.4. Pressure rate-temperature profiles of HAN (24mass%) decomposition in a glass cell with/without catalyst.....	50

	Page
Figure 4.5. Temperature-time behaviors of the exotherm durations in Fig. 4.1 .....	52
Figure 4.6. Kinetic analysis of HAN (24mass%) decomposition in a glass cell without catalyst .....	54
Figure 4.7. Kinetic analysis of HAN (24mass%) decomposition in a glass cell with SS316Ti bar .....	55
Figure 4.8. Kinetic analysis of HAN (24mass%) decomposition in a glass cell with SS 316 bar .....	55
Figure 4.9. Temperature-time profiles of the industrial HAN sample (17mass%) decomposition in different cells .....	58
Figure 4.10. Pressure-time profiles of the industrial HAN sample (17mass%) decomposition in different cells .....	58
Figure 4.11. Self-heating rate-temperature profiles of the industrial HAN sample (17mass%) decomposition in different cells .....	59
Figure 4.12. Pressure rate-temperature profiles of the industrial HAN sample (17mass%) decomposition in different cells .....	59
Figure 4.13. Temperature-time behaviors of the exotherm durations in Fig. 4.9 .....	61
Figure 4.14. Kinetic analysis of the industrial HAN sample (17mass%) decomposition in a glass cell.....	62
Figure 4.15. Kinetic analysis of the industrial HAN sample (17mass%) decomposition in a titanium cell .....	62
Figure 4.16. Kinetic analysis of the industrial HAN sample (17mass%) decomposition in a stainless steel cell.....	63
Figure 4.17. Linear relationship between $\phi$ and $\Delta H_{rxn}$ .....	64
Figure 4.18. Onset temperature vs. soak time at various soak temperatures.....	68
Figure 4.19. Onset pressure vs. soak time at various soak temperatures.....	69
Figure 4.20. Maximum storage time prediction for soak temperature of 90°C.....	70
Figure 4.21. Maximum storage time prediction for soak temperature of 110°C.....	71

	Page
Figure 4.22. The maximum storage time trend based on isothermal aging testing ....	71
Figure 4.23. Temperature-time profiles of the industrial HAN sample (17mass%) decomposition in a stainless steel cell.....	73
Figure 4.24. Pressure-time profiles of the industrial HAN sample (17mass%) decomposition in a stainless steel cell.....	74
Figure 4.25. Self-heating rate-temperature profiles of the industrial HAN sample (17mass%) decomposition in a stainless steel cell.....	74
Figure 4.26. Pressure rate-temperature profiles of the industrial HAN sample (17mass%) decomposition in a stainless steel cell.....	75
Figure 4.27. Temperature-time behaviors of the exotherm durations in Fig. 4.23 .....	75
Figure 4.28. Simulation of test 1 .....	78
Figure 4.29. Simulation of test 2 .....	78
Figure 4.30. Simulation of test 3 .....	79

## CHAPTER I

### INTRODUCTION

All chemicals can be viewed as a double-edged sword. If you use them properly, they will drive the improvement of technology and the development of the economy. However, if some unwanted side or decomposition reactions happen, chemicals may pose hazards that threaten human life and cause tremendous damage to property. The U.S. Chemical Safety and Hazard Investigation Board issued a report, *Incident Data — Reactive Hazard Investigation* that analyzed 167 chemical incidents from 1980 to 2001 in the USA (U.S. Chemical Safety and Hazard Investigation Board, 2003). These incidents were distributed among chemical manufacturing (raw material storage, chemical processing, and product storage) and other industrial activities (such as bulk chemicals storage). According to the report, thirty-seven incidents occurred in storage areas or involved storage tanks of reactive chemicals. Because chemicals are usually stored in large quantities, they may cause catastrophic consequences during an incident. In order to control reactive hazards and prevent similar incidents, the study of safe storage and handling conditions for reactive chemicals is necessary. However, reactive chemicals usually have complicated runaway pathways as part of their decomposition reaction systems. It is therefore a challenge to define safe storage and handling conditions for industries

that manufacture, handle, and store reactive chemicals.

Hydroxylamine nitrate (HAN) is an important agent for the nuclear industry and the U.S. Army. High concentrations of HAN are used as an oxidizer in gun propellant mixtures, and at low concentrations HAN is used as a decontamination agent for equipment treatment in nuclear material processing. According to a technical report from the U.S. Department of Energy, HAN has been involved in several incidents from 1972 to 1997. One major HAN incident was an explosion on May 14, 1997, in the Chemical Preparation Room of the Plutonium Reclamation Facility at the Hanford Plutonium Finishing Plant (U.S. Department of Energy, 1998). The investigation of this incident showed that understanding the thermal decomposition behavior of HAN during storage and handling is significant to avoid similar incidents. With this safety objective, this research focused on effects of various container materials on the decomposition of HAN and on determining a method to predict safe storage boundaries.

Calorimetry is a very useful method for studying thermal behavior and evaluating potential thermal hazards of runaway reactions (Sempere et al., 1997; Tseng et al., 2005). Calorimetry used for thermal stability and runaway study can be categorized into two types: screening level calorimetry and advanced calorimetry. Screening level calorimetry is used for rapid tests of thermal hazards of reactive chemicals. For chemicals that show potential hazards in screening tests, advanced calorimetry is employed to evaluate thermal behavior.

Advanced calorimetry mainly refers to adiabatic calorimetry, which can simulate the worst-case scenario of thermal hazards in exothermic reactions. Adiabatic calorimetric tests can measure the maximum temperature, pressure, and self-heating rates during an exothermic reaction. These data can be used in the design of safety relief systems, process control, and for assessing hazards due to chemical reactivity. In addition, the behavior of temperature or pressure versus time of a reaction in adiabatic calorimetric tests can be used to analyze the kinetics of reactions.

The simplest kinetics applied to thermal decomposition of hazardous materials is the  $n$ -th order model, which has been illustrated clearly in operating principles of adiabatic calorimeters. It can generally well represent adiabatic data. However, for some complicated reactions such as autocatalytical decompositions, it cannot be guaranteed that  $n$ -th order kinetics will work satisfactorily, especially for the explosion periods of autocatalytic decompositions. Much work has been done on seeking more formal kinetic models for simulating calorimetric data. As a result, some commercialized kinetic modeling software has been generated.

The Thermal Safety Software (TSS) series developed by ChemInform St. Petersburg Ltd. (CISP) is a type of kinetic modeling software. For all kinds of calorimetric data, the TSS provides not only the  $n$ -th order model, but also other kinetic models such as the generalized auto-catalysis model, auto-catalytic stage (“proto”) model, Avrami-Eforfeev’s model (topo chemical reaction), generalized topo

chemical model, and the Jander model.

In this work, the Automatic Pressure Tracking Adiabatic Calorimeter (APTAC) was employed to conduct experiments for studying HAN thermal decomposition. The  $n$ -th order kinetic model was used for simulating HAN decomposition behavior during the induction period. The overall kinetic simulation for HAN decomposition was performed using the TSS software. Based on the current results, a method to predict safety conditions during storage and handling of HAN has been proposed.

Chapter II presents a review of calorimetry used in thermal hazards study. Besides screening level calorimetry and advanced calorimetry, miniature calorimetry as a new member of the calorimetry family is reviewed. The APTAC is emphasized because it is the instrument used in this research. Chapter III presents a background of thermal and catalytic HAN decomposition and provides experimental details of samples, equipment, calibration, and experimental methods. Chapter IV presents and discusses experimental data from the APTAC testing including kinetic analysis with the  $n$ -th order and the TSS software. Chapter V summarizes the conclusions and addresses future work on this topic.

This research is useful for HAN manufactures and customers, because it provides them with a study of the effects of different materials used for HAN containers on the decomposition of HAN and proposes an approach to determine safe boundaries for HAN storage and handling. The experimental data obtained in this work not only can help with aspects of process safety design including emergency

relief systems, process control, and process equipment selection, but also is a useful reference for the associated theoretical study of autocatalytic decomposition behavior.

## CHAPTER II

### CALORIMETRY APPROACH FOR THE STUDY OF THERMAL HAZARDS

#### 2.1. Introduction

Thermal hazards have been reported as one of the major hazards in chemical process facilities, and they are usually caused by chemical exotherm behavior due to instability, incompatibility, oxidization, flammability, or explosibility. The calorimetry approach is mainly applied for the study of thermal stability and runaway reactions. Thermal stability is defined as “the resistance to permanent change in properties caused solely by heat” (<http://composite.about.com/library/glossary/t/bldef-t5525.htm>). Runaway means “a thermally unstable reaction system which shows an accelerating increase of temperature and reaction rate which may result in an explosion” (CCPS, 1995). A runaway reaction may occur if the heat removal rate is less than the heat generation rate for an exothermic reaction. Many factors can lead to runaway, including rapid decomposition or oxidation reactions, reactants overloading or mischarging, incorrect handling of catalyst, cooling system failure, or loss of agitation.

Calorimetry is “the science of measuring the heat of chemical reaction and physical changes” (<http://en.wikipedia.org/wiki/Calorimetry>). In the area of process safety, it is a powerful approach for studying thermal behavior and evaluating the

thermal hazards of a runaway reaction (Gustin, 1993; Maschio, et al, 1999; Duh, et al, 1996; Donoghue, 1997). This technique, which can be used to conduct thermodynamic and kinetic analyses, measures the behaviors of temperature, pressure, power output, temperature increase rate, and pressure increase rate with respect to time. The resulting information can help to prevent runaway reactions, design emergency relief systems, and study thermal stability and storage compatibility (Gustin et al., 1993; Barreda et al., 2005; Lu et al., 2004; Botros et al., 2006, Rota et al., 2002; Fauske, 2000).

Calorimetry for thermal safety investigation in industries and academia can be classified into two types based on operation cost and testing time: screening level calorimetry and advanced calorimetry. These types will be introduced in the following sections, followed by a comparison among commonly used calorimeters. Moreover, a new member of the calorimetry family – miniature calorimetry, will be discussed in this chapter. As the instrument used in this research, the Automatic Pressure Tracking Adiabatic Calorimeter (APTAC) will be emphasized in a separate section.

## **2.2. Screening Level Calorimetry**

Calorimetry screening provides inexpensive and rapid testing, requires minimal expertise, and yields information that guides more detailed analysis. In industries, screening level calorimetry is employed as a minimum best practice (MBP)

for safety management, which results in an acceptable level of risk with consideration of cost effectiveness. The screening calorimetry in common use includes Differential Thermal Analysis (DTA), Differential Scanning Calorimetry (DSC), Reactive System Screening Tool (RSST), Thermogravimetric Analysis (TGA), and Isoperibolic Calorimetry.

### **2.2.1. Differential Thermal Analysis (DTA)**

Differential Thermal Analysis is a “fingerprinting” technique. It can provide information on chemical reactions, phase transformations, and structure changes for a sample under study. Usually, it connects a voltmeter with two thermocouples, which are placed in a reference material (inert substance) such as  $\text{Al}_2\text{O}_3$  and a sample material, respectively. When the sample and reference material are subjected to an identical temperature scanning program, temperature differences between them are monitored as functions of temperature or time (CCPS, 1995). The principle of DTA is that the input energy will steadily raise the temperature of the reference material, which will be converted to latent heat during a phase transition of the sample. Figure 2.1 below shows a DTA instrument from Orton Instruments.



Fig.2.1. DTA from Orton Instruments  
(<http://www.ortonceramic.com/instruments/pdf/DTA.pdf>)

### **2.2.2. Differential Scanning Calorimetry (DSC)**

Differential Scanning Calorimetry is a technique by which the input energy difference for establishing a nearly zero temperature difference between a sample substance of up to a few mg and inert reference material is measured as a function of temperature while the sample and reference material are subjected to an identical temperature scanning program. DSC can be categorized into two types, power compensation DSC and heat-flux DSC, which are discussed in detail by Bhadeshia (2002). Figure 2.2 is a picture of a DSC calorimeter from Netzsch Instruments Inc.

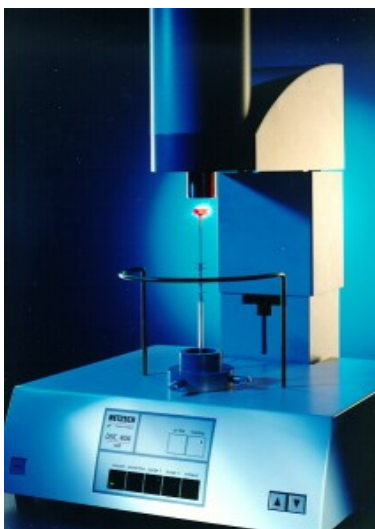


Fig.2.2. DSC-404C Pegasus®  
(<http://www.e-thermal.com/dsc404c.htm>)

### 2.2.3. Reactive System Screening Tool (RSST)

The Reactive System Screening Tool developed by Fauske & Associates is a near-adiabatic calorimeter that characterizes reaction thermal nature rapidly with a single heating scan. The sample substance is placed in a small open glass cell (about 10mL) that is contained in a stainless steel vessel pressurized with nitrogen. The resulting RSST data yield rates of temperature and pressure rise due to runaway reaction, which provides information about exothermic reactions and design emergency relief devices (Fauske, 1993). The RSST is not very sensitive and can only detect self-heat rates higher than  $1^{\circ}\text{C}/\text{min}$ . However, it is frequently used for screening reactive chemicals due to its relative affordable price and ease of use. The RSST and its control unit are shown in Figure 2.3.



Fig.2.3. RSST including a pressure vessel and control unit  
(<http://www.chem.mtu.edu/~crowl/rsst.htm>)

The Advanced Reactive System Screening Tool (ARRST), based on the RSST, is also manufactured by Fauske & Associates. Retaining the easy-to-use and inexpensive characteristics of the RSST, the ARSST adopts new Windows software, which adds many features such as wider scan rates (0~30°C/min), a heat-wait-search (HWS) heating mode, and isothermal operation at elevated temperatures. As a result, the sensitivity of onset detection is increased down to 0.1°C/min. A detailed introduction of the ARSST was presented by Burelbach (2000).

#### **2.2.4. Thermogravimetric Analysis (TGA)**

Thermogravimetric Analysis is a technique for studying thermal stability of chemicals in which the weight loss percentage of a sample is measured as a function of temperature or time while the sample is being heated at a fixed rate. Information about the composition of the sample is indicated by the mass loss during a specific

temperature range. It is commonly used for determining material characteristics, degradation temperature, and decomposition point of explosives. Many companies produce TGA apparatus, such as Linseis, Mettler, Perkin Elmer, and TA Instruments.

A typical TGA apparatus is shown in Figure 2.4 below.



Fig.2.4. TGA

(<http://www.ptli.com/testlopedia/tests/TGA-E1131.asp>)

### **2.2.5. Isoperibolic Calorimetry**

Isoperibolic Calorimetry is used to investigate the thermal behavior of exothermic reactions. In this type of calorimeter, a surrounding jacket is maintained at constant temperature while the temperature of the sample cell and its bucket are raised due to heat released by sample decomposition or combustion. Commercial isoperibolic calorimeters include SENSITIVE DETECTOR OF EXOTHERMIC PROCESSES (SEDEX), SIKAREX, and RADEX, whose photo is shown in Figure 2.5.



Fig.2.5. RADEX cell (left), SEDEX cell (middle), and SIKAREX cell (right)  
([http://www.systag.ch/e530tsc5.htm# Measuring\\_cells](http://www.systag.ch/e530tsc5.htm# Measuring_cells))

### 2.3. Advanced Calorimetry

Advanced calorimetry used for thermal safety study includes adiabatic calorimetry and reaction calorimetry. Adiabatic calorimetry is designed to investigate worst-case scenarios for exothermic reactions, which has been proven to be a good way to evaluate thermal hazards of reactive chemicals under runaway conditions since the dynamic data of runaway reactions is measured directly. Reaction calorimetry investigates heat flow due to exothermic reaction by simulating real process conditions. Reaction calorimetry belongs to the general class of isothermal calorimetry that cannot measure the runaway data directly. Therefore, adiabatic calorimetry is preferred for runaway reaction studies.

Compared with screening level calorimetry, adiabatic calorimetry is not only

time-consuming and expensive but also requires more experiment and interpretation skills. However, adiabatic calorimetry is usually employed as an available best practice (ABP) to study the greatest reduction in risk for safety management. It minimizes heat losses during operation by adjusting the surrounding temperature to match the sample temperature, which simulates the worst-case scenario of a runaway reaction. The kinetic and thermodynamic data obtained by adiabatic calorimeter can be applied to build computer models of reaction kinetics and runaway simulations (Grolmes & King, 1995; Townsend et al., 1995; Liaw et al., 2001). The resulting information can be used to conduct consequence analysis in risk assessment. Commonly used adiabatic calorimeters include the Accelerating Rate Calorimeter (ARC), Automatic Pressure Tracking Adiabatic Calorimeter (APTAC), Vent Sizing Package (VSP), Phi-tec, and Dewar flask. Hereinto, ARC and APTAC are discussed in this section. For other adiabatic calorimeters, information can be found in the open literature (Yue, 1994; Gigante et al., 2003; Nomen et al., 1995).

### **2.3.1. Accelerating Rate Calorimeter (ARC)**

In 1978, Dow Chemical Company developed the Accelerating Rate Calorimeter, which became the most widely used adiabatic calorimeter for substances ranging from explosives to detergents and batteries to resins. Later on, Thermal Hazard Technology reengineered the original ARC and extended its application to make it more users friendly. In the ARC, a sample cell made of

stainless steel, titanium, tantalum, or Hastelloy is placed in an insulated container as shown in Figure 2.6. Two heating modes (heat-wait-search and heating) are available for the ARC. In the heat-wait-search mode, the ARC heats the sample material with a fixed temperature increment, then switches to wait mode for stabilizing the temperatures of the sample and containment vessel, and finally changes to a search mode. If an exotherm is detected during the search mode, the ARC goes into the adiabatic mode and follows the exotherm. Otherwise, it heats the sample material to the next search stage at a higher temperature. For the heat mode, the sample material is heated continuously until an exotherm is detected, and then the ARC switches to the adiabatic mode to follow the exotherm.

The ARC can detect exotherms as low as  $0.01^{\circ}\text{C}/\text{min}$ . The operating temperature can be up to  $400^{\circ}\text{C}$  and the pressure up to 200 bars. The data obtained from ARC testing are temperature and pressure as functions of time, which are used to calculate the maximum self heat rates, maximum pressure rates, onset temperatures, and reaction kinetics parameters. The major problem with the ARC is the high thermal inertia of the reaction vessel as a result of using a thick wall sample cell and a relative small quantity of sample. Moreover, due to the limited cell heating up to  $20^{\circ}\text{C}/\text{min}$ , the ARC is not appropriate to study under adiabatic conditions fast exotherms such as some autocatalytic reactions.

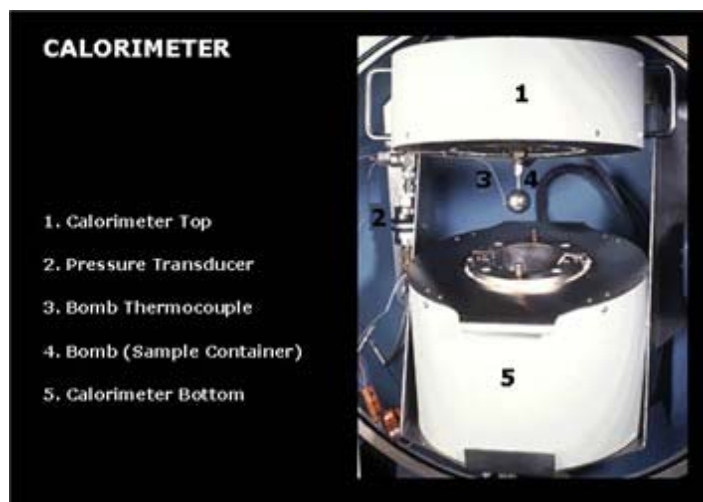


Fig.2.6. Close-up view of ARC  
(<http://www.chem.mtu.edu/~crowl/arc.htm>)

### 2.3.2. Automatic Pressure Tracking Adiabatic Calorimeter (APTAC)

The Automatic Pressure Tracking Adiabatic Calorimeter was developed from the ARC and has many unique features. Its dynamic calorimetric range is about 20 times wider than other adiabatic calorimeters (up to 400°C/min). Reagent can be added into the sample cell and the sample can be vented during an experiment, which extends the applications of adiabatic calorimetry. Because the APTAC performs closed-cell testing, the resulting data are more accurate than open-cell calorimeters such as the RSST or ARSST. In addition, a pressure compensation mechanism in which the sample pressure is matched outside the cell enables the APTAC to use thin-wall sample cells (made of glass, stainless steel, titanium, etc.). This improvement combined with the larger sample size dramatically reduces the thermal inertia of the sample cell.

The APTAC is capable of studying exothermic reactions at temperatures ranging from ambient to 500°C and pressures ranging from vacuum to 2000 psia. It has various modes such as heat-wait-search, heat-soak-search, heat ramps, and isothermal. Figure 2.7 is an overall view of APTAC™ system, and Figure 2.8 is a schematic of APTAC™ pressure vessel.



Fig.2.7. Overall view of the APTAC™ system  
(<http://www.calorimeters.net/Overview%20Products-Services/aptac.htm>)

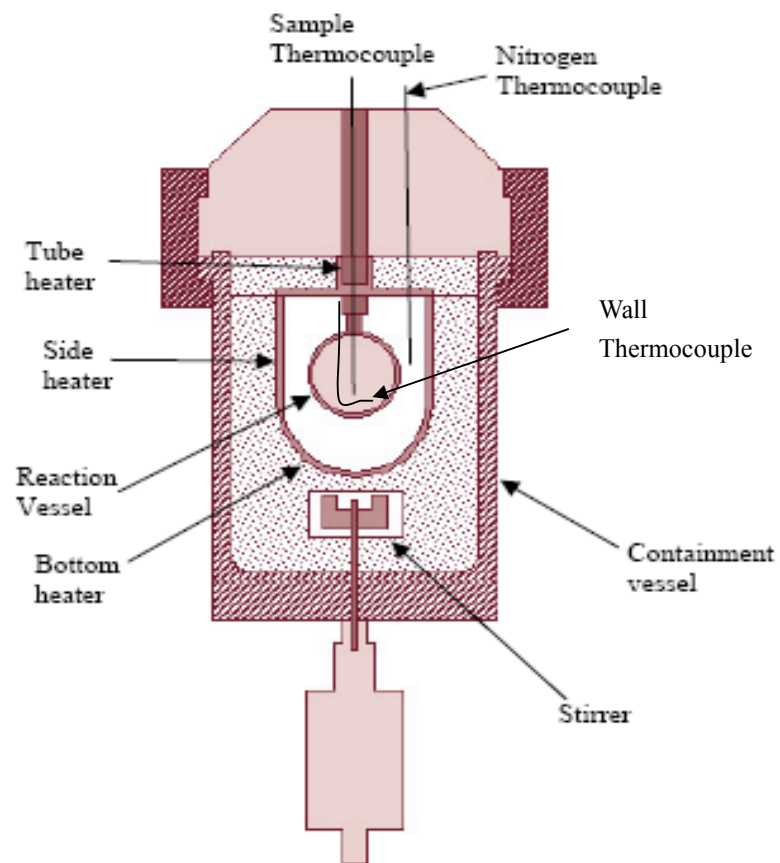


Fig.2.8. Schematic of the APTAC pressure vessel  
(Adapted from Wei, 2005)

#### **2.4. Comparison of Calorimeters**

No calorimeter can be used for all purposes because each one has its own strengths and weaknesses based on the principle of measurement and range of operation. Kersten et al. (2005) have conducted a Round-Robin test with di-tertiary-butyl peroxide in the ARC, Phi-Tec, Pressure Dewar calorimeter (Dewar), temperature controlled reactor (CRVM), and the APTAC for comparing the accuracy and reliability of these adiabatic calorimeters. After these experiments, they concluded that no specific type of equipment was superior to the others from an overall point of view. However, if some requirements or limitations are specified, an appropriate calorimeter may be selected for a specific application. A summary and comparison of common calorimeters are listed in Table 1.1, which may help to choose appropriate tools for specific studies of thermal hazards.

Table 1.1.

Comparison of commonly used calorimeters (Modified from <http://www.harsnet.de/links/Calorimeters.htm>)

Calorimeter	TS <sup>U</sup>	Calwin	DSC	HP27	Radex
Pressure range		-1 to 60 bar			
Temperature range	0 to 400°C	-20 to 200 °C	Up to 750°C		
Typical sample size	5g	500g	1mg	2 to 10 mg	1 to 5 g (1 to 5 mL)
Objective and method	Thermal stability screening	Isoperibolic	Isothermal test, thermal stability screening	Thermal stability, high pressure DSC	Thermal stability screening method
Thermal sensitivity	1W/g	<0.1mW/g	~3 μW/mg	1mW/g	5 J (0.1C x 50 J/C Heat Cap Radex)
Advantages*	1, 2, 3, 4, 7, 8	1,3,7	1, 2, 3	1, 2, 3, 8	1 (multiple tests at once), 3, pressure data
Disadvantages**	8		4, 8	4, 6, 8	1 (cleaning), 4, 5
Data obtained	Onset temperature, pressure	ΔH, C <sub>p</sub> , pressure	ΔH, C <sub>p</sub> , limited kinetic data	ΔH, kinetic data	ΔH, relative onset temperature
Price	Single test	Low	Low	Low	Medium
	Interpretation	Low to medium	Medium	Medium	Medium
	Instrument	Low to medium	Low	Medium	High
Skills	Experimentation	Low	Medium	Medium	Medium
	Interpretation	Medium to high	Low	High	High
Manufacturer	Hazard Evaluation Laboratory Limited (HEL)	uniHH	Netzsch Instruments Inc.	Mettler	SYSTAG, System Technik AG

\* Advantages: 1. Quick; 2. Only small sample needed; 3. Wide temperature range; 4. Sensitivity to T; 5. Low Phi-factor; 6. Accurate global kinetics; 7. Low price; 8. Small effort; 9. Other

\*\*Disadvantages: 1. Time consuming; 2. Large sample required; 3. Restricted temperature range; 4. Insensitivity to T; 5. Medium/high Phi-factor; 6. More test runs needed; 7. Very expensive; 8. Cannot imitate process conditions; 9. Other

Table 1.1. (Continued)

Calorimeter	TGA	DTA	Similar	ARSST	ARC
Pressure range	1 bar		Up to 60 bar		
Temperature range	200°C	Up to 1500°C	-40 to 300°C		
Typical sample size	10 to 20 mg	1mg	750g	1 to 10 mL	5g (5mL)
Objective and method	Differential thermal analysis, detection of volatiles, composition, thermal stability	Thermal stability, screen reactive system	Isothermal calorimeter	Thermal stability screening, runaway characterization, vent sizing	Adiabatic test, thermal stability
Thermal sensitivity	0.0001 W	< 0.0005 $\mu$ V	<0.1mW/g	1mW/g	0.01°C/min
Advantages*	1, 2, 3, 6, 7	1, 2, 3	1, 9 (can simulate actual process)	1, 2, 3, 4, 5, 6	2, 3, 5, 9 (Pressure data)
Disadvantages**	8	4, 8	2	6, 8	1, 5, 7, 9 (measured heat rates Phi-dependant, needs modeling)
Data obtained	Humidity, change of mass versus temperature	$\Delta$ H, limited kinetic data	$\Delta$ H, C <sub>p</sub> , kinetic data, power output, pressure, gas evolution rate	Kinetic data, onset temperature, adiabatic temperature rise	$\Delta$ H, kinetic data, onset temperature
Price	Single test Interpretation Instrument	Medium High High	Low	Medium Medium High	Medium Medium Low
Skills	Experimentation Interpretation	High High	Medium High	Medium High	High High
Manufacturer	Mettler	Orton Instruments	HEL	Fauske	Thermal Hazard Technology

Table 1.1. (Continued)

Calorimeter	Open Cup ARC	VSP	PHI-TECI	APTAC	Dewar Flask
Pressure range		Up to 1000 psia	0 to 138 bar	Up to 2000 psia	
Temperature range		-50 to 1000°C	0 to 500°C	Up to 500°C	-20 to 200°C
Typical sample size	10g (20mL Powder)	120mL (sample cell)	8g	130mL (sample cell)	200 to 500 mL
Objective and method	Adiabatic test, solids oxidative stability, storage stability	Adiabatic test, thermal stability	Adiabatic testing, thermal stability, runaway characterization	Adiabatic testing, thermal stability, runaway characterization	Adiabatic testing, thermal stability
Thermal sensitivity	0.01°C/min	0.05°C/min	0.02°C/min	0.04°C/min	0.5W/kg
Advantages*	5, air flow at elevated temperature,	3, 5, 9 (Pressure compensation)	1, 2, 3, 4, 6, 9 (Pressure compensation)	3, 5, 6, 9 (Pressure compensation)	3, 4, 5, 7, 9 (accurate data)
Disadvantages**	1, 2	1, 2	8	1, 7, 9 (measured heat rates Phi –dependant, needs modeling)	1, 2
Data obtained	Kinetic data (zero order)	$\Delta H$ , kinetic data, onset temperature, pressure	$\Delta H$ , kinetic data, onset temperature, pressure	$\Delta H$ , kinetic data, onset temperature, pressure, pressure	$\Delta H$ , $C_p$ , the induction time
Price	Single test	High	High	High	High
	Interpretation		Medium	Medium	
	Instrument	High	Medium	High to very high	Low
Skills	Experimentation	High	Medium	Medium	Medium
	Interpretation	High	High	High	Medium
Manufacturer		Fauske	HEL	TIAX	

## 2.5. Miniature Calorimetry

With the development of nanotechnology and microfabrication, miniature calorimetry as the new member in the calorimetry family has been gradually applied in the area of process safety. Currently, miniature calorimetry used in safety studies includes isothermal nanocalorimetry and isothermal microcalorimetry.

Isothermal nanocalorimetry is a technique based on similar principles such as the DSC, but the calorimeter cell size is reduced to the micrometer or nanometer scale. A commercialized isothermal nanocalorimeter (INC) developed by Calorimeter Sciences Corp. (CSC) has been applied in measurement of pharmaceutical shelf life, hazards evaluation of explosive storage, and the study of chemical stability. This INC can detect a heat flow change as low as 1 nanocalorie/second. Such high sensitivity is a prerequisite for calorimetric study of samples in limited quantity or with a hazardous nature. More information about the INC is available on the website of Calorimeter Sciences Corp. (<http://www.calorimetriesciences.com/Calorimeters.html>).

Isothermal microcalorimetry can monitor the heat flow generated by a chemical, physical, or biological process as the sample is maintained at constant temperature. The heat flow can be used to calculate the heat generated or consumed by the sample placed in the calorimeter. Commercialized isothermal microcalorimeters include the Tian-Calvet microcalorimeter and the Thermal

Activity Monitor (TAM).

The Tian-Calvet microcalorimeter is an isothermal microcalorimeter used for the study of thermal decomposition including the determination of kinetics and the evaluation and prediction of reaction progress. It can be used if the ARC indicates an onset temperature of reaction within 50°C of the temperature required for the process. Its sample size is 1~10mL compared with 100mL in the DSC. Moreover, the Tian-Calvet microcalorimeter can obtain more accurate data than the usual DSC. A detailed introduction to the Tian-Calvet microcalorimeter can be found on the website of Setaram Instrumentation (<http://www.setaram.com/>).

The Thermal Activity Monitor was developed at the University of Lund (Suurkuusk & Wadsö, 1982) and was commercialized by LKB Instruments in Sweden. It is designed for detecting chemical activity that may develop into a thermal runaway during storage or handling of bulk quantities. The third generation, TAM III, allows multi-sample measurements to be performed simultaneously for up to 48 hours. Its scanning mode can be set to less than 2°C/hr for an isothermal step. The application of the TAM in the pharmaceuticals and biomaterials can be found in the literature (Lechuga-Ballesteros et al., 2003; Zimehl et al., 2002).

## **2.6. APTAC Details**

Because the APTAC is the instrument used in this research, detailed information on its operation modes, data acquired, and general principles of

operation will be discussed under the following subtitles.

### **2.6.1. Operation Modes**

The APTAC has several heating strategies for the sample including heat-wait-search, heat-soak-search (also called iso-aging), heat-ramp by fixed temperature difference, heat-ramp by rate, heat-ramp by rate with exothermal detection, and isothermal. Heat-wait-search and heat soak-search are used in this work. Information about the other strategies can be found in the control and operation manual of the APTAC.

In the heat-wait-search, the APTAC heats the sample with a specified temperature rate (say 2°C/min) to a starting temperature, then changes to wait mode to allow for the temperatures of sample and containment vessel to stabilize, and finally switches to search mode to detect exothermal behavior. During the process, the self-heating rate of the sample is polled and compared with a predefined sensitivity threshold. When the self-heating rate of the sample exceeds this threshold, an exotherm is detected by the system. If an exotherm is detected during the search mode, the APTAC will go into the adiabatic mode and follow the exotherm. Otherwise, the sample material will be heated to the next higher predefined temperature for the next exotherm search. The standard stabilization and searching times are 25 minutes.

The iso-aging can be used to study the effects of inhibitors added to the

reactants. In this strategy, the sample material is heated first to a preset soak temperature. The APTAC requires time for temperature stabilization of the pressure vessel and sample (default value is 25 minutes) and then proceeds to the search mode during which the APTAC maintains a constant sample temperature. During the process, the self-heating rate of the sample is polled and compared with a predefined sensitivity threshold. When the self-heating rate of the sample exceeds this threshold, an exotherm is detected by the system. If an exotherm is detected in the search mode, the APTAC will automatically switch to the adiabatic mode and follow the exotherm. Otherwise, the APTAC will stay in the search mode until the predefined soak time is ended and then proceed to a standard heat-wait-search.

### **2.6.2. Data Acquired**

The data measured directly by the APTAC includes elapsed time, sample temperature, reaction vessel temperature, containment vessel temperature, sample pressure containment pressure, sample self-heating rate, and pressure rate of sample. Important data curves that can be obtained from the APTAC software are temperature versus time, pressure versus time, temperature versus pressure, heat rate versus temperature, and pressure rate versus temperature profiles. These data and the shapes of the curves can provide information about potential hazards posed by the reaction that occurred in the system. Moreover, there are some important parameters that may be used for further kinetic analysis of runaway reactions or for simulation

during the design of safety-relief devices. Useful reaction characterization parameters include:

- Onset temperature ( $T_{\text{on}}$ ): “the temperature at which a detectable temperature increase is first observed due to a chemical reaction” (defined by CCPS, 1995). Its value depends on the sensitivity of the temperature measuring equipment. Usually, the more the thermally sensitivity, the lower the measured onset temperature. The onset temperature is important information for safe storage and handling of hazardous materials. A safety margin used in industry is 50°C or more above the onset temperature to prevent undesired reactions.
- Maximum adiabatic temperature ( $T_{\text{max}}$ ): the maximum value during an exothermic process.  $T_{\text{max}}$  is an important parameter for kinetic analysis of a runaway reaction.
- Maximum pressure ( $P_{\text{max}}$ ): the maximum value of pressure during an exothermic process. The major risk posed by a runaway reaction is the mechanical failure of reactor or container due to overpressure. The  $P_{\text{max}}$  is important also for the design of safety relief valves.
- Maximum self-heating rate ( $dT/dt_{\text{max}}$ ). This value is used in the design of safety relief devices.
- Maximum pressure rate ( $dP/dt_{\text{max}}$ ). This value is used in the design of safety relief devices.

- Time to maximum rate (TMR): the time from the self-heating rate at the onset temperature to the maximum self-heating rate. This time is used to estimate the response time of an emergency system to avoid a runaway reaction.
- Noncondensed pressure: the pressure in the gas phase of a sample when the system is cooled down after a runaway reaction has finished. This value is useful for the thermodynamic simulation of runaway reactions.

### 2.6.3. General Principles of Operation

Townsend and Tou (1980) illustrated data interpretation with the n-th order kinetics for the ARC. Because the APTAC has similar principles to the ARC, the data interpretation for the ARC is also suitable for the APTAC. Those general principles of operation are reviewed here.

For an exothermic reaction, a runaway situation may occur if the heat generated from the reaction is greater than the heat removed by the cooling system. This phenomenon can be explained by the fact that the rate constant of a reaction increases exponentially with temperature. The Arrhenius equation gives a quantitative expression for this event:

$$k = k_0 \exp(-E_a / RT) \quad (1)$$

where  $k$  is the rate constant,  $k_0$  is the frequency factor,  $E_a$  is the activation energy for the chemical reaction, and  $R$  is gas constant. Actually, a more general form of the

constant rate has been proposed as (Townsend & Tou, 1980):

$$k = k_0 T^j \exp(-E_a / RT) \quad (2)$$

where  $j$  is 0 in the Arrhenius equation, 0.5 in collision theory, and 1 in absolute rate theory. However, the term of  $T^j$  is overshadowed by the exponential factor, because the latter has wider variation. To simplify the model,  $j$  is taken as 0 whenever considering the rate constant.

If the reaction is assumed to occur with homogeneous and  $n$ -th order kinetics for a single reactant A, the reaction rate law of gives the reaction rate in terms of the rate constant, concentration of species, and the reaction order:

$$r_A = \frac{dC_A}{dt} = -kC_A^n \quad (3)$$

where  $r_A$  is the reaction rate of component A,  $k$  is the rate constant,  $n$  is the reaction order, and  $C$  is the concentration of component A.

For an exothermic reaction under adiabatic conditions (e.g., in an adiabatic calorimeter), the heat produced from the initial reaction will cause a rise in temperature that will in turn expedite the rate of reaction as shown in equations (1) and (3). This acceleration effect will lead the system to a maximum temperature and consume the concentration of reactant. Therefore, the reaction rate is expected to achieve a maximum value at a temperature peak and then decrease to zero at the end of the reaction. During the process of exotherm, the concentration of the reactant at any temperature or time is given by:

$$C = \frac{T_F - T}{T_F - T_o} * C_o = \frac{T_F - T}{\Delta T} * C_o \quad (4)$$

where  $C_o$  is the initial concentration;  $C$  is the concentration at any temperature  $T$ , and  $T_o$  and  $T_F$  are the initial and final temperatures, respectively.

The overall reaction heat generated is expressed as:

$$\Delta H = mC_V \Delta T \quad (5)$$

where  $\Delta H$  is the overall reaction heat in terms of enthalpy,  $m$  is the mass of the sample,  $C_V$  is the average heat capacity at constant volume of the reaction system over the temperature range, and  $\Delta T$  is the adiabatic temperature rise.

By differentiating equation (4), the self-heat rate  $dT/dt$  is obtained and then substituted into equation (3):

$$\frac{dT}{dt} = k \left( \frac{T_F - T}{\Delta T} \right)^n \Delta T C_o^{n-1} \quad (6)$$

If a pseudo kinetic constant  $k^*$  is defined as the following:

$$k^* = k C_o^{n-1} = \frac{dT / dt}{\left( \frac{T_F - T}{\Delta T} \right)^n \Delta T} \quad (7)$$

a relationship between  $\ln(k^*)$  and  $1/T$  can be derived by combining equations (1) and (7):

$$\ln(k^*) = \ln(C_o^{n-1} k_0) - \frac{E_a}{R} \left( \frac{1}{T} \right) \quad (8)$$

Given a correct reaction order, the  $\ln(k^*)$  versus  $1/T$  plot should be a straight line with slope of  $E_a/R$  and intercept of  $C_o^{n-1} k_0$ . The activation energy  $E_a$  and the

frequency factor  $k_0$  for the Arrhenius equation can be calculated based on the slope and intercept of the plot.

For a reaction with high activation energy (say, greater than 20 kcal/mol), the time after  $t_m$  (defined as the time at the maximum self-heat rate) is negligible because the reaction decays quickly after  $t_m$ . Therefore, the time of reaction can be estimated by the time to maximum self-heat rate (TMR). By rewriting equation (6) into the expression of  $dt$  and integrating  $dt$  from  $t_0$  (the time at the onset temperature) to  $t_m$ , TMR can be calculated by:

$$TMR = \int_{t_0}^{t_m} dt = \int_{T_0}^{T_m} \frac{dT}{k \left( \frac{T_F - T}{\Delta T} \right)^n \Delta TC_o^{n-1}} \quad (9)$$

where  $T_0$  is the onset temperature, and  $T_m$  is the temperature at the maximum self-heat rate. These parameters are determined through APTAC tests as discussed above.

In the above equations, the reaction heat energy is assumed to heat the reaction system itself. But in reality, a portion of the reaction heat is used to heat the reaction vessel that is the sample cell in the APTAC. This part of heat loss must be corrected using the following energy balance:

$$m_s C_{Vs} \Delta T = (m_s C_{Vs} + m_b C_{Vb}) \Delta T_s \quad (10)$$

where  $m_s$  is the mass of the sample,  $C_{Vs}$  is the average heat capacity of the sample,  $m_b$  is the mass of the sample cell, and  $C_{Vb}$  is the average heat capacity of the sample

cell,  $\Delta T$  is the corrected adiabatic temperature rise, and  $\Delta T_s$  is the adiabatic temperature rise measured experimentally. If a new parameter called the thermal inertia factor ( $\phi$ ) is defined as:

$$\phi = \frac{m_s C_{Vs} + m_b C_{Vb}}{m_s C_{Vs}} \quad (11)$$

equation (10) can be written:

$$\Delta T = \phi \Delta T_s \quad (12)$$

Commonly,  $1/\phi$  indicates the degree of adiabaticity of the calorimeter. For an industrial runaway reaction under adiabatic surroundings, the  $\phi$  factor approaches and is generally equal to 1.

Considering the correction of  $\phi$ , the adiabatic final temperature ( $T_F$ ) is:

$$T_F = T_0 + \phi \Delta T_s \quad (13)$$

Equations (4), (5), and (6) also become:

$$C = \frac{T_{Fs} - T_s}{\Delta T_s} * C_o \quad (14)$$

$$\Delta H = m C_V \phi \Delta T_s \quad (15)$$

$$\frac{dT}{dt}_s = k \left( \frac{T_{Fs} - T_s}{\Delta T_s} \right)^n \Delta T_s C_o^{n-1} \quad (16)$$

where the subscript “s” indicates the measured value in an experiment.

## CHAPTER III

### EXPERIMENTAL DETAILS

#### 3.1. Introduction

Hydroxylamine Nitrate (HAN), an important agent for the nuclear industry and the U.S. Army, has been involved in several incidents. One major incident was the 1997 Hanford explosion (U.S. Department of Energy, 1998). According to the incident report from the U.S. Department of Energy (1998), the concentration of HAN in aqueous solution had increased due to evaporation over the preceding four years, and iron from the inner surface of the HAN container could have acted as a decomposition catalyst. The higher HAN concentration, effect of iron contaminant, and increased ambient temperature due to inadequate ventilation expedited the violent decomposition of HAN.

Generally, HAN aqueous solution at relatively low HAN concentration up to 24 mass% is used in industries. It is a clear and odorless liquid. The molecular formula of HAN is  $\text{NH}_2\text{OH}\cdot\text{HNO}_3$ , and the gas phase structure of HAN is shown in Figure 3.1. HAN is thermally unstable and can decompose autocatalytically at elevated temperatures or in the presence of metal contaminants.

The kinetic mechanism of HAN decomposition has been investigated by several groups (Dijk & Priest, 1984; Rafeev & Rubtsov, 1993; Schoppelrei & Brill, 1997; Oxley & Brower, 1988). However, no formalized kinetic modeling has been

developed to simulate HAN runaway behavior and predict its safe boundaries for storage and handling. The major impediment is that HAN decomposition is an autocatalytic reaction with a complicated reaction pathway. This research has focused on the catalytic effects of stainless steel, titanium, and stainless steel with titanium on the HAN decomposition, and developing a kinetic model for HAN decomposition in storage tanks or other containers. Experiments were conducted with the Automatic Pressure Tracking Adiabatic Calorimeter (APTAC).

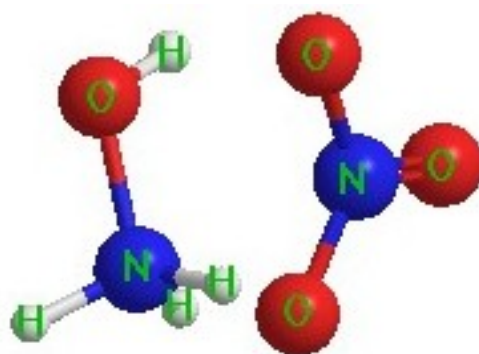


Fig.3.1. Gas phase structure of HAN  
([http://psc.tamu.edu/research/reactive\\_chem\\_lab/HAN.htm](http://psc.tamu.edu/research/reactive_chem_lab/HAN.htm))

This chapter presents experimental details on equipment, samples, methods, and thermocouple calibration. In addition, background on the mechanism of HAN reaction with nitrous acid, HAN thermal decomposition, HAN decomposition under iron catalysis, and autocatalytic decomposition hazards are also provided.

### 3.2. Background

#### 3.2.1. Mechanism of HAN Reacting with Nitrous Acid

The mechanism of HAN reacting with nitrous acid has been proposed by Gowland and Stedman (1981), as represented below:



The overall reaction can be summarized by two competing reactions:



In reaction (21), more nitrous acid is generated than is consumed, which accounts for the autocatalytic phenomena. But at low temperatures and low  $\text{HNO}_3$  and iron concentrations, reaction (22) will dominate.

#### 3.2.2. Mechanism of HAN Thermal Decomposition

Oxley and Brower (1988) proved that HAN decomposition products are comprised of nitric acid, water, nitrous oxide, and nitrogen. In the gas products, the ratio of nitrous oxide ( $\text{N}_2\text{O}$ ) to nitrogen varied from 2:1 to 4:1. They also proposed two possible overall reactions, which are shown below:





Wei et al. (2004) studied the detailed mechanism of HAN thermal decomposition by Gaussian 03 quantum calculations. In their publication, a mechanism network shown in Figure 3.2 was presented. Nitrous acid as an intermediate of HAN decomposition can react with HA (hydroxylamine) to accelerate the overall decomposition.

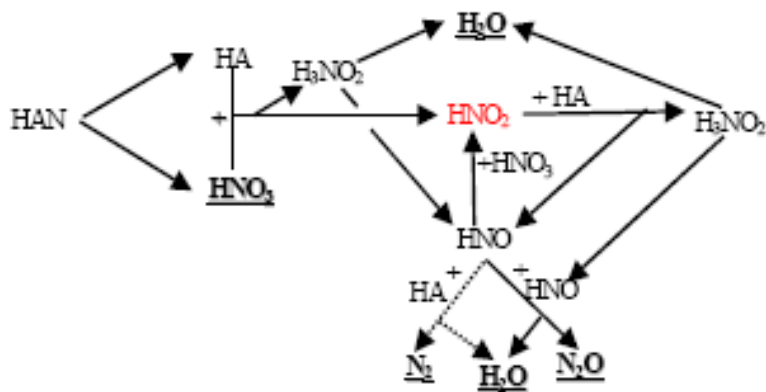
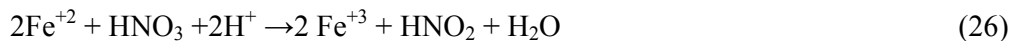


Fig.3.2. Mechanism of HAN decomposition proposed by Wei et al. (2004)

### 3.2.3. Mechanism of Iron Catalyzed HAN Decomposition

Iron can act as a catalyst to trigger HAN decomposition. This mechanism is given by (25) and (26) (U.S. Department of Energy, 1998):



The overall reaction under iron catalysis is shown as:



According to Klein's study (U.S. Department of Energy, 1998), in the presence of iron the ratio of  $\text{N}_2\text{O}$  to  $\text{N}_2$  in gas products for HAN decomposition was determined to be 36:1. Therefore, compared to nitrous oxide, the amount of nitrogen produced is negligible so it does not appear in the overall reaction (27).

#### **3.2.4. Autocatalytic Decomposition Hazards**

Autocatalytic reaction refers to a type of reaction that generates the catalyst (or reactant) as a product. Autocatalytic reactions consist of three periods: induction, explosion, and decay. During the induction period, the product that acts as a catalyst is generated and accumulated. Once this catalytic product reaches a critical amount, the explosion period starts and the temperature versus time curve exhibits a sharp jump to approximately the maximum temperature. However, the explosion period only lasts for a short time (may be less than a couple of seconds). After that, the system enters the decay period due to the depletion of reactants. The rapid increase in temperature and pressure during the explosion period poses a challenge to the design of protection and mitigation measures relating to runaway reactions. The existence of the induction period also poses a hazard for the extended storage for the chemicals that undergo autocatalytic decomposition.

Dien et al. (1994) proposed a method to estimate the "time to maximum rate under adiabatic conditions" ( $\text{TMR}_{\text{ad}}$ ) for autocatalytic decomposition based on a first-order reaction in competition with a Prout-Tompkins step, i.e.  $\text{A} \rightarrow \text{B}$ ,  $\text{A} + \text{B} \rightarrow 2\text{B}$ .

The kinetic parameters obtained from temperature-time curves in DSC testing can be validated by ARC experiments. The  $TMR_{ad}$  calculated from the kinetic model is used to determine the runaway time which can be used to plan corresponding countermeasures.

Autocatalytic decomposition hazards can be measured and assessed using general isothermal and adiabatic calorimeters. Bou-Diab and Fierz (2002) developed a screening method based on dynamic DSC measurements to identify autocatalytic decompositions. They found that autocatalytic decomposition occurred when the apparent activation energy was higher than 220kJ/mol. A border value of the apparent activation energy, 180-220kJ/mol, was suggested for use in screening autocatalytic decomposition hazards. Wei et al. (2004) studied the autocatalytic decomposition behavior of energetic materials using the APTAC. It has been proved that APTAC can be a reliable and efficient screening tool to identify autocatalytic decomposition hazards.

### **3.3. Experimental Details**

#### **3.3.1. Samples**

Hydroxylamine nitrate (HAN) (24mass%) in aqueous solution purchased from Aldrich (catalog number 438235), and an industrial HAN sample (17mass%, aqueous solution) were used in this study without further purification and analysis. The ppm concentrations of trace elements in the industrial HAN sample were

assumed to have negligible effect on the behavior of HAN decomposition.

Two kinds of materials, SS316 Ti and SS316, were used as catalysts to test their effects on HAN decomposition. Before they were added to the glass cell the catalysts were mechanically cut into bars. In order to obtain comparable results, the surface areas of catalyst bars were designed to be equal (about 2.5 cm<sup>2</sup>).

### **3.3.2. Equipment**

The experimental tests were carried out in the Automatic Pressure Tracking Adiabatic Calorimeter (APTAC<sup>TM</sup>) manufactured by TIAX, LLC. The APTAC is capable of studying exothermic reactions with temperatures up to 500°C and pressures up to 2000 psia in several testing modes (e.g., heat-wait-search, iso-aging, isothermal, and heat ramps). The principle of the APTAC operation is to minimize heat loss by adjusting the surrounding temperature to match the sample temperature. This property is very useful in simulating the worst-case scenario of an industrial runaway reaction. The APTAC can detect exotherms with a temperature rise rate of 0.04-400 °C/min and a pressure rise rate of 0.01-10,000 psia/min.

In the present work, a 100mL glass thick-wall cell, a 130mL titanium thin-wall cell, and a 130mL stainless steel thin-wall cell were used as sample cells. The surface area of the catalyst bar was measured by the 150mm dial caliper (manufactured by Chicago Brand) before it was placed into the HAN sample. In order to avoid contact of HAN with the metal sheath of thermocouple, a

Teflon-coated thermocouple (Omega part number OSK2K974/TJ8-NNIN-04OU-12-PFA-SB-T-OTP-M) was used throughout the experiments.

### 3.3.3. Methods

The heat-wait-search (HWS) and the iso-aging modes were used in this work. In the heat-wait-search, the sample was heated at  $2^{\circ}\text{C}/\text{min}$  until it reaches a predefined starting temperature. Then the system changed to wait mode to stabilize the temperature of sample and containment vessel and finally went to search mode to detect an exotherm. Before an exotherm was detected, a default time of 25 minutes was spent on each waiting or searching step. The threshold self-heating rate was chosen as  $0.05^{\circ}\text{C}/\text{min}$  throughout the experiment. If the self-heating rate of the sample exceeded this threshold during the search mode, the system automatically entered the adiabatic mode and proceeded with the exotherm until the sample was depleted or one of shutdown criteria was satisfied. Otherwise, the sample was heated to the next higher predefined temperature for the next search.

In the iso-aging mode, the sample was heated to a preset soak temperature. The APTAC took 25 minutes to stabilize the temperatures of the containment vessel and the sample and then switched to search mode for soaking the sample at that temperature. In this mode, the APTAC tracked the temperature of the sample to keep the system isothermal. In this process, the self-heating rate of the sample was compared with the predefined threshold ( $0.05^{\circ}\text{C}/\text{min}$ ). Once the self-heating rate of

the sample exceeded the threshold, the APTAC would automatically switch to adiabatic mode and follow the exotherm. If no exotherm was detected during the soak period, the APTAC would continue to proceed with a standard heat-wait-search. The iso-aging mode is designed to study the effect of inhibitors or additives on exothermic behavior of a sample material. In this work, the iso-aging mode was used to test the effect of surrounding temperatures on the autocatalytic decomposition of HAN.

Because the decomposition products of HAN in the liquid phase are water and nitrous acid, sample cells were cleaned with deionized water first and then with acetone before use. The same treatment was also applied to the catalyst bars before they were placed into the HAN-water solutions. The Teflon-coated thermocouple was flashed with deionized water and then acetone to remove contaminants from the sheath surface before placing into the sample cell. The pressure unbalance criterion was set at 80 psia for the glass cell and 100 psia for the titanium and stainless steel cells. It was not necessary to use sample stirring in these tests because only a small amount of HAN (several grams) was used in each experiment.

#### **3.3.4. Thermocouple Calibration**

Thermocouple (TC) calibration of the APTAC is necessary to maintain accurate temperature measurements. There are two kinds of TC calibration: relative and absolute. The relative calibration is used to make sure that the sample, cell wall,

and nitrogen thermocouples provide the same outputs if they are surrounded by the same temperature, while the absolute calibration checks the accuracy of absolute temperature of thermocouple measurements.

#### **3.3.4.1. Relative Calibration**

The adiabatic surrounding of the APTAC is obtained by adjusting the nitrogen temperature to be approximately the same as the temperature of the sample. Any deviation (negative or positive) between these two temperatures will cause system error for the APTAC testing. The purpose of relative calibration is to minimize either negative or positive drift of the system. It has been shown that 1°C of deviation may cause a drift rate of 0.1°C/min at modest pressures. The higher the pressure, the greater the drift rate for the same temperature difference (heat transfer rate through the sample cell wall depends on the surrounding pressure). For an exotherm detection level of 0.01°C/min, the thermocouples must be calibrated to within 0.1°C or even less. Because the practical exotherm detection level changes with pressure, the APTAC specifies its exothermal detection level as 0.04°C/min. Whenever a sample cell or thermocouple is replaced, a relative calibration must be done. Moreover, a schedule of relative calibration must be maintained. Normally, a relative calibration is recommended every 10 runs.

An empty sample cell is usually used in a relative calibration. By selecting “set up” on the menu bar and then choosing the “calibration” item, a dialog window

about calibration input data will be reached. A set of parameters (such as cooling down temperature, ending temperature, operating pressure, heating rate, etc.) must be input before starting a calibration. The starting temperature for calibration is defaulted to 50°C. The ending temperature must be chosen within the normal operating range of the thermocouple. For example, the Teflon-coated thermocouple cannot withstand high temperature. Its working range is up to ~ 210°C. To ensure that the 200°C point can be measured, 210°C may be chosen as the ending temperature.

After the calibration is completed, a thermocouple offset versus temperature curve is generated and stored automatically. This calibration curve covers the range from -50°C to 500°C and records data every 50-degree interval. For the data that cannot be obtained during calibration (-50°C, 0°C, 250°C, 300°C, 350°C, 400°C, 450°C, and 500°C for Teflon-coated thermocouple), the operator must manually input the points by extrapolating from the measured calibration data and then entering the data into the appropriate boxes in the Default Tabs 6 and 7. Figures 3.3 to 3.5 are the temperature-time curve, pressure-time curve, and thermocouple offset profile, respectively, for the calibration of the Teflon-coated thermocouple (Omega part number is OSK2K974/TJ8-NNIN-04OU-12-PFA-SB-T-OTP-M) in a glass cell. Figure 3.6 shows the corresponding Default Tabs 6 and 7 for this calibration.

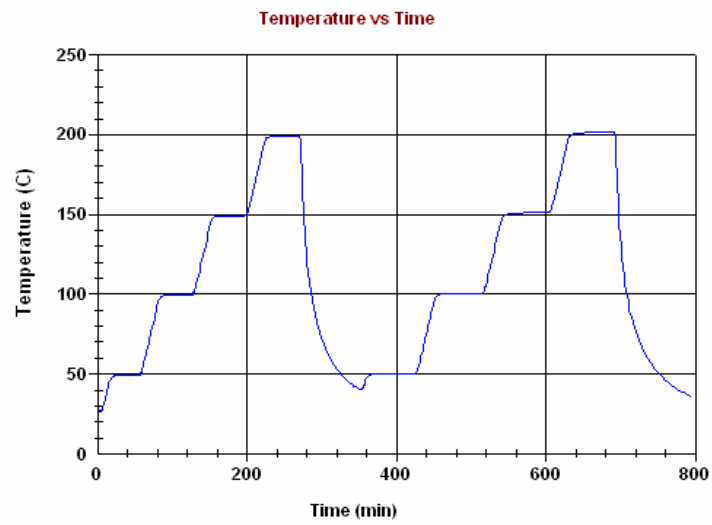


Fig.3.3. Temperature vs. time for the calibration test with initial pressure at 300 psia

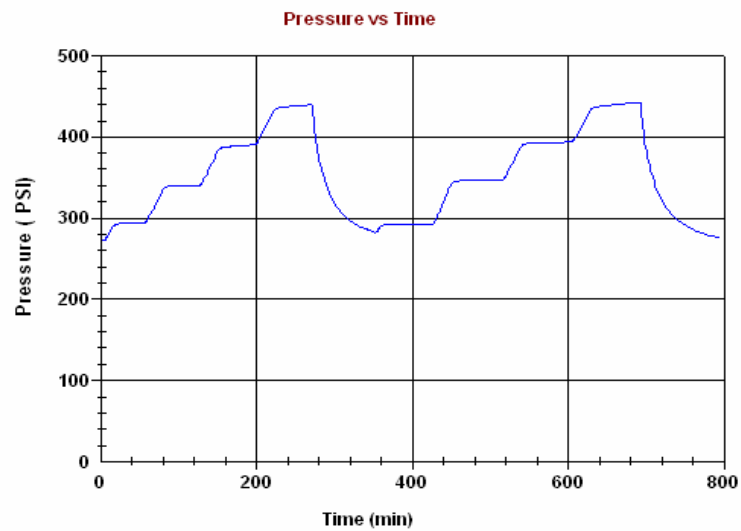


Fig.3.4. Pressure vs. time for the calibration test with initial pressure at 300 psia

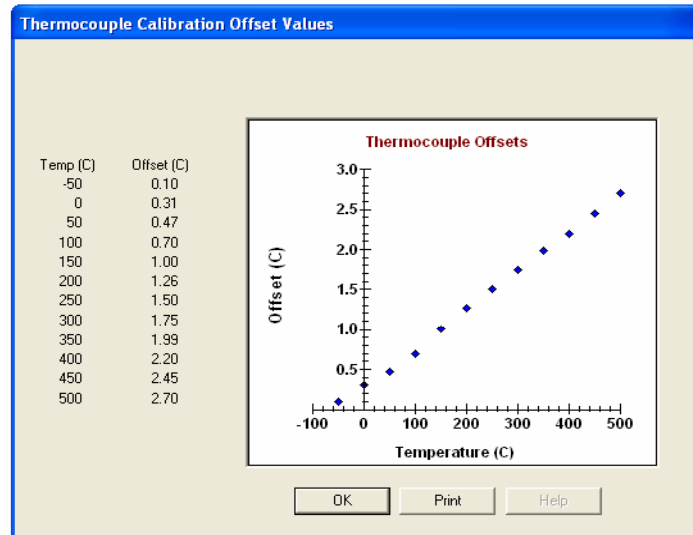


Fig.3.5. Thermocouple offset vs. temperature profile

The figure shows two screenshots of the "Default Parameters Setup" window. The left screenshot shows the "Thermocouple Calibration Offsets: -50 C to 300 C" tab, and the right screenshot shows the "Thermocouple Calibration Offsets: 350 C to 500 C" tab. Both windows also display "Transducer Zero (PSI)" values for various components.

Sample	Bomb Wall	Nitrogen
-50	0.1	0
0	0.31	0
50	0.474336	0.196478
100	0.697033	0.435001
150	1.00407	0.720411
200	1.26408	0.965713
250	1.5	0
300	1.75	0

Sample	Bomb Wall	Nitrogen
350	1.99	0
400	2.2	0
450	2.45	0
500	2.7	0

Component	Value (PSI)
Sample	81
Pressure Vessel	13.8
Simple Vent	-9.4
1-Shot	17.3
Condenser	0
Gas Collector	0
.....	0
.....	0

Fig.3.6. Default Tabs 6 and 7

#### **3.3.4.2. Absolute Calibration**

The thermocouple signal conditioning units in the APTAC system are set and linearized for type N thermocouples. When a new type N thermocouple is placed into an ice water mixture, if the reading is not 0°C, it is necessary to use the APTAC software to adjust the zero point. Specifically, the nitrogen thermocouple is placed in ice water and its offset from 0°C is recorded. This offset is entered into the thermocouple offset data point in the Default Tab 2. Then the APTAC automatically adds this value to all type N thermocouples, such as the sample, cell wall, and nitrogen thermocouples.

## **CHAPTER IV**

### **EXPERIMENTAL RESULTS AND DISCUSSION**

#### **4.1. HAN Decomposition in Glass Cell with SS316Ti or SS316**

##### **4.1.1. Objective**

As mentioned in Chapter III, iron has a catalytic effect on hydroxylamine nitrate (HAN) decomposition. In industry, stainless steel tanks (such as SS316Ti or SS316) are used to store HAN in warehouses. Because it is a sensitive parameter for the hydroxylamine family compounds, the effect of iron on HAN decomposition must be investigated. A set of tests was designed to study catalytic effects of SS316Ti and SS316 on HAN decomposition.

The HAN sample (24mass%) was purchased from Aldrich. A 100mL glass cell was used as a sample cell in these tests because it can provide a relatively neutral environment for HAN decomposition (Wei et al, 2004). Two materials, SS316Ti and SS316, were used as catalysts. The SS316Ti material was provided by an industrial company, and the SS316 material used in the tests was prepared by the chemical engineering mechanical shop. Before being loaded into glass cell, the large pieces of catalysts were cut into bars with surface areas of  $\sim 2.5\text{cm}^2$ . HAN decomposition tests in a glass cell without catalyst were also conducted. The APTAC heat-wait-search mode was employed to study the exothermic behavior of HAN decomposition.

### 4.1.2 Results

The 24mass% HAN with no catalyst, with the SS316Ti catalyst bar, and with the SS316 catalyst bar in the glass cell were examined by the HWS mode of the APTAC and the experimental results are shown in Figures 4.1 to 4.4. Table 4.1 summarizes important parameters such as the onset temperature, maximum temperature, maximum pressure, self-heating rate at onset temperature, maximum self-heating rate, maximum pressure rise rate, non-condensable pressure at 50°C, and reaction heat for each case. The presented uncertainties are within one standard deviation based on three replicas. Phi factors and reaction heats (energies of reaction) cannot be measured directly by the APTAC and were calculated using equations (11) and (15) in Chapter II. The average heat capacity of HAN used in the thermal inertia calculation was estimated to equal liquid water's heat capacity (4.18 J/g/°C) because it is not available in literature and water is a major product of decomposition. The average heat capacity of titanium and stainless steel were estimated to be 0.544 J/g/°C and 0.5 J/g/°C, respectively (The references are given on the websites of <http://www.stanford.edu/~eboyden3/constants.html> and <http://www.lenntech.com/Stainless-steel-316L.htm>).

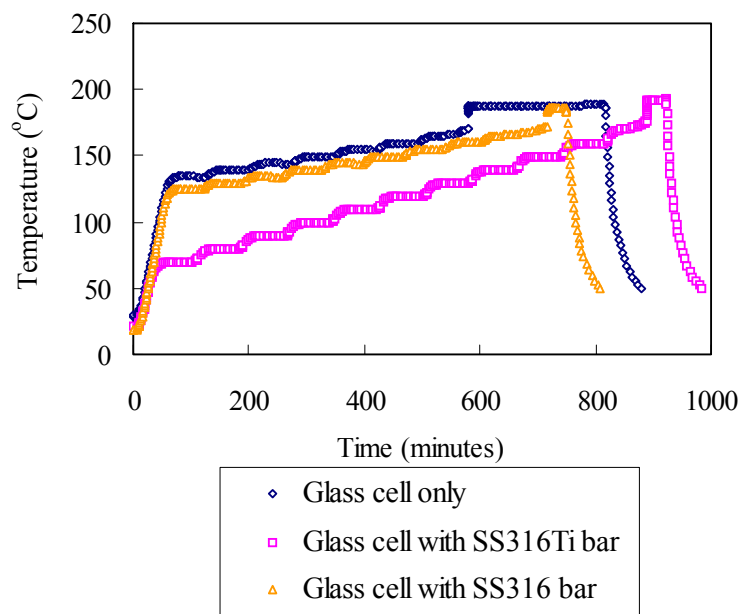


Fig.4.1. Temperature-time profiles of HAN (24mass%) decomposition in a glass cell with/without catalyst

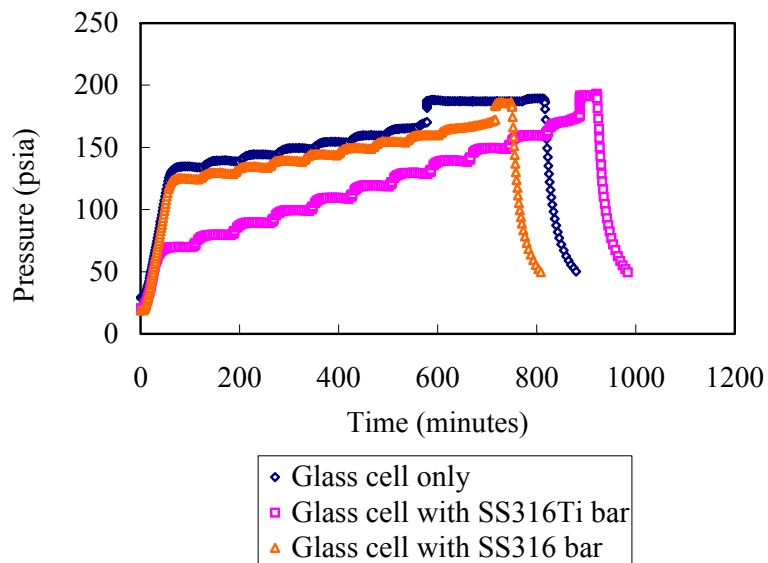


Fig.4.2. Pressure-time profiles of HAN (24mass%) decomposition in a glass cell with/without catalyst

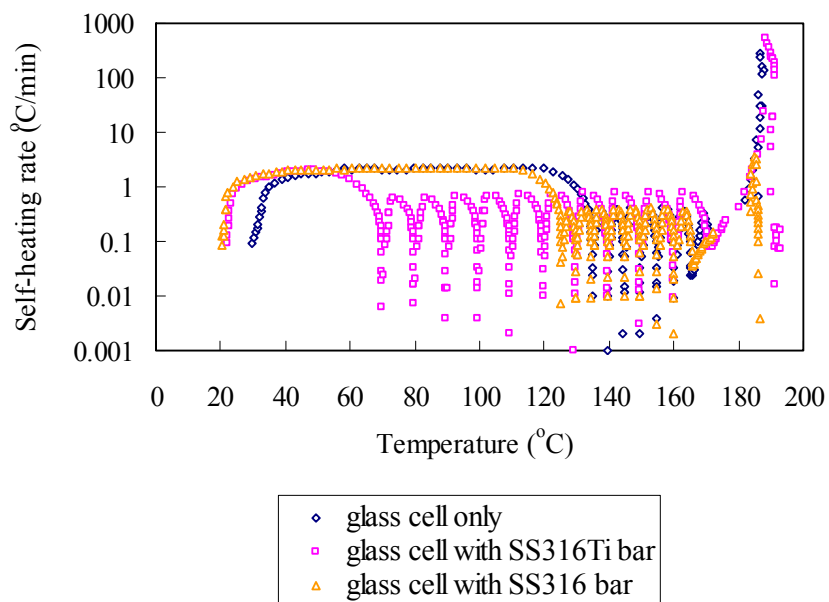


Fig.4.3. Self-heating rate-temperature profiles of HAN (24mass%) decomposition in a glass cell with/without catalyst

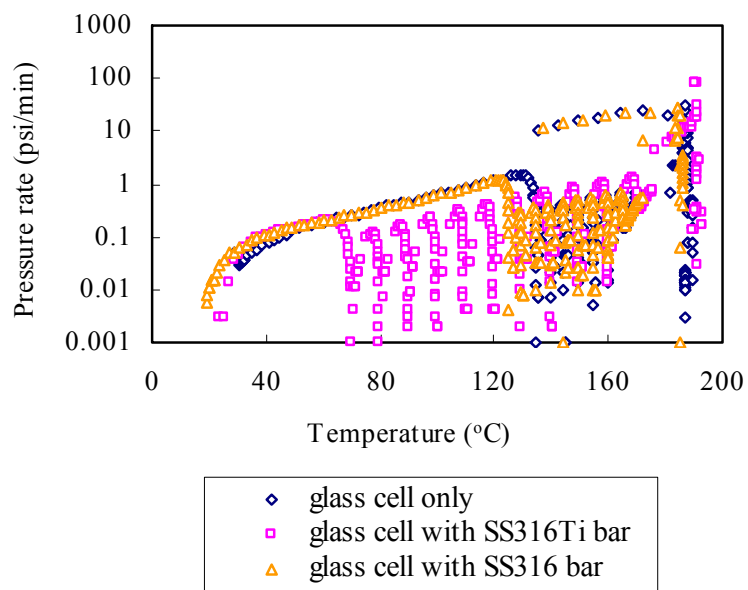


Fig.4.4. Pressure rate-temperature profiles of HAN (24mass%) decomposition in a glass cell with/without catalyst

Table 4.1.  
HWS of HAN decomposition (24mass%) in a glass cell with/without catalyst bar

HAN (24mass%) 3.7g								Phi	
	$T_0$ °C	$T_{max}$ °C	$P_{max}$ psia	$dT/dt_0$ °C/min	$dT/dt_{max}$ °C/min	$dP/dt_{max}$ psi/min	Non-condensable psia (@50°C)	factor $\phi$	$\Delta H_{rxn}$ kJ/mol
Glass cell	169±3	188±1	249±6	0.10±0.07	310±50	27±7	62±4	3.2	-65±11
Glass cell with SS316 Ti*	170±3	188±3	246±14	0.10±0.00	512±75	46±30	58±4	3.2	-62±12
Glass cell with SS316**	164±6	184±3	229±8	0.07±0.02	367±1	28±2	51±7	3.0	-68±10

\* The surface area of the SS316Ti bar is 2.23cm<sup>2</sup>, and the glass cell is 52 g.

\*\* The surface area of the SS 316 bar is 2.54cm<sup>2</sup>, and the glass cell is 49 g.

#### 4.1.3. Discussion

Because the catalyst test pieces were mechanically cut, the surface areas of the catalysts could not be controlled exactly. There was about a 0.3cm<sup>2</sup> difference between the surface areas of the two catalyst bars. We assumed that this difference did not affect the experimental results. Actually, the test data are consistent with this assumption.

The data in Table 4.1 show that the onset temperature decreased by 5°C in the presence of the SS316 bar. But for the cases of the glass cell only and the glass cell with the SS 316Ti bar, the onset temperatures are almost same. These results indicate that under almost equal catalytic surface area, SS316 significantly expedites HAN decomposition, while SS316Ti does not exhibit catalytic behavior. But if the exotherm durations in Figure 4.1 are amplified (shown in Figure 4.5), one can observe that the induction period is a few seconds for the glass cell, about 20 minutes for the glass cell with SS 316Ti, and almost 50 minutes for the glass cell with SS316.

This implies that SS316Ti does catalyze HAN decomposition because the induction period exists but is weaker than SS316 with this amount of surface area. For the case of the glass cell only, it is reasonable to assume that the glass material provides a neutral test environment. In order to confirm the catalytic effect of SS316Ti, the surface area of SS316Ti should be increased in future studies.

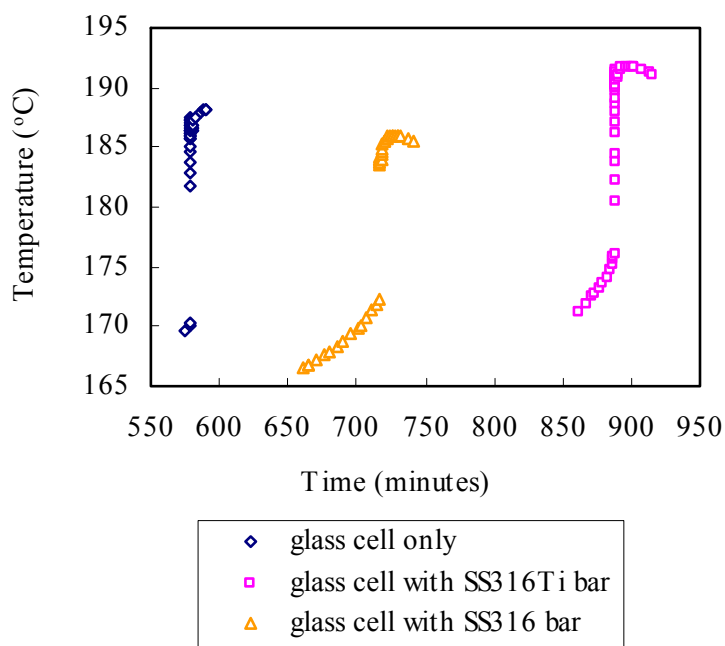


Fig.4.5. Temperature-time behaviors of the exotherm durations in Fig. 4.1

The overall reaction heats (shown in Table 4.1) are close for the three cases. This result suggests that an overall reaction thermal energy does not change in the presence of a catalyst, which is not surprising because a catalyst only changes the

reaction pathway, not the overall reaction.

The thermal decomposition of HAN is an autocatalytic reaction that includes an induction period, explosion period, and decay period. The maximum rates of self-heating and pressure rise for HAN decompositions vary. This variation is partly because the exotherm in the explosion period is so fast that the APTAC at its measurement rate misses some of the critical data points. As shown in Chapter III, the mechanism of this reaction is complicated because many intermediates are generated and can react with each other. Without further analyzing the composition and concentration of all important intermediates, it is very difficult to model the whole decomposition process. However, for the safe storage and handling study, our interest focuses only on the induction period, because the goal of this study is to prevent rapid HAN decomposition from the beginning by addressing HAN storage in tanks or containers before it exceeds its safety threshold.

According to the general principles of the APTAC described in Chapter II, a relationship between  $\ln(k^*)$  and  $1/T$  is given by:

$$\ln(k^*) = \ln(C_o^{n-1}k_0) - \frac{E_a}{R} \left(\frac{1}{T}\right)$$

Given a correct reaction order, the  $\ln(k^*)$  versus  $-1/T$  plot should be a straight line with a slope of  $E_a/R$  and an intercept of  $C_o^{n-1}k_0$ . The overall activation energy  $E_a$  and the frequency factor  $k_0$  in the Arrhenius equation can be calculated based on the slope and intercept of the plot.

To simplify the problem, the first order kinetic model was used to represent the experimental data for the induction period in these three cases. Figures 4.6, 4.7, and 4.8 show kinetic analysis of HAN decompositions in the glass cell with/without catalyst. It can be observed that the first order kinetic model (linear fitting of  $\ln(k^*)$  vs.  $-1000/T$ ) matches the experimental data very well. In these figures, the slope of the fit line corresponds to  $E_a/R$  and the intercept of the fit line corresponds to  $\ln(k_0)$ .  $E_a$  and  $k_0$  are estimated and listed in Table 4.2.

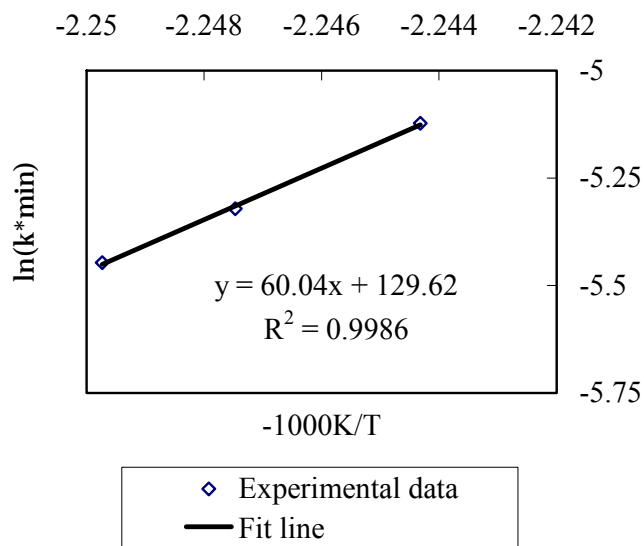


Fig.4.6. Kinetic analysis of HAN (24mass%) decomposition in a glass cell without catalyst

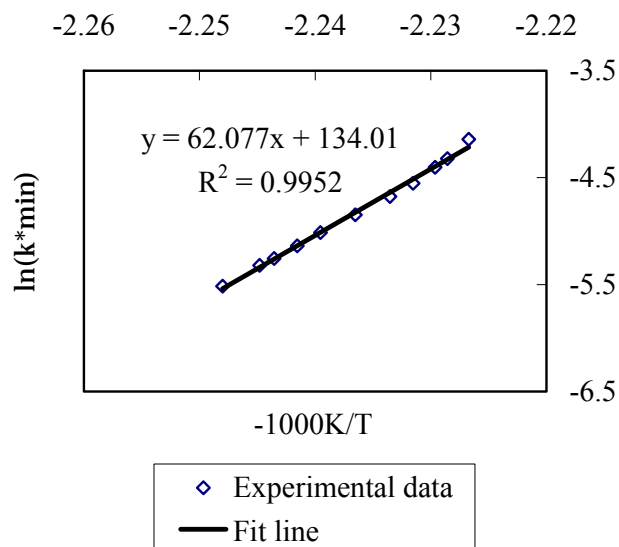


Fig.4.7. Kinetic analysis of HAN (24mass%) decomposition in a glass cell with SS316Ti bar

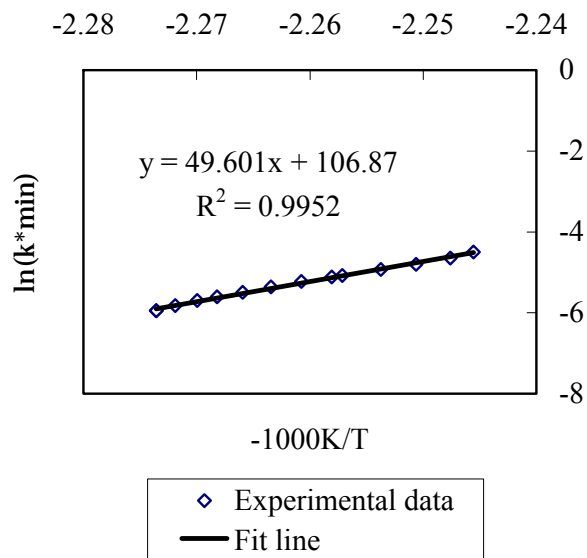


Fig.4.8. Kinetic analysis of HAN (24mass%) decomposition in a glass cell with SS316 bar

Table 4.2.

Summary of kinetic parameters of HAN (24mass%) in a glass cell with/without catalysts

1 <sup>st</sup> order kinetics	Ea (kJ/mol)	k <sub>0</sub> (min <sup>-1</sup> )
Glass cell	499	1.9*10 <sup>56</sup>
Glass cell with SS316Ti bar	516	1.6*10 <sup>58</sup>
Glass cell with SS316 bar	412	2.6*10 <sup>46</sup>

As mentioned above, SS316 shows a significant catalytic impact on the HAN decomposition compared with SS316Ti. This can be explained from the apparent overall activation energies listed in Table 4.2. The glass cell with the SS316 bar has the lowest value for apparent activation energy. Therefore, it is possible that a SS316Ti tank is superior to a SS316 tank for 24mass% HAN storage.

## 4.2. HAN Decomposition in Glass, Titanium, and Stainless Steel Cells

### 4.2.1. Objective

In the previous section, we suggested increasing the surface area of the SS316Ti catalyst for further studies. However, the size of catalyst used in this experiment was limited by the amount of HAN. Only a small amount of HAN can be used in a test since HAN decomposition is rapid. If a larger amount of HAN is used, the APTAC may not be able to follow the reaction adiabatically. Therefore, HAN decomposition in sample cells of SS316Ti and SS316 can be used for increasing the catalyst surface area for a small amount of HAN. A titanium sample cell instead of a SS316Ti cell was employed because the latter was not available from TIAX, LLC or

other sources. A series of tests was conducted in glass, titanium, and stainless steel cells to study the catalytic effect of iron and titanium on HAN decomposition.

The HAN sample (17mass%) was provided by an industrial company. The titanium and stainless steel cells had a volume of ~130mL (standard) and the glass cell had a volume of ~100mL. The APTAC heat-wait-search mode was used for onset temperature search in these tests.

#### 4.2.2. Results

The experimental results of this set of parallel tests are presented in Table 4.3 and Figures 4.9 to 4.12. In Table 4.3, the uncertainties presented are within one standard deviation based on three replicas.

Table 4.3.  
HWS of the industrial HAN (17mass%) decomposition in different cells

HAN (17mass%)	$T_0$	$T_{max}$	$P_{max}$	$dT/dt_0$	$dT/dt_{max}$	$dP/dt_{max}$	Non-condensable factor	$\Delta H_{rxn}$	
4.8g	$^{\circ}C$	$^{\circ}C$	psia	$^{\circ}C/min$	$^{\circ}C/min$	psi/min	psia (@50 $^{\circ}C$ )	$\phi$	kJ/mol
Glass cell	169 $\pm$ 2	191 $\pm$ 4	255 $\pm$ 24	0.06 $\pm$ 0.04	8 $\pm$ 4	94 $\pm$ 89	62 $\pm$ 3	3.1	-88 $\pm$ 13
Ti cell	158 $\pm$ 3	176 $\pm$ 1	182 $\pm$ 5	0.06 $\pm$ 0.01	246 $\pm$ 40	12 $\pm$ 3	42 $\pm$ 1	1.9	-51 $\pm$ 6
SS cell	148 $\pm$ 3	167 $\pm$ 4	158 $\pm$ 11	0.06 $\pm$ 0.04	4 $\pm$ 0	20 $\pm$ 5	45 $\pm$ 1	2.4	-67 $\pm$ 9

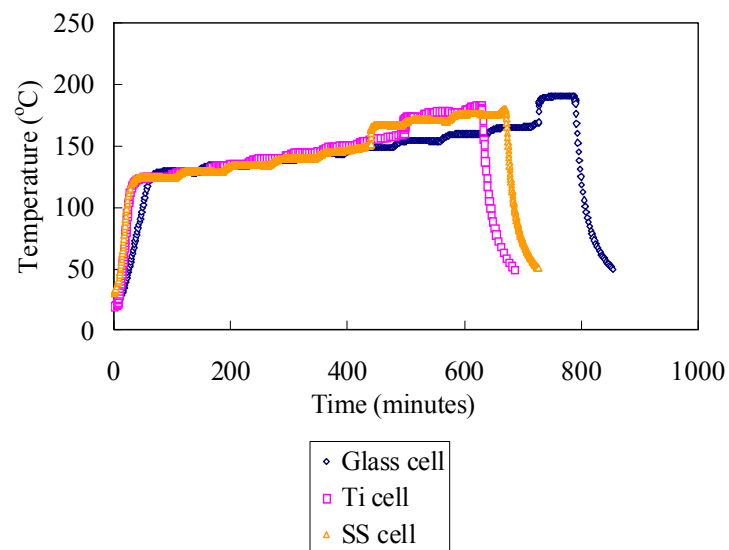


Fig.4.9. Temperature-time profiles of the industrial HAN sample (17mass%) decomposition in different cells

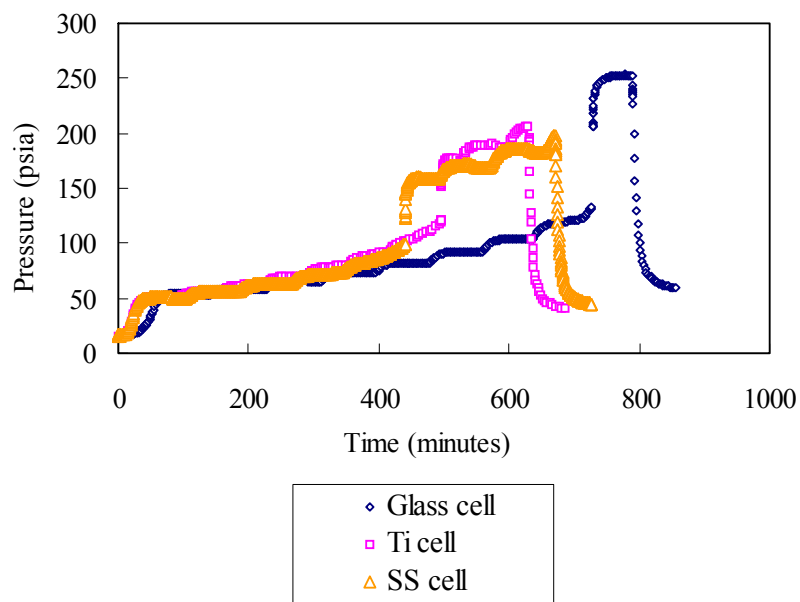


Fig.4.10. Pressure-time profiles of the industrial HAN sample (17mass%) decomposition in different cells

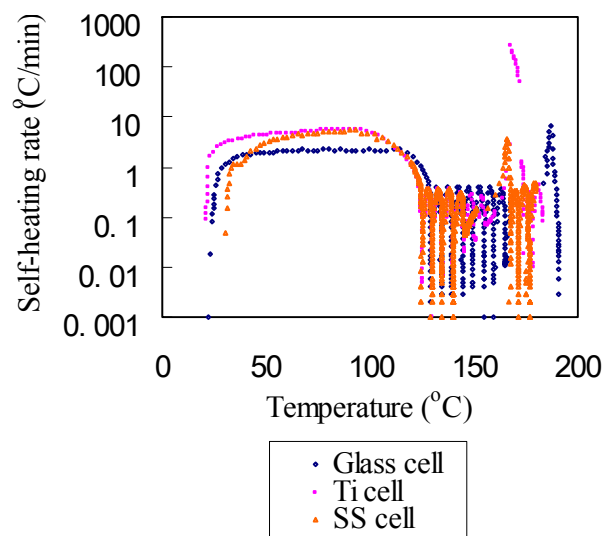


Fig.4.11. Self-heating rate-temperature profiles of the industrial HAN sample (17mass%) decomposition in different cells

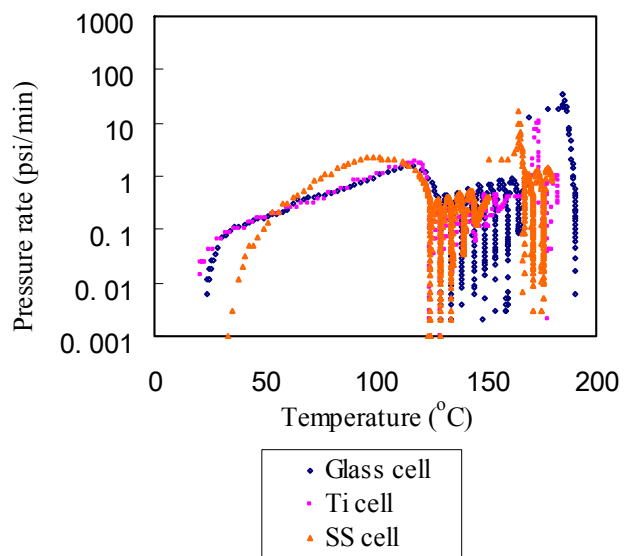


Fig.4.12. Pressure rate- temperature profiles of the industrial HAN sample (17mass%) decomposition in different cells

### 4.2.3. Discussion

In the temperature-time plot shown in Figure 4.9, the onset of self-heating of HAN in the glass cell starts at about 170°C and continues to a maximum temperature of 191°C. However, for the titanium or stainless steel cell, an obvious reduction in onset temperature and maximum temperature for adiabatic rise is observed. Similar trends are also displayed in the pressure-time behavior (shown in Figure 4.10).

The exotherm durations in Figure 4.9 are extracted and amplified in Figure 4.13. The induction periods are approximately 40 minutes for the titanium cell and 50 minutes for the stainless steel cell, and almost zero for glass cell. Therefore, the glass cell offers a more neutral surrounding, while titanium and stainless steel catalyze HAN decomposition. Moreover, these results suggested that stainless steel has a stronger catalytic effect than titanium. From safety point of view, titanium or stainless steel containing titanium should provide a more stable environment than stainless steel for a HAN container material.

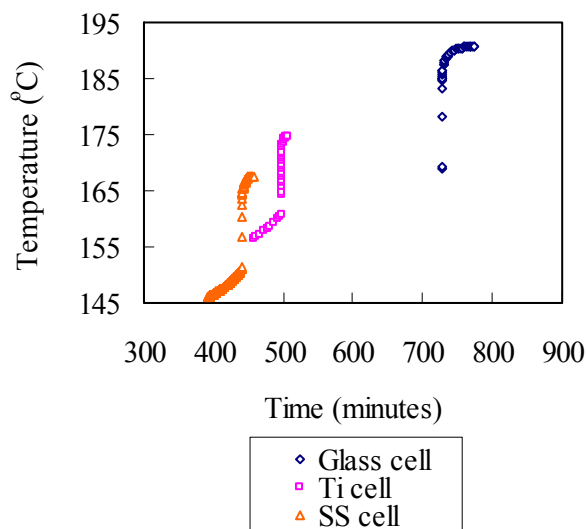


Fig.4.13. Temperature-time behaviors of the exotherm durations in Fig. 4.9

Again, the first-order kinetic model was applied to fit the experimental data for the induction period in all three cases. Figures 4.14 to 4.16 show kinetic analysis of HAN decomposition in glass, titanium, and stainless steel cells. In the cases of glass and titanium cells, the linear fit (first order kinetic model) matches experimental data well. But for the case of stainless steel cell, the experimental data display nonlinear behavior (Figure 4.16), which may be caused by a heterogeneous catalytic reaction of HAN decomposition. See section 4.3.2. for more details.

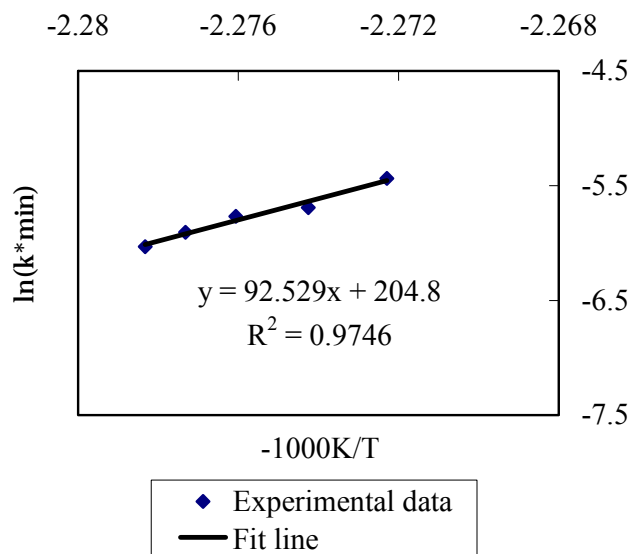


Fig.4.14. Kinetic analysis of the industrial HAN sample (17mass%) decomposition in a glass cell

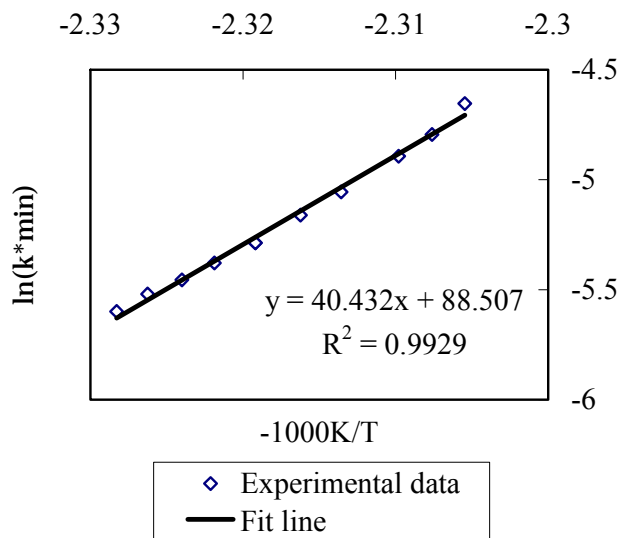


Fig.4.15. Kinetic analysis of the industrial HAN sample (17mass%) decomposition in a titanium cell

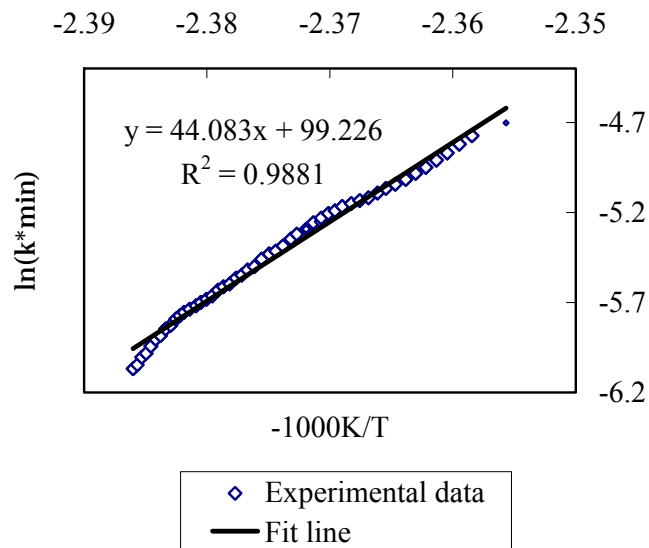


Fig.4.16. Kinetic analysis of the industrial HAN sample (17mass%) decomposition in a stainless steel cell

The apparent activation energies ( $E_a$ ) and frequency factors ( $k_0$ ) for these three cases can be estimated using the slopes and intercepts of the fit equations. Table 4.4 lists the values of  $E_a$  and  $k_0$ . The stainless steel cell has greater value of  $E_a$  than the titanium cell. This result seems not consistent with the previous conclusion that stainless steel has a stronger catalytic effect than titanium. The stainless steel cell, however, exhibits a typical heterogeneous catalysis on the HAN decomposition (see section 4.3.2 for more details). However, n-th order kinetics was applied to analyze the experimental data using perhaps an inaccurate assumption of homogeneous reaction.

Table 4.4.

Summary of kinetic parameters of the industrial HAN sample (17mass%) in different cells

1 <sup>st</sup> order kinetics	Ea (kJ/mol)	k <sub>0</sub> (min <sup>-1</sup> )
Glass cell	769	8.8*10 <sup>88</sup>
Titanium cell	336	2.8*10 <sup>38</sup>
Stainless steel cell	366	1.2*10 <sup>43</sup>

In Figure 4.17, the relationship between the reaction heat ( $\Delta H_{\text{rxn}}$ ) and the thermal inertial ( $\phi$ ) is linear. This means the total heat generated in the reaction for the same amount of HAN is the same in the glass, titanium, and stainless steel cells. As stated above, the catalytic effect of a container material only changes the reaction pathway, not the overall reaction.

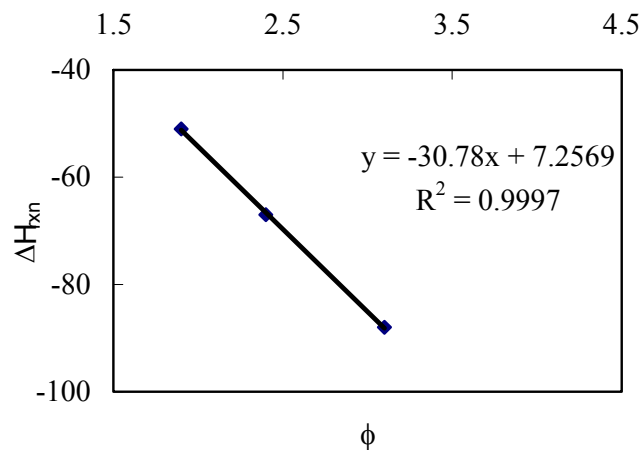


Fig.4.17. Linear relationship between  $\phi$  and  $\Delta H_{\text{rxn}}$

### **4.3. Searching for Safe Boundary Conditions During HAN Storage and Handling**

In this study, the final objective is to predict safe boundary conditions for HAN storage and handling. Usually, environmental temperature, HAN temperature, tank pressure, and storage time can be observed or recorded easily for warehouse storage and process handling. Therefore, predicting a safe boundary aims at defining the safe threshold pressure and maximum safe storage time for an average storage temperature.

There are two possible ways to predict the safe boundary of HAN storage. One is an experimental approach. This requires the soak temperature to be as close as possible to the ambient temperature of warehouse (since this temperature varies with weather, season, and location, a conservative value such as 50°C can be adopted). Given a certain soak time, the onset of exotherm behavior can be detected using an appropriate instrument. However, the lower the soak temperature, the more soak time that is needed to detect the exotherm. The other approach is simulation, i.e., a combination of experimental work and kinetic simulation. If it is possible to develop a validated kinetic-based model, a simulation under real storage conditions can be generated and the associated safety boundary can be predicted.

### **4.3.1. Isothermal Aging Testing of the Industrial HAN Sample in a Stainless Steel Cell**

#### **4.3.1.1. Objective**

Although titanium or stainless steel containing titanium may be better than stainless steel for a HAN container material, the research to find a safe boundary for HAN storage in a stainless steel container is still attractive for HAN manufacturers and customers, because titanium costs more than stainless steel.

Isothermal aging testing can be used to study the effect of inhibitors or additives on exothermal behavior of a sample material. In this research, isothermal aging testing was applied to test the effect of the aging factor on the autocatalytic decomposition of HAN. Specifically, the trend of HAN autocatalytic decomposition at different soak temperatures with varying soak times was determined during a series of isothermal aging tests. This is a straightforward experimental approach, because the safe storage time or pressure for a specific soak temperature (or warehouse temperature) can be estimated by extrapolating from experimental data.

#### **4.3.1.2. Results**

The isothermal aging tests were performed using the industrial HAN sample (17mass%) in a stainless steel cell (thin wall) with the APTAC iso-aging mode. Because it is not practical to run experiments at lower temperature (such as 50°C)

due to extremely long testing times, parallel isothermal aging tests at higher temperatures (120°C, 110°C, and 90°C) were performed with the soak times varied from several hundred to a few thousand minutes. The important experimental parameters are summarized in Table 4.5. As mentioned in Chapter II, if no exotherm was detected in the soak stage, the system would convert to a standard heat-wait-search, and an exotherm could be detected in this mode. Table 4.5 shows that the exotherm was detected in the heat-wait-search mode for most cases. Only for the run marked with a star was the exotherm detected during the soak stage. The onset temperatures and pressures at various combinations of soak times and soak temperatures are also shown in Figures 4.18 and 4.19. The behaviors of temperature-time, pressure-time, self-heating rate-temperature, and pressure rate-temperature for each test are included in the Appendix A.

Table 4.5.

Iso-aging results of the industrial HAN decomposition in a stainless steel cell

HAN (17mass%) 4.8g	Soak time min	T <sub>0</sub> °C	P <sub>0</sub> psia	T <sub>max</sub> °C	P <sub>max</sub> psia	dT/dt <sub>0</sub> °C/min	dT/dt <sub>max</sub> °C/min	dP/dt <sub>max</sub> psi/min	Non-condensable psia (@50°C)
Without soak	0	146	85	168	159	0.05	3.6	17	45
T <sub>soak</sub> =120°C	900	145	92	154	125	0.05	4.3	127	43
	1,150	132	73	141	100	0.19	22	39	40
	1,218*	124	63	143	108	0.05	42	35	45
T <sub>soak</sub> =110°C	1,000	131	74	166	168	0.05	26	184	54
	1,200	121	63	143	108	0.05	26	34	45
T <sub>soak</sub> =90°C	900	141	86	170	179	0.05	19	1,018	53
	1,500	137	78	159	142	0.05	15	201	47
	2,000	141	86	158	135	0.08	5	235	43
	2,500	136	79	153	123	0.05	6	153	44

\* The exotherm was detected during the soak stage. Each listed value is the average value within three experimental replicas.

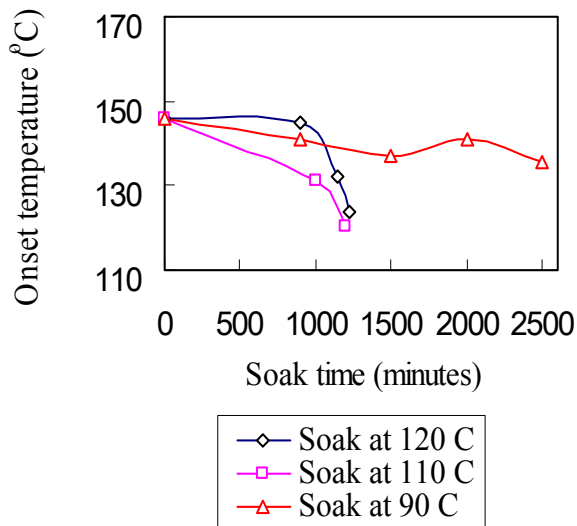


Fig.4.18. Onset temperature vs. soak time at various soak temperatures

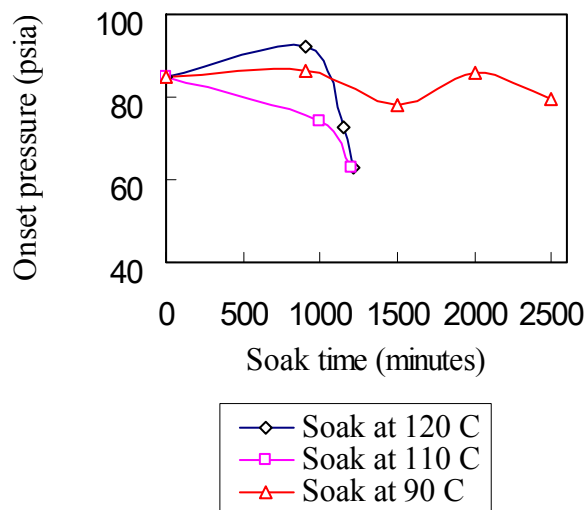


Fig.4.19. Onset pressure vs. soak time at various soak temperatures

#### 4.3.1.3. Discussion

As expected, the overall trend is that the measured onset temperature decreases with increasing soak time for any fixed soak temperature. But for the case of soak at 90°C, it is difficult to observe a big difference in onset temperature for soaking times within a few thousand minutes. When the industrial HAN sample was soaked at 120°C, the lowest onset temperatures (124°C) was close to the environment temperature (i.e. soak temperature) after a certain soak time. Since catalytic effect of iron always exists for HAN stored in stainless steel tanks, this conclusion should also be applied for lower temperatures such as ambient temperatures for warehouse storage. Hence, there is a maximum safe storage time after which the onset of decomposition will occur at environmental temperatures.

In the case of soak at 120°C, the maximum storage time was measured directly. For soaking at 90°C and 110°C, the maximum storage times can be predicted by extrapolating the experimental data, which is shown in Figures 4.20 and 4.21. The predicted maximum storage times are about 16,000 minutes (~267hrs, ~11days) for 90°C and 1,350 minutes (~23hrs, ~1day) for 110°C.

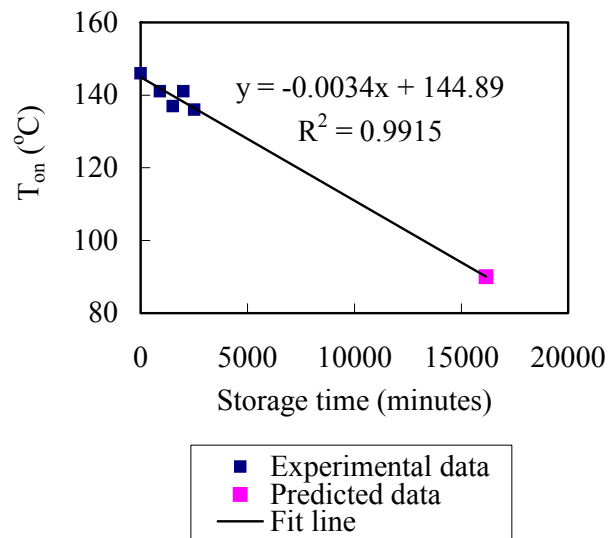


Fig.4.20. Maximum storage time prediction for soak temperature of 90°C

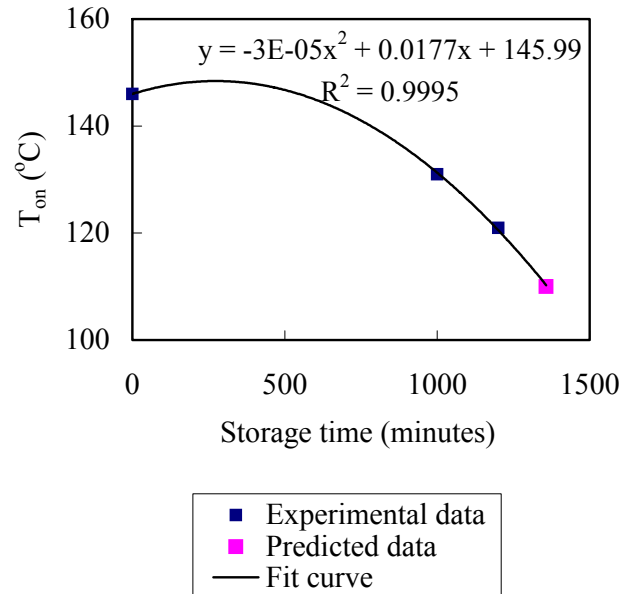


Fig.4.21. Maximum storage time prediction for soak temperature of 110°C

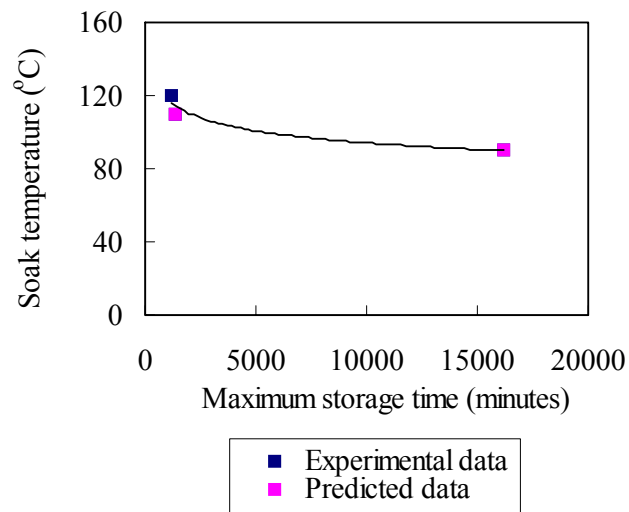


Fig.4.22. The maximum storage time trend based on isothermal aging testing

With the above prediction, the trend of maximum storage time versus soak temperature is displayed in Figure 4.22. Because there are only three points in this

figure, many curves could be employed in a fit. However, provided sufficient experimental data are collected over a sufficient range of decreasing temperature, the maximum storage time at ambient temperature in a warehouse can, in principle, be predicted.

Similar approaches can be employed to predict the onset pressure at maximum storage time for each case. However, because the variation of pressure in measurement is much larger than that of temperature for this reactive system, it is more reliable to search for the threshold pressure for HAN safe storage by kinetic simulation.

#### **4.3.2. HAN Decomposition in a Stainless Steel Cell with Various Thermal Inertias**

##### **4.3.2.1. Objective**

In order to predict the safe threshold pressure during warehouse storage and process handling of HAN, it is necessary to develop a kinetic-based model for its autocatalytic decomposition. For this purpose, a set of tests for the thermal decomposition of different masses of HAN was measured in a stainless steel cell.

##### **4.3.2.2. Results**

Different amounts of the industrial HAN sample (17mass%) in the same stainless steel cell were examined using the heat-wait-search mode of the APTAC.

The experimental data are reported in Table 4.6. The behaviors of temperature vs. time and pressure-time, self-heating rate-temperature, and pressure rate-temperature are displayed in Figures 4.23 to 4.26. The exotherm parts in Figure 4.23 are extracted and magnified in Figure 4.27.

Table 4.6.

HWS results of thermal decomposition for different masses of the industrial HAN sample in a stainless steel cell

HAN (17mass%) in SS cell	$T_0$ °C	$P_0$ psi	$T_{max}$ °C	$P_{max}$ psia	$dT/dt_0$ °C/min	$dT/dt_{max}$ °C/min	$dp/dt_{max}$ psi/min	Non-condensable Psi (@50°C)	Phi factor	$\Delta H_{rxn}$ kJ/mol
4.8g (test 1)	146	85	168	159	0.05	3.6	17	45	2.4	76
4.3g (test 2)	146	83	167	155	0.05	5.2	76	43	2.6	77
3.9g (test 3)	146	86	163	140	0.05	3.7	15	38	2.8	73

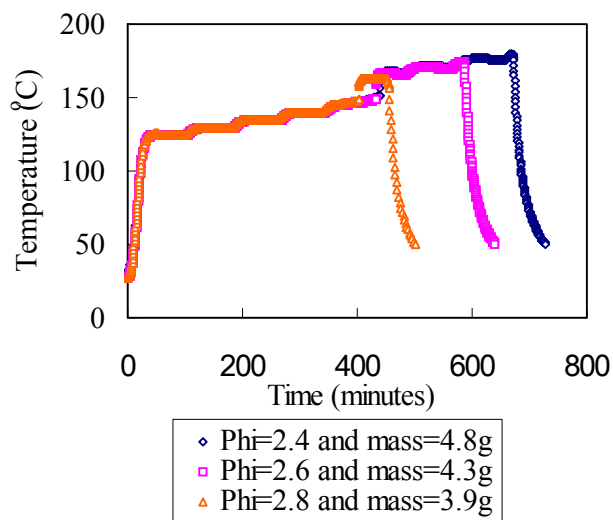


Fig.4.23. Temperature-time profiles of the industrial HAN sample (17mass%) decomposition in a stainless steel cell

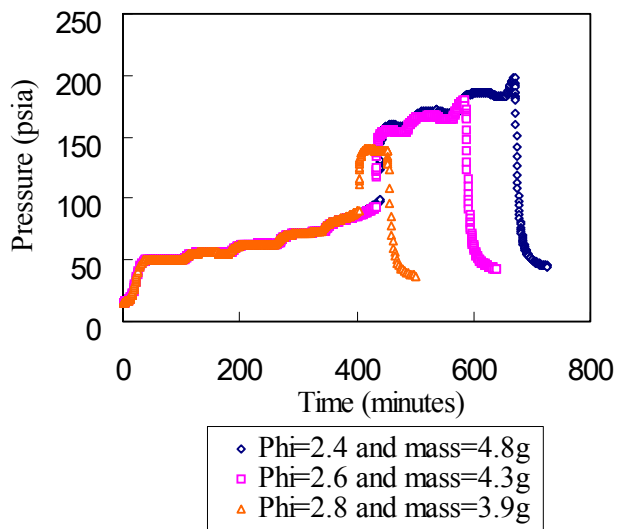


Fig.4.24. Pressure-time profiles of the industrial HAN sample (17mass%) decomposition in a stainless steel cell

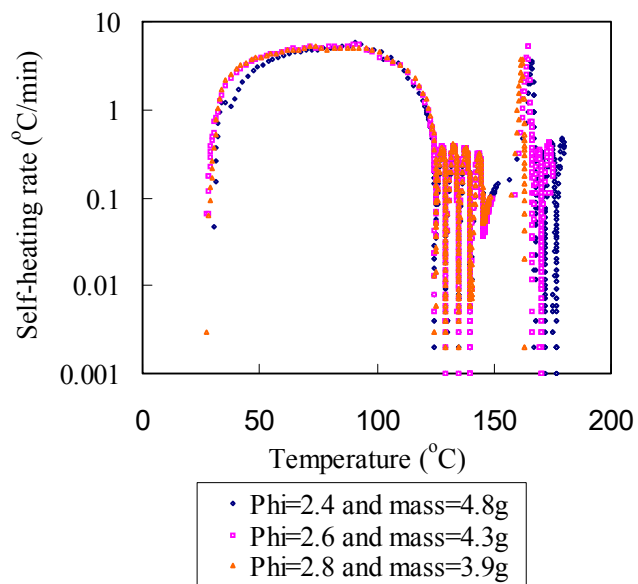


Fig.4.25. Self-heating rate-temperature profiles of the industrial HAN sample (17mass%) decomposition in a stainless steel cell

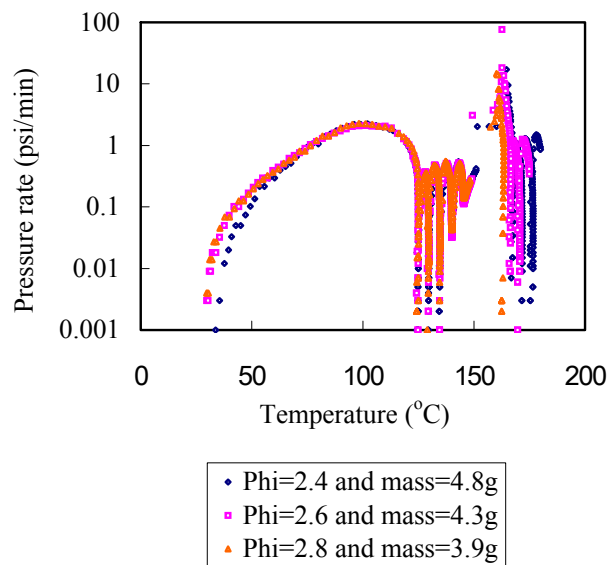


Fig.4.26. Pressure rate-temperature profiles of the industrial HAN sample (17mass%) decomposition in a stainless steel cell

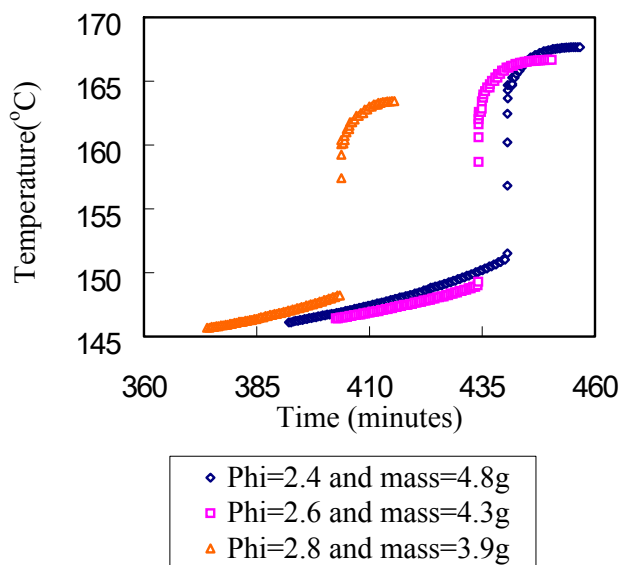


Fig.4.27. Temperature-time behaviors of the exotherm durations in Fig. 4.23

#### 4.3.2.3. Discussion

An important observation from Figure 4.27 is that the induction period is extended with an increase in sample mass. The shortest induction period corresponds to the smallest sample amount. This is opposite of the normal homogeneously catalytic reaction in which the largest amount of sample has the shortest induction period. Therefore, the HAN decomposition catalyzed by the inner surface of the cell material is a typical heterogeneous reaction. Moreover, the higher ratio of contact surface to sample mass contributes to a stronger catalytic effect due to a heterogeneous interaction.

The kinetic simulation for heterogeneous reaction should be built on the reaction mechanism. However, the mechanism of HAN heterogeneous catalytic decomposition is not available in the literature. To simulate the kinetics of HAN decomposition in a stainless steel cell, a pseudo-homogeneous reaction was assumed in this work. Adiabatic Data Processing software (ADPro) and Formal Kinetics Evaluation software (ForK) in the Thermal Safety Software package (developed by ChemInform St. Petersburg Ltd.) were used for kinetic simulation of these three tests. The full autocatalysis model was successfully applied to simulate the kinetics of HAN decomposition in the stainless steel cell. The kinetic scheme is described below:



A→C Proto (autocatalytic stage) Equation:  $d\alpha/dt = k_0 e^{-E_a/RT} \alpha^{n1} (1 - \alpha)^{n2}$

where  $\alpha$  is the degree of conversion of HAN ( $\alpha$  is defined as  $(C_{A0}-C_A)/C_{A0}$ ;  $0 \leq \alpha \leq 1$ ),  $k_0$  is the frequency factor in the Arrhenius equation,  $n$ ,  $n1$ , and  $n2$  are reaction orders, and  $E_a$  is the activation energy. The kinetic parameters for the initiation stage and autocatalytic stage are reported in Table 4.7 and Table 4.8. The simulation results are presented in Figure 4.28 to 4.30.

Table 4.7.

Parameters of initiation stage (A→B) during HAN decomposition

Parameters	Units	Value
$\ln(k_0)$	$\ln(1/\text{sec})$	33.48
$E_a$	$\text{kJ/mol}$	151.42
$n$	-	2.0
$Q^*$	$\text{kJ/kg}$	181.27

\*Heat effects were calculated per unit of mass of the solution

Table 4.8.

Parameters of autocatalytic stage (A→C) during HAN decomposition

Parameter	Units	Test 1	Test 2	Test 3
$\ln(k_0)$	$\ln(1/\text{sec})$	31.59	32.61	33.87
$E_a$	$\text{kJ/mol}$	120.6	120.6	120.6
$n1$	-	4.0	4.0	4.0
$n2$	-	1.0	1.0	1.0
$Q^*$	$\text{kJ/kg}$	181.27	181.27	181.27
$k_0$	$1/\text{sec}$	$5.22 \cdot 10^{13}$	$1.46 \cdot 10^{14}$	$5.126 \cdot 10^{14}$

\*Heat effects were calculated per unit of mass of the solution

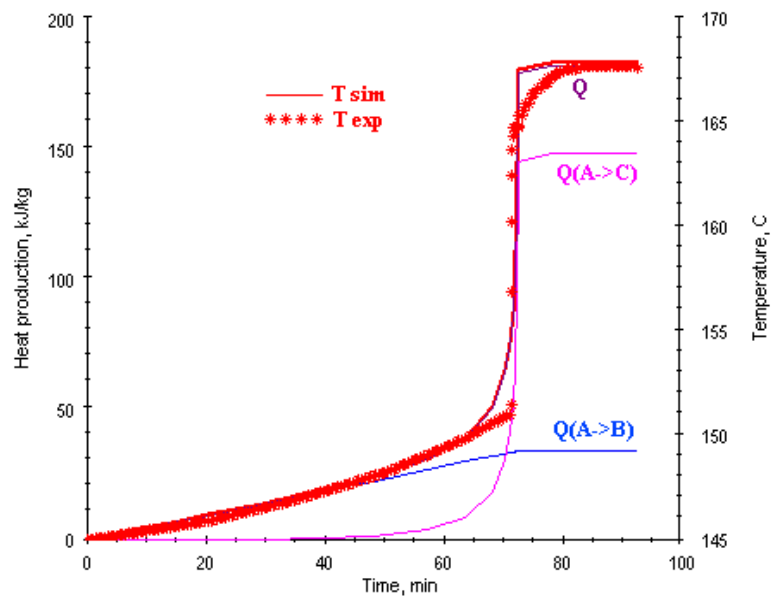


Fig.4.28. Simulation of test 1

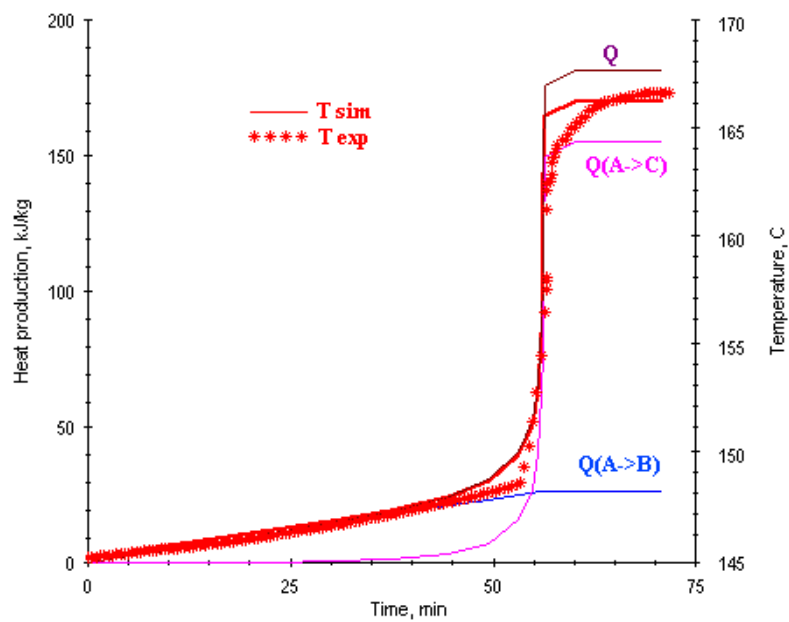


Fig.4.29. Simulation of test 2

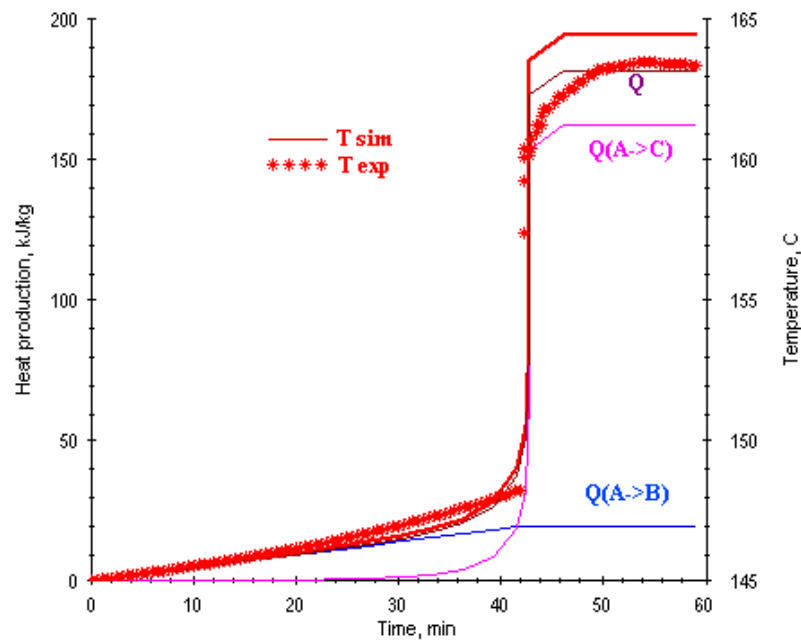


Fig.4.30. Simulation of test 3

As a result, the initiation stage of HAN decomposition was simulated by second order kinetics, and the autocatalytic stage was simulated by the proto model (the kinetic function is  $\alpha^{n1} (1 - \alpha)^{n2}$ ). The simulation curves shown in Figures 4.28 to 4.30 match the experimental data. Currently, this kinetic model cannot be used directly for safe threshold pressure predictions. The model must be validated or modified using additional experimental data. After a validated kinetic-based model is developed, the simulation under real storage condition will be generated by the TSS, and the safe threshold pressures before runaway can be estimated.

## **CHAPTER V**

### **CONCLUSIONS AND FUTURE WORK**

#### **5.1. Conclusions**

In this work, hydroxylamine nitrate (HAN) aqueous solution decomposition in the presence of titanium, stainless steel with titanium, or stainless steel was investigated with the Automatic Pressure Tracking Adiabatic Calorimeter (APTAC). Titanium, stainless steel with titanium, and stainless steel exhibit catalytic effects on the decomposition of HAN but their existence does not change the overall reaction enthalpy of decomposition. Compared with stainless steel, titanium and stainless steel with titanium are better choices for container materials during storage of HAN aqueous solution.

An isothermal aging approach was proposed to predict the maximum storage time of HAN. Sufficient experimental data could be used to predict the maximum safe storage time of HAN at ambient temperature in these container materials.

A kinetics-based simulation was suggested to predict safe threshold pressures for warehouse storage and process handling. First order kinetics was used to represent the induction period data of HAN decomposition for initial estimation. In the case of HAN decomposition in a stainless steel cell, a full autocatalysis model was proposed to simulate the kinetics. Adiabatic Data Processing software (ADPro) and Formal Kinetics Evaluation software (ForK) in the Thermal Safety Software

package were employed to perform this simulation.

## 5.2. Future Work

This work aims to find safe boundary condition for warehouse storage and process handling of HAN aqueous solution. Additional work is needed to achieve the final objective of this research, i.e., predictions of the maximum safe storage time and the safe threshold pressure at ambient temperature.

First of all, a great deal of calorimetric data from the APTAC is required from isothermal aging testing for reliable predictions of maximum HAN storage time. If possible, calorimeters with higher thermal sensitivity should be used to conduct experiments to increase the accuracy of testing. Secondly, the full autocatalysis mode proposed to simulate HAN decomposition in a stainless steel cell must be validated or modified by further experiments. In addition, the ratio of cell contact surface to HAN mass is an important factor for this heterogeneous catalytic reaction. For industrial storage, this ratio is much smaller than the ratio in experimental tests. For example, if 2,000 pounds of HAN (24mass%) with a density of  $1.118\text{g/cm}^3$  is stored in a stainless steel tank with a 2.6ft inside diameter and a 5.3 ft height, the ratio of contact surface to mass is about  $0.05\text{ cm}^2/\text{g}$ . But in the laboratory experiments, if 4.8g HAN used in a 130mL stainless steel cell, this ratio is about  $2.4\text{cm}^2/\text{g}$ . This is almost 50 times greater than the ratio from the tank example. This difference must be considered in scaling up predictions.

## REFERENCES

- Barreda, D. G. G., Vazquez, J., Lopez-Aleman, P. L., Villares, P., & Jimenez-Garay, R. (2005). A comparative study on the glass-forming ability of some alloys in the Sb-As-Se system by differential scanning calorimetry. *Journal of Physics and Chemistry of Solids*, 66 (10), 1783-1787.
- Bhadeshia, H. K. D. H. (2002). Differential scanning calorimetry. <http://www.msm.cam.ac.uk/phasetrans/2002/Thermal2.pdf>
- Botros, S. H., Moustafa, A. F., & Ibrahim, S. A. (2006). Improvement of the homogeneity of SBR/NBR blends using polyglycidylmethacrylate-g-butadiene rubber. *Journal of Applied Polymer Science*, 99 (4), 1559-1567.
- Bou-Diab, L., & Fierz, H. (2002). Autocatalytic decomposition reactions, hazards and detection. *Journal of Hazardous Materials*, 93 (1), 137-146.
- Burelbach, J. P. (2000). Advanced reactive screening system tool (ARSST). *28th Annual Conference, North American Thermal Analysis Society*. <http://www.fauske.com/Download/Chemical/Papers/C29.pdf>
- Center for Chemical Process Safety (CCPS) (1995). *Guidelines for chemical reactivity evaluation and application to process design*. New York: AIChE, CCPS.
- Dien, J-M., Fierz, H., Stoessel, F., & Kille, G. (1994). The thermal risk of autocatalytic decompositions: a kinetic study. *Chimia*, 48 (12), 542-550.
- Dijk, C. A. V., & Priest, R. G. (1984). Thermal decomposition of hydroxylammonium nitrate at kilobar pressure. *Combustion and Flame*, 57 (1), 15-24.
- Donoghue, E. (1997). Identifying hazardous chemical reactivity - a brief introduction. *Journal of Thermal Analysis*, 49 (3), 1609-1616.

- Duh, Y.S., Hsu, C.C., Kao, C.S., & Yu, S.W. (1996). Applications of reaction calorimetry in reaction kinetics and thermal hazard evaluation. *Thermochimica Acta*, 285 (1), 67-79.
- Fauske, H. K. (1993). U.S. Patent 5,229,074
- Fauske, H. K. (2000). Properly size vents for nonreactive and reactive chemicals. *Chemical Engineering Progress*, 96 (2), 17-29.
- Gigante, L., Lunghi, A., Martinelli, S., Cardillo, P., Picello, L., Bortolaso, R., Galvagni, M., & Rota, R. (2003). Calorimetric approach and simulation for scale-up of a Friedel-Crafts reaction. *Organic Process Research & Development*, 7 (6), 1079-1082.
- Gowland, R. J., & Stedman, G. (1981). Kinetic and product studies on the decomposition of hydroxylamine in nitric-acid. *Journal of Inorganic & Nuclear Chemistry*, 43 (11), 2859-2862.
- Grolmes, M. A., & King, M. J. (1995). Simulation of vented pressure-vessel tests for organic peroxides. *Journal of Hazardous Materials*, 44 (2-3), 253-266.
- Gustin, J. L. (1993). Thermal-stability screening and reaction calorimetry-application to runaway reaction hazard assessment and process safety management. *Journal of Loss Prevention in the Process Industries*, 6 (5), 275-291.
- Gustin, J. L., Fillon, J., Treand, G., & Elbiyaali, K. (1993). The phenol + formaldehyde runaway reaction – runaway reaction-vent sizing for reactor protection. *Journal of Loss Prevention in the Process Industries*, 6 (2), 103-113.
- Kersten, R. J. A., Boers, M. N., Stork, M. M., & Visser, C. (2005). Results of a Round-Robin with di-tertiary-butyl peroxide in various adiabatic equipment for assessment of runaway reaction hazards. *Journal of Loss Prevention in the Process Industries*, 18 (3), 145-151.
- Lechuga-Ballesteros, D., Bakri, A., & Miller, D. P. (2003). Microcalorimetric measurement of the interactions between water vapor and amorphous pharmaceutical solids. *Pharmaceutical Research*, 20 (2), 308-318.

- Liaw, H. J., Chen, C. J., & Yur, C. C. (2001). The multiple runaway-reaction behavior prediction of MEK-oxidation reactions. *Journal of Loss Prevention in the Process Industries*, 14 (5), 371-378.
- Lu, K. T., Luo, K. M., Lin, S. H., Su, S. H., & Hu, K. H. (2004). The acid-catalyzed phenol-formaldehyde reaction - Critical runaway conditions and stability criterion. *Process Safety and Environmental Protection*, 82 (B1), 37-47.
- Maschio, G., Feliu, J.A., Ligthart, J., Ferrara, I., & Bassani, C. (1999). The use of adiabatic calorimetry for the process analysis and safety evaluation in free radical polymerization. *Journal of Thermal Analysis and Calorimetry*, 58 (1), 201-214.
- Nomen, R., Sempere, J., Serra, E., & Pena, M. A. (1995). Safety subjects 5. Simple experiments to determine the thermal potential of a process: Adiabatic Dewar calorimetry. *Afinidad*, 52 (459), 291-295.
- Oxley, J. C., & Brower, K. R. (1988). Thermal decomposition of hydroxylamine nitrate. *Proceedings of SPIE-The International Society for Optical Engineering*, 872, 63-70.
- Rafeev, V. A., & Rubtsov, Y. I. (1993). Kinetics and mechanism of thermal decomposition of hydroxylammonium nitrate, *Russian Chemical Bulletin*, 42, 1811-1815.
- Rota, R., Ruggeri, G., Morbidelli, M., & Ditali, S. (2002). Influence of calorimetric approximations on the design of emergency relief systems. *Journal of Loss Prevention in the Process Industries*, 15 (1), 49-61.
- Schoppelrei, J. W., & Brill, T. B. (1997). Spectroscopy of hydrothermal reactions. 7. Kinetics of aqueous  $[\text{NH}_3\text{OH}]\text{NO}_3$  at 463-523 K and 27.5 MPa by infrared spectroscopy. *Journal of Physical Chemistry A*, 101 (46), 8593-8596.
- Sempere, J., Nomen, R., Serra, R., & Cardillo, P. (1997). Thermal hazard assessment using closed-cell adiabatic calorimetry. *Journal of Loss Prevention in the Process Industries*, 10 (1), 55-62.
- Suurkuusk, J. & Wadsö, I. (1982). A multichannel micro-calorimetry system.

*Chemica Scripta*, 20 (4), 155-163

- Townsend, D. I., & Tou, J. C. (1980). Thermal hazard evaluation by an acceleration rate calorimeter. *Thermochimica Acta*, 37 (1), 1-30.
- Townsend, D. I., Ferguson, H. D., Erguson, H. D., & Kohlbrand, H. T. (1995). Application of ARC(TM) thermokinetic data to the design of safety schemes for industrial reactors. *Process Safety Progress*, 14 (1), 71-76.
- Tseng, J. M., Shu, C. M., & Yu, Y. C. (2005). Thermal hazard simulations for methyl ethyl ketone peroxide induced by contaminants. *Korean Journal of Chemical Engineering*, 22 (6), 797-802.
- U.S. Chemical Safety and Hazard Investigation Board (2003). Hazard investigation: improving reactive hazard management. [http://www.csb.gov/completed\\_investigations/docs/ReactiveIncidentDataReport.pdf](http://www.csb.gov/completed_investigations/docs/ReactiveIncidentDataReport.pdf)
- U.S. Department of Energy (1998). Technical report on hydroxylamine nitrate. [http://www.eh.doe.gov/chem\\_safety//Docs/hydroxlyamine.pdf](http://www.eh.doe.gov/chem_safety//Docs/hydroxlyamine.pdf)
- Wei, C., W. J. Rogers, & M. S. Mannan. (2004). Detection of autocatalytic decomposition behavior of energetic materials using APTAC. *Proceedings of the 32nd North American Thermal Analysis Society Conference*. Williamsburg, Virginia.
- Wei, C. (2005). *Thermal runaway reaction hazard and decomposition mechanism of the hydroxylamine system*. PhD Dissertation, Texas A&M University, College Station, Texas.
- Yue, M. H., Sharkey, J. J., & Leung, J. C. (1994). Relief vent sizing for a Grignard reaction. *Journal of Loss Prevention in the Process Industries*, 7 (5), 413-418.
- Zimehl, R., Drews, J., & Fischer-Brandies, H. (2002). Thermometric monitoring of setting biomaterials. *Thermochimica Acta*, 382 (1-2), 161-168.

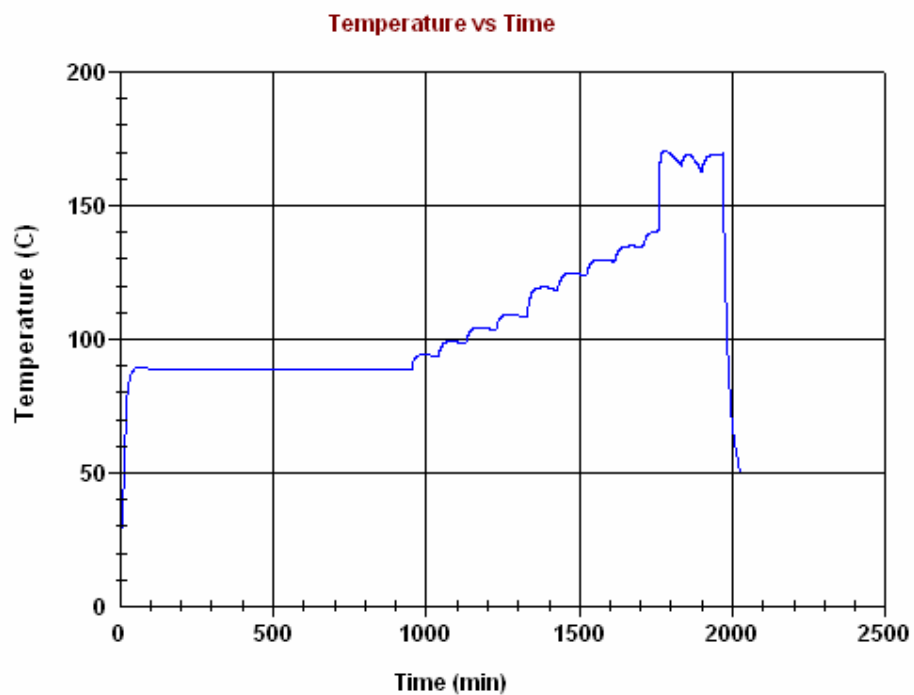
**APPENDIX A****FIGURES OF ISOTHERMAL AGING TESTS OF  
INDUSTRIAL HAN SAMPLE IN A STAINLESS  
STEEL CELL WITH THE APTAC**

Fig.A.1. Temperature as a function of time for soak temperature of 90°C and soak time of 900 minutes

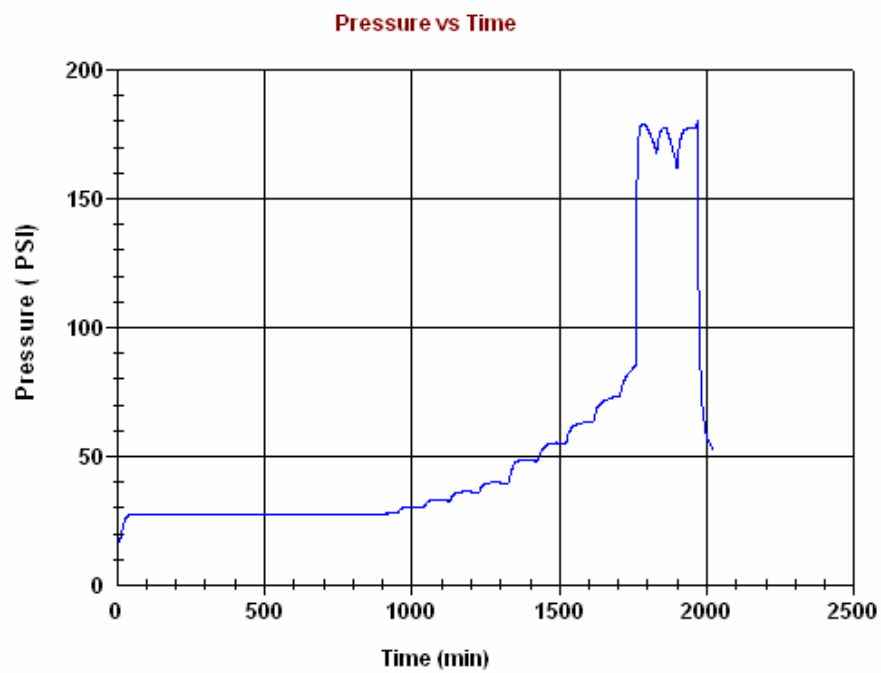


Fig.A.2. Pressure as a function of time for soak temperature of 90°C and soak time of 900 minutes

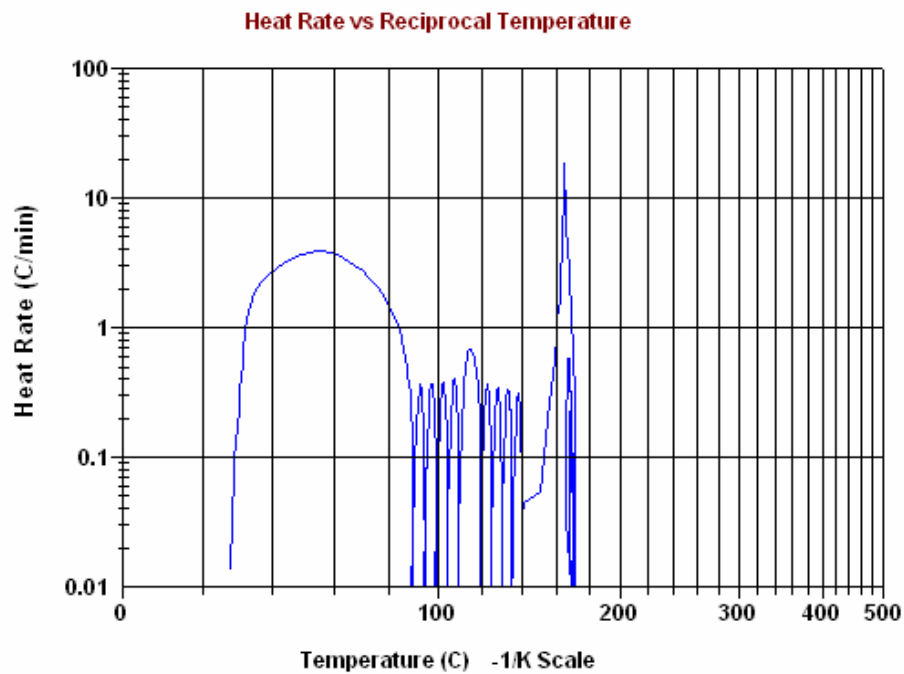


Fig.A.3. Heat rate as a function of temperature for soak temperature of 90°C and soak time of 900 minutes

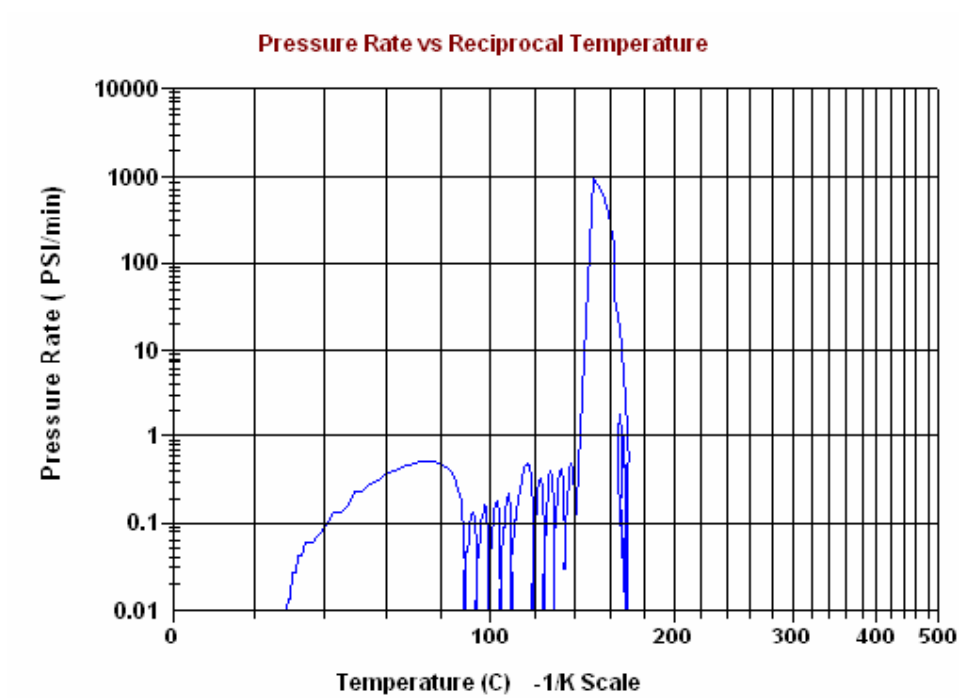


Fig.A.4. Pressure rate as a function of temperature for soak temperature of 90°C and soak time of 900 minutes

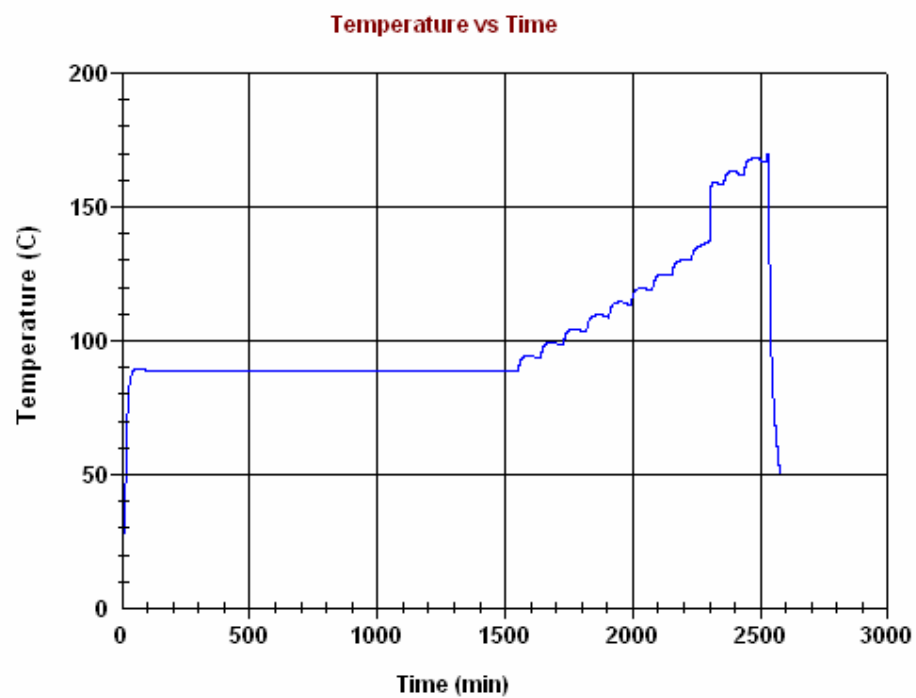


Fig.A.5. Temperature as a function of time for soak temperature of 90°C and soak

time of 1,500 minutes

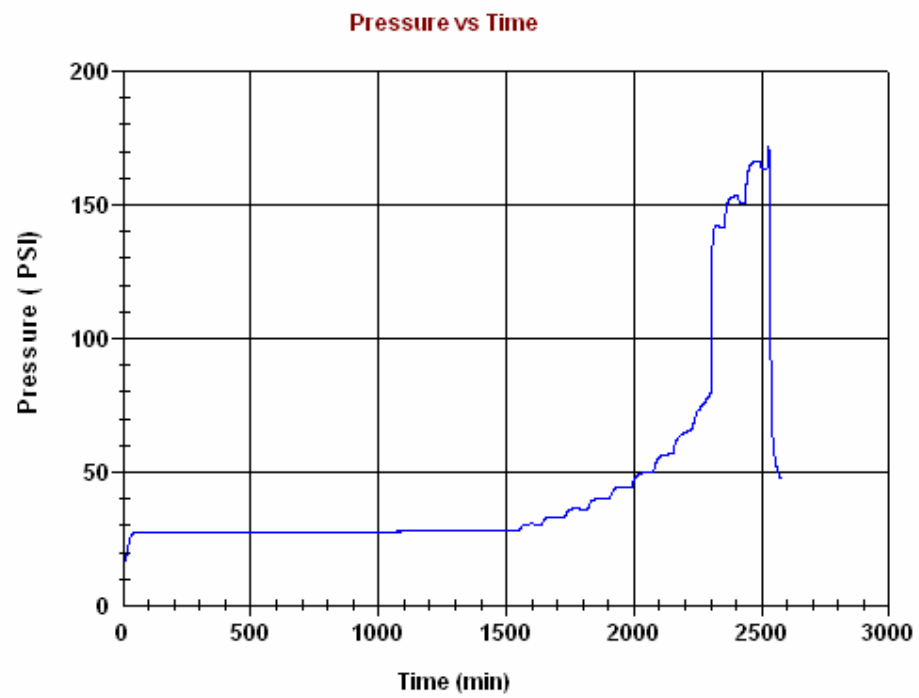


Fig.A.6. Pressure as a function of time for soak temperature of 90°C and soak time of 1,500 minutes

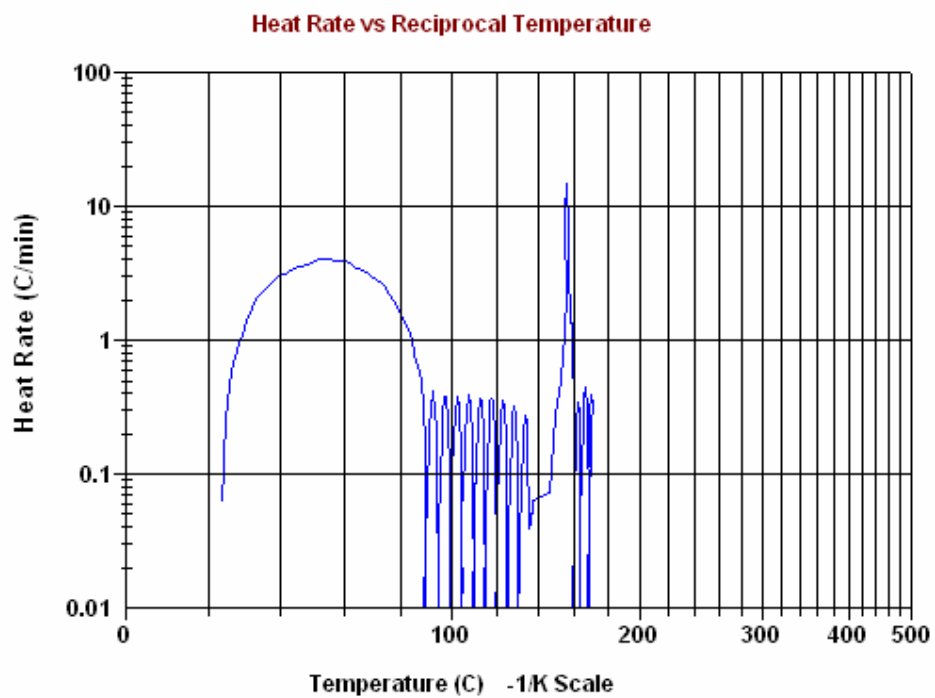


Fig.A.7. Heat rate as a function of temperature for soak temperature of 90°C and soak time of 1,500 minutes

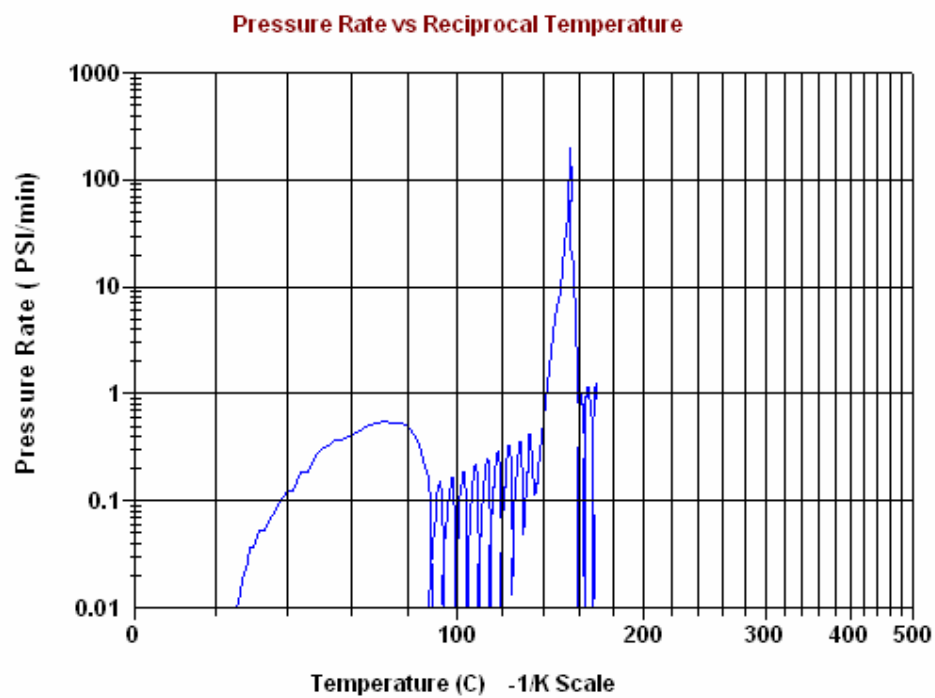


Fig.A.8. Pressure rate as a function of temperature for soak temperature of 90°C and soak time of 1,500 minutes

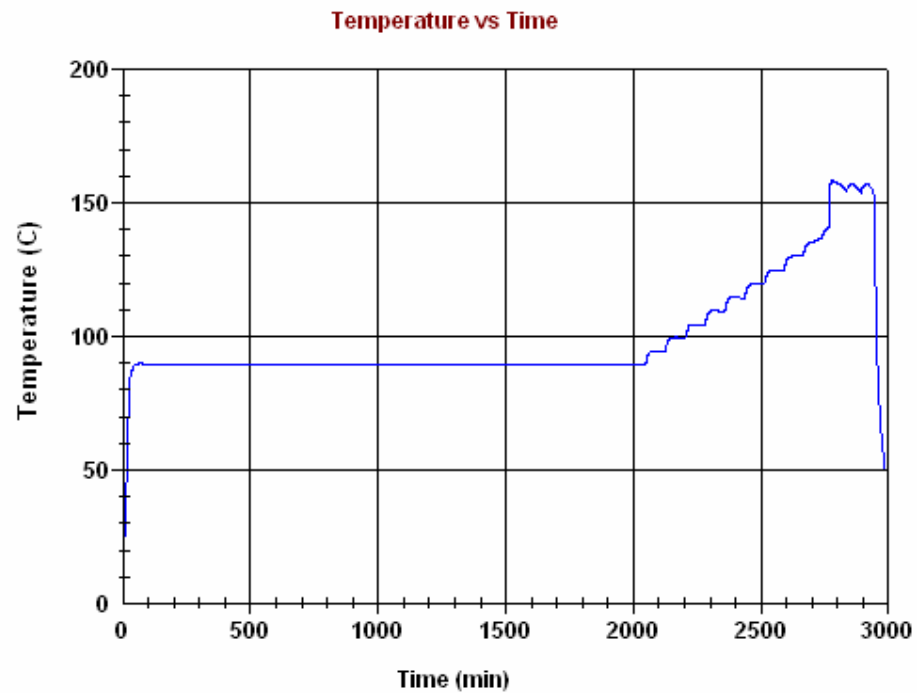


Fig.A.9. Temperature as a function of time for soak temperature of 90°C and soak time of 2,000 minutes

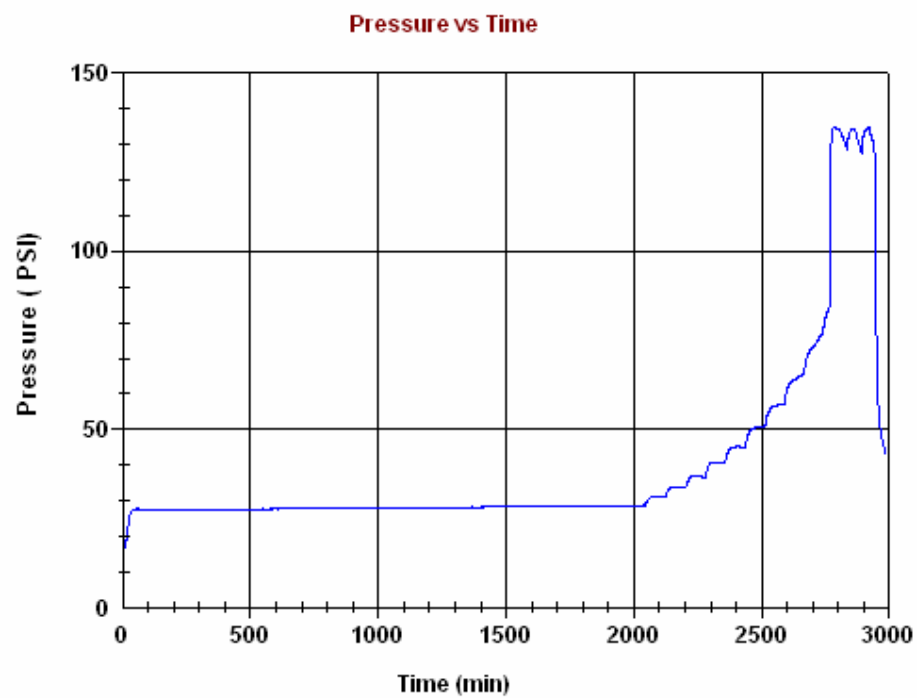


Fig.A.10. Pressure as a function of time for soak temperature of 90°C and soak time of 2,000 minutes

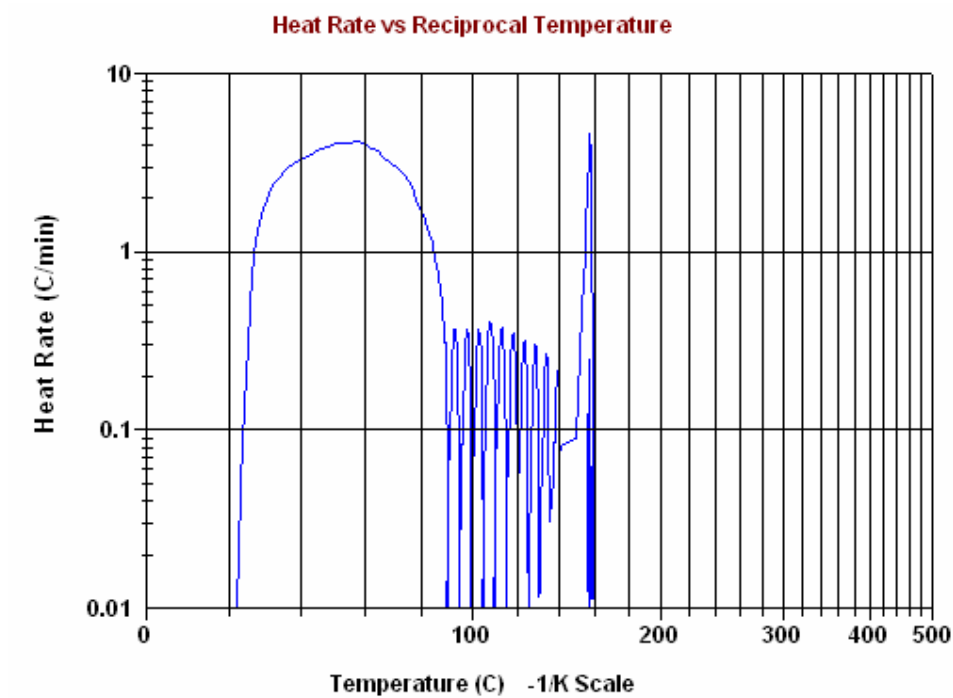


Fig.A.11. Heat rate as a function of temperature for soak temperature of 90°C and soak time of 2,000 minutes

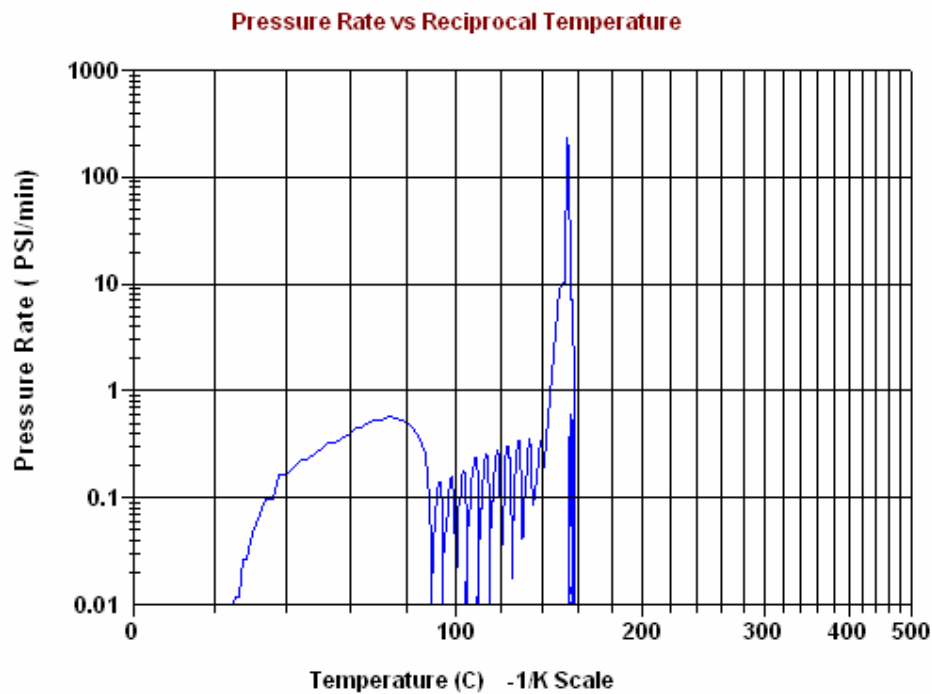


Fig.A.12. Pressure rate as a function of temperature for soak temperature of 90°C and soak time of 2,000 minutes

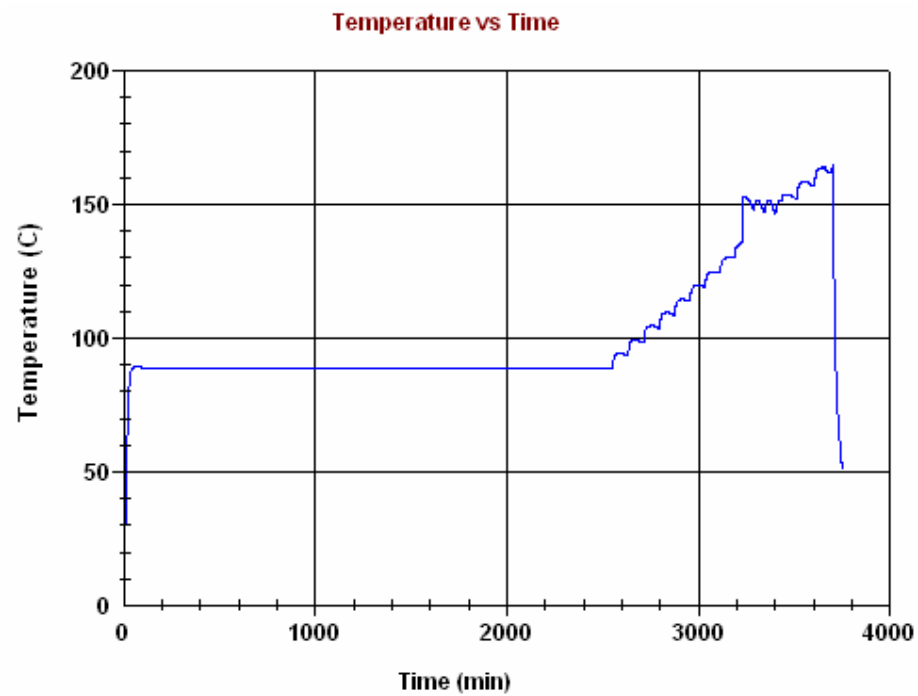


Fig.A.13. Temperature as a function of time for soak temperature of 90°C and soak time of 2,500 minutes

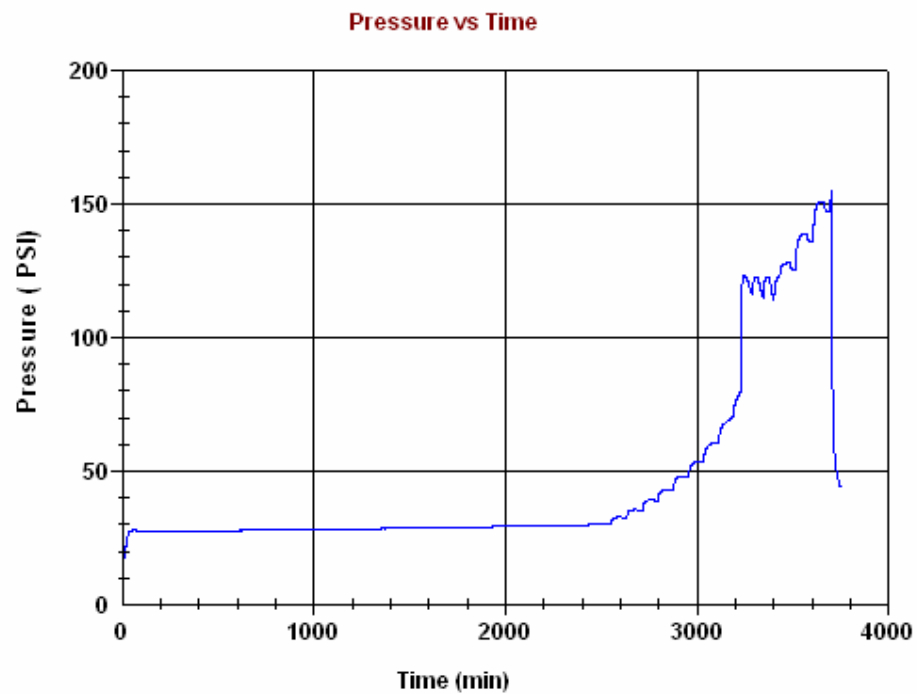


Fig.A.14. Pressure as a function of time for soak temperature of 90°C and soak time of 2,500 minutes

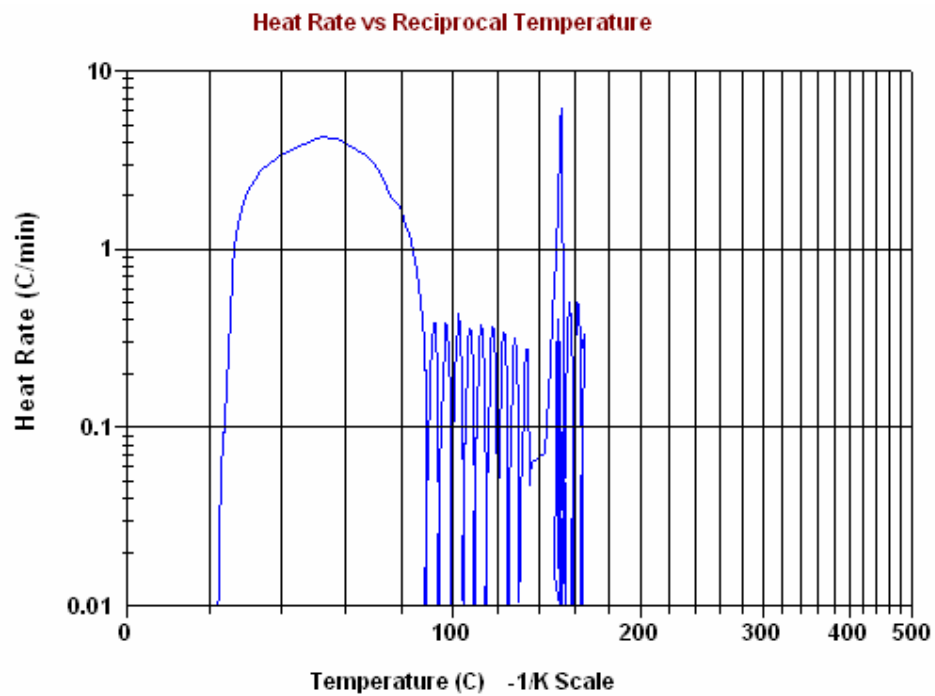


Fig.A.15. Heat rate as a function of temperature for soak temperature of 90°C and soak time of 2,500 minutes

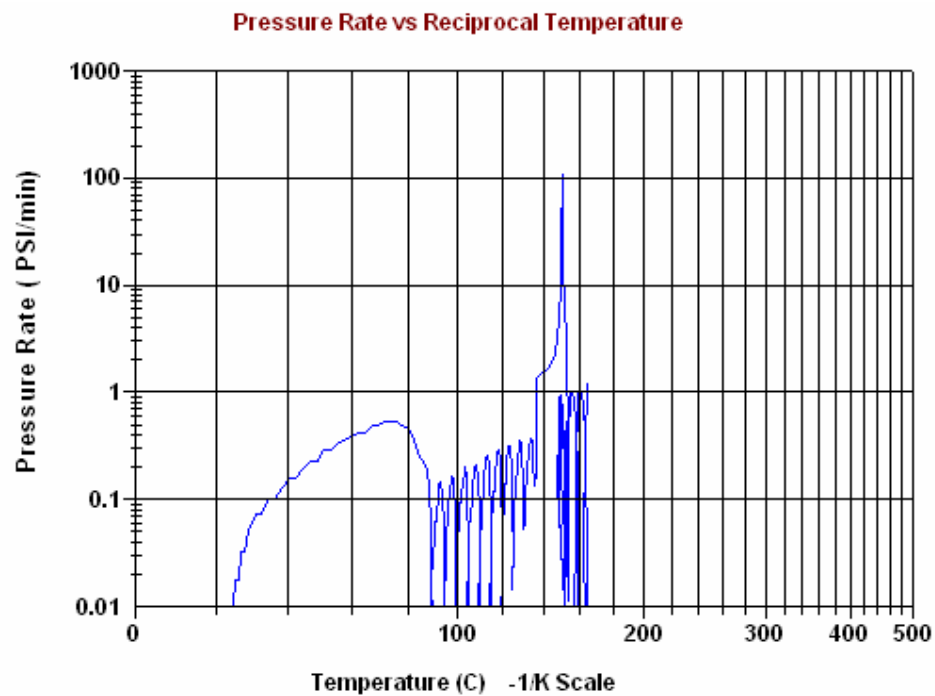


Fig.A.16. Pressure rate as a function of temperature for soak temperature of 90°C and soak time of 2,500 minutes

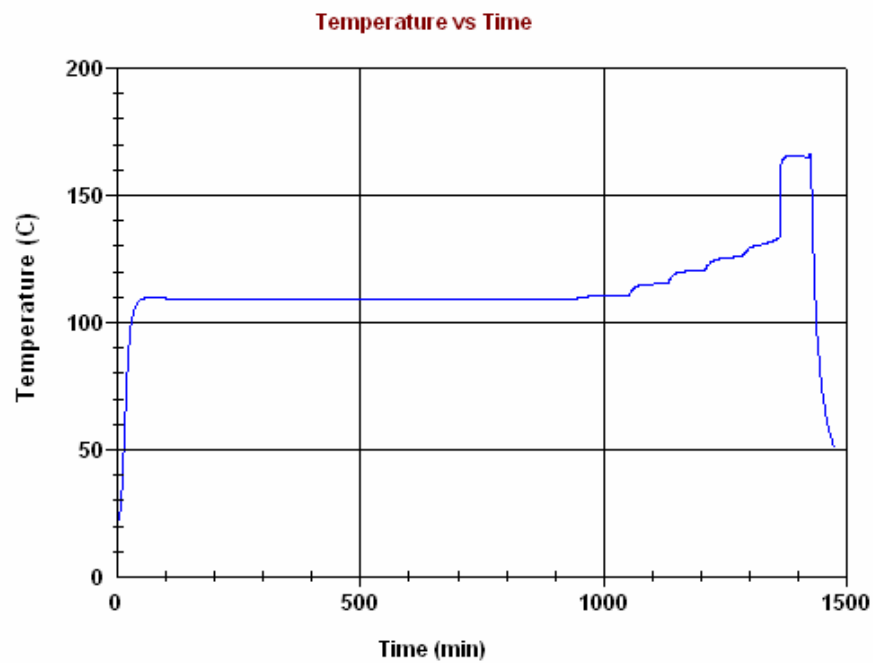


Fig.A.17. Temperature as a function of time for soak temperature of 110°C and soak time of 1,000 minutes

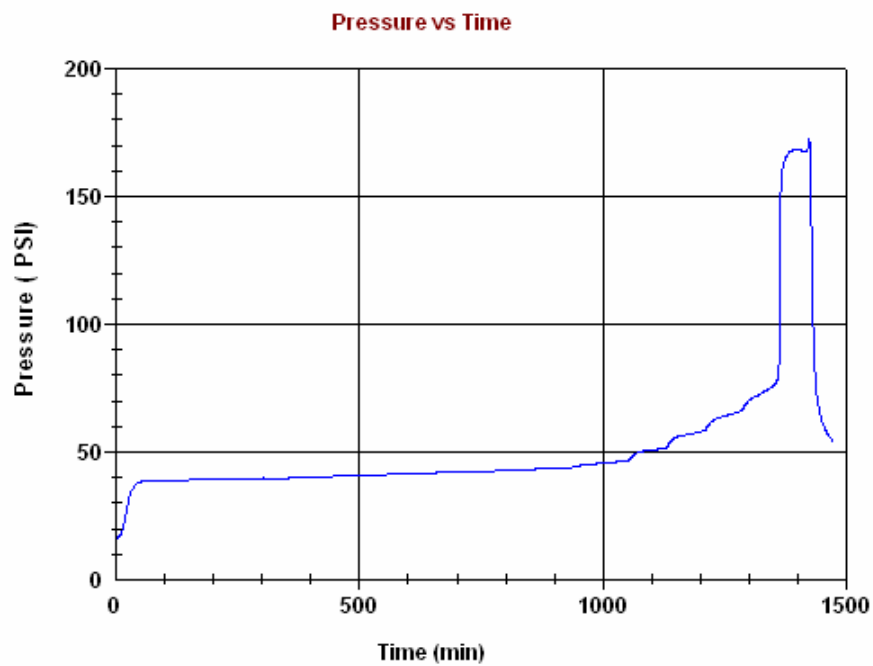


Fig.A.18. Pressure as a function of time for soak temperature of 110°C and soak time of 1,000 minutes

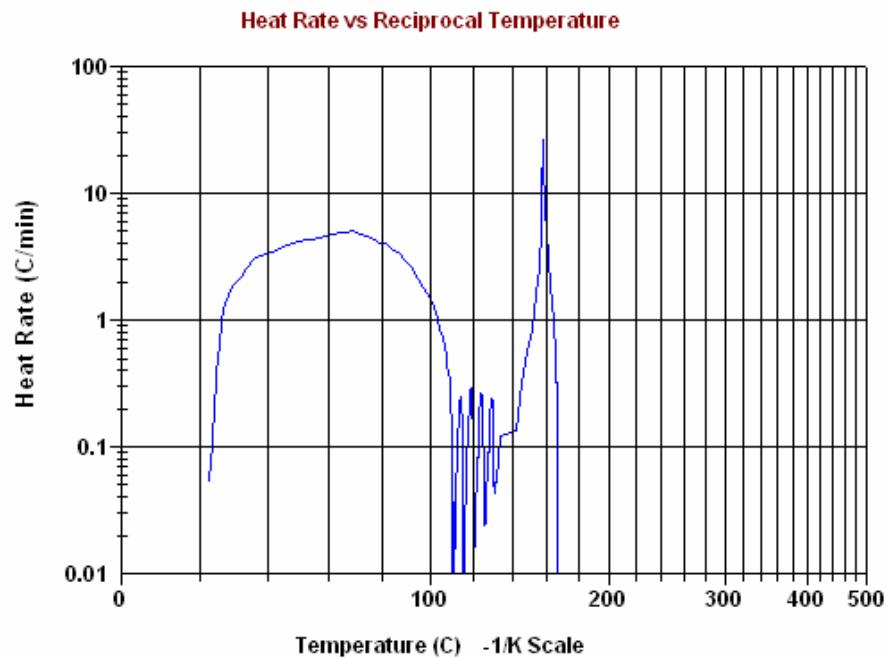


Fig.A.19. Heat rate as a function of temperature for soak temperature of 110°C and soak time of 1,000 minutes

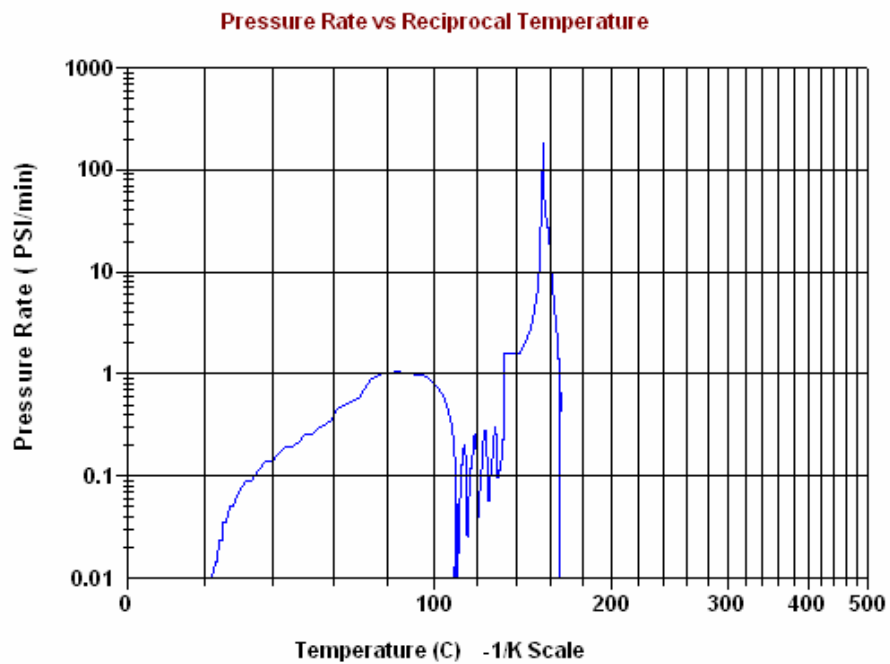


Fig.A.20. Pressure rate as a function of temperature for soak temperature of 110°C and soak time of 1,000 minutes

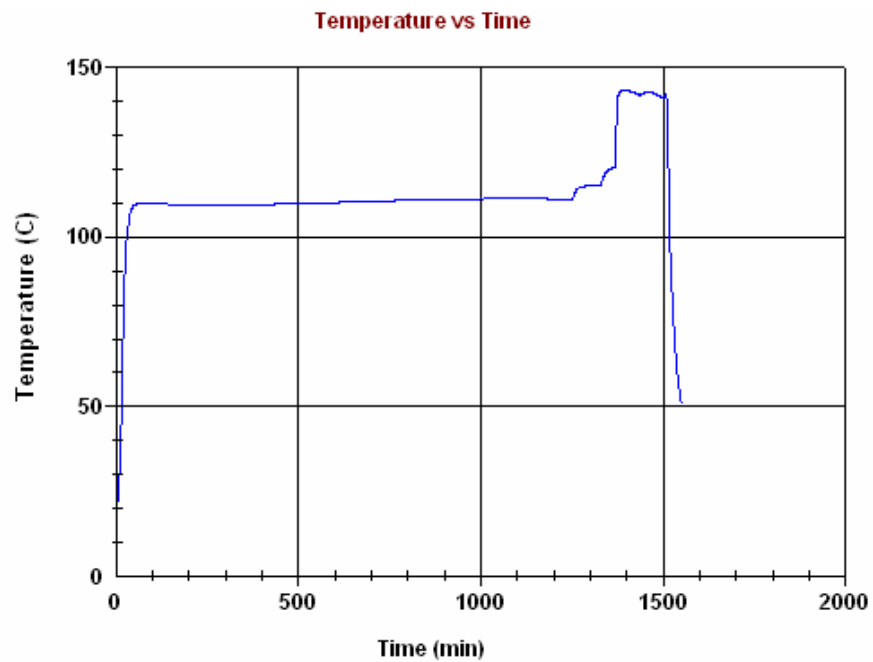


Fig.A.21. Temperature as a function of time for soak temperature of 110°C and soak time of 1,200 minutes

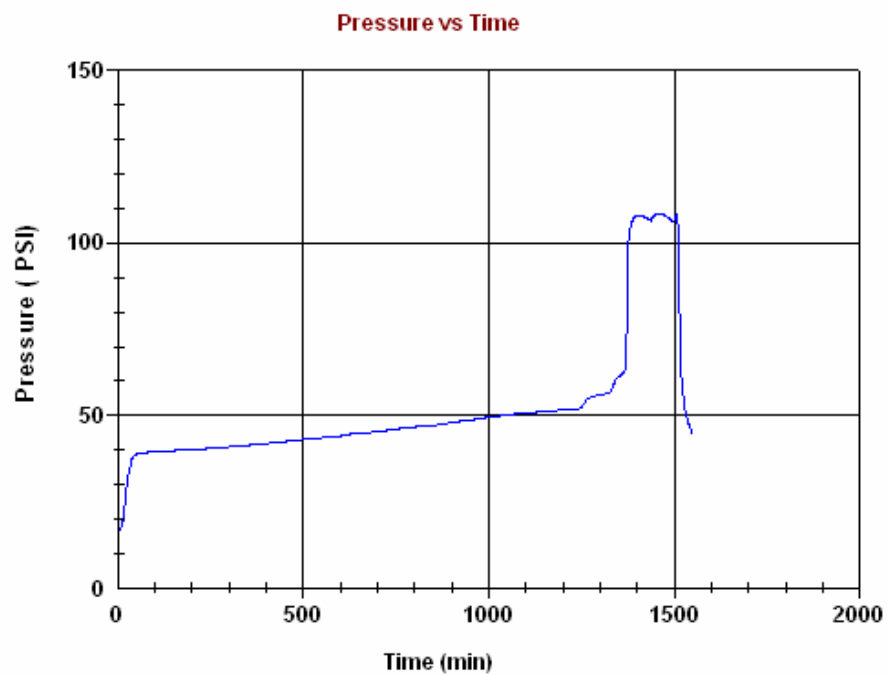


Fig.A.22. Pressure as a function of time for soak temperature of 110°C and soak time of 1,200 minutes

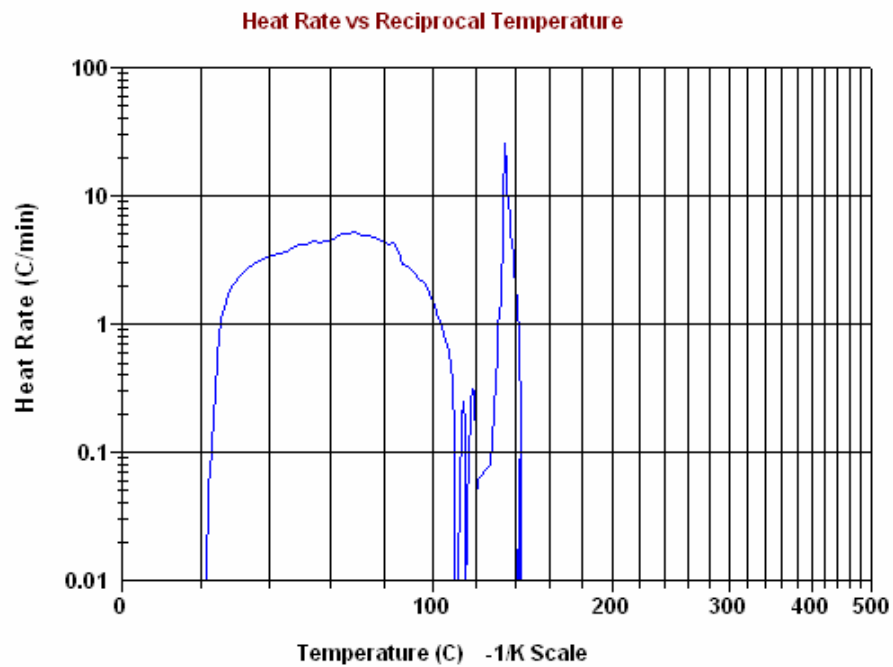


Fig.A.23. Heat rate as a function of temperature for soak temperature of 110°C and soak time of 1,200 minutes

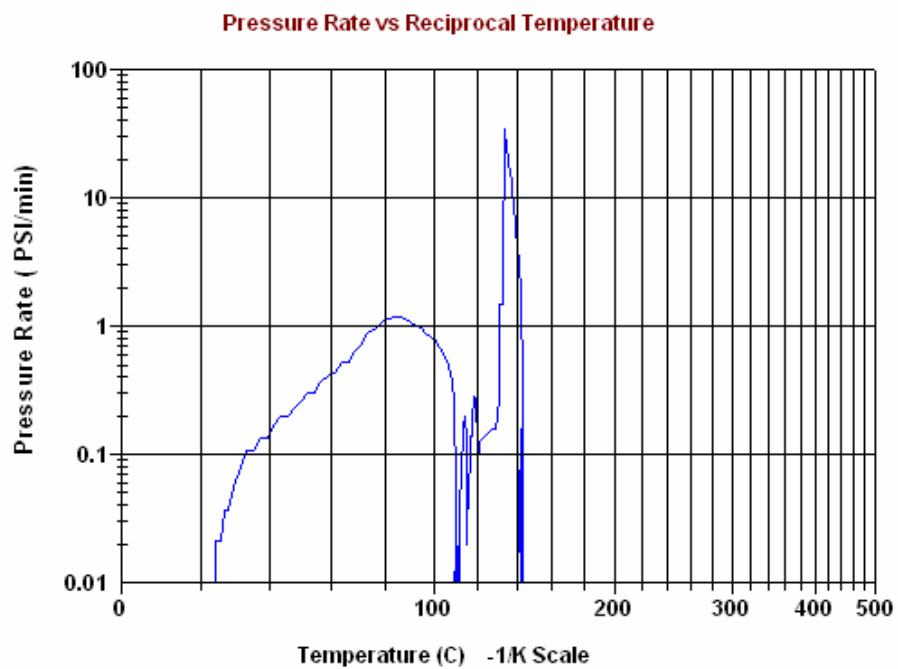


Fig.A.24. Pressure rate as a function of temperature for soak temperature of 110°C and soak time of 1,200 minutes

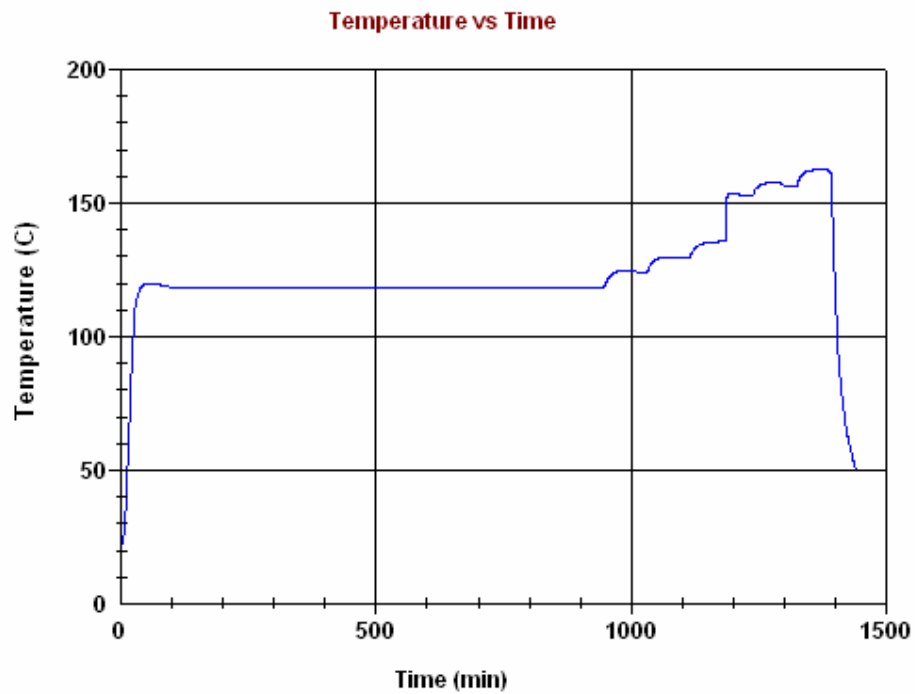


Fig.A.25. Temperature as a function of time for soak temperature of 120°C and soak time of 900 minutes

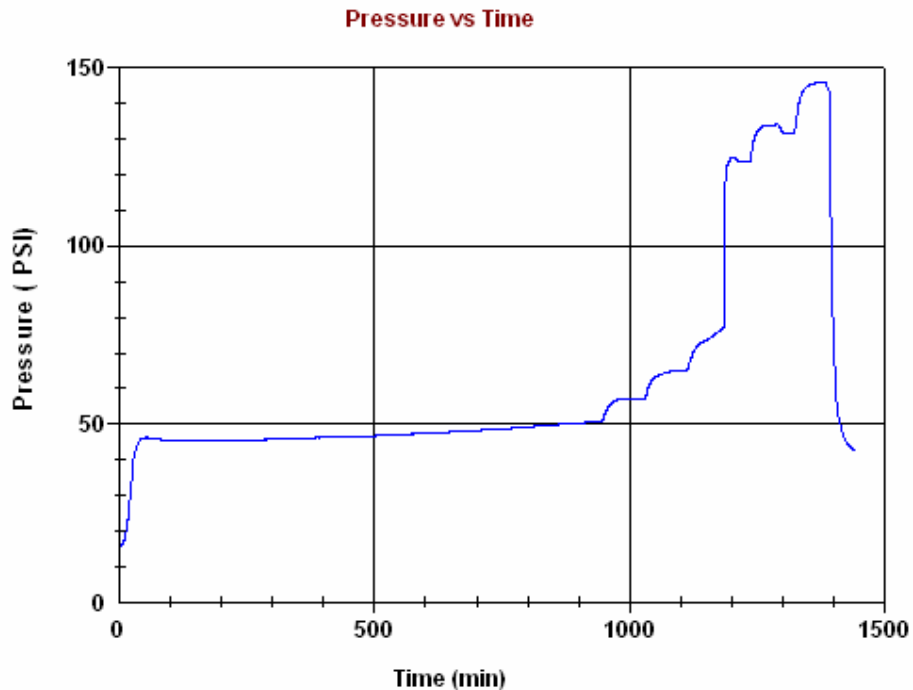


Fig.A.26. Pressure as a function of time for soak temperature of 120°C and soak time of 900 minutes

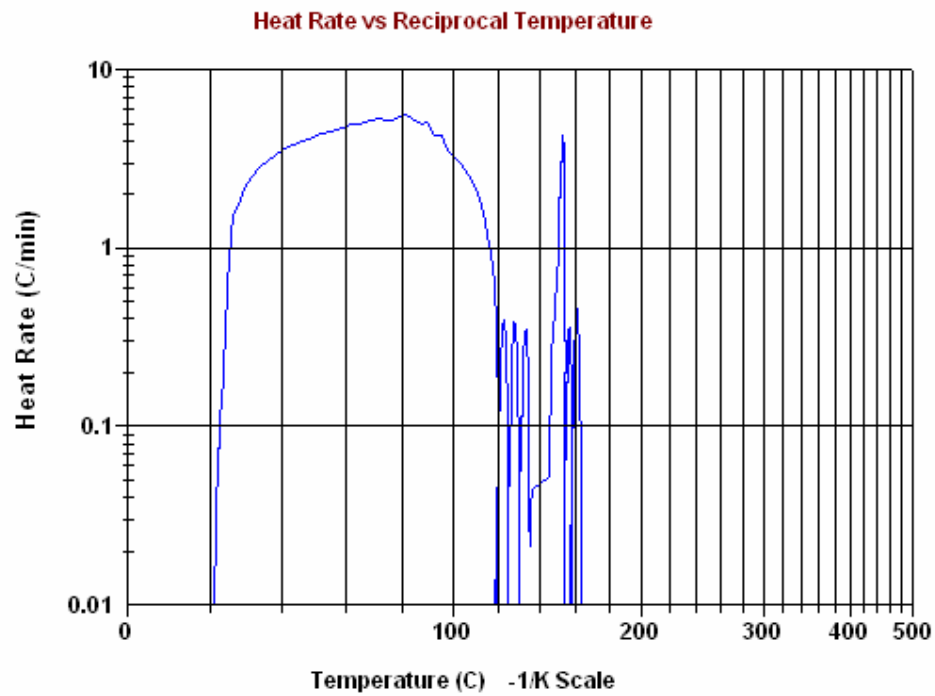


Fig.A.27. Heat rate as a function of temperature for soak temperature of 120°C and soak time of 900 minutes

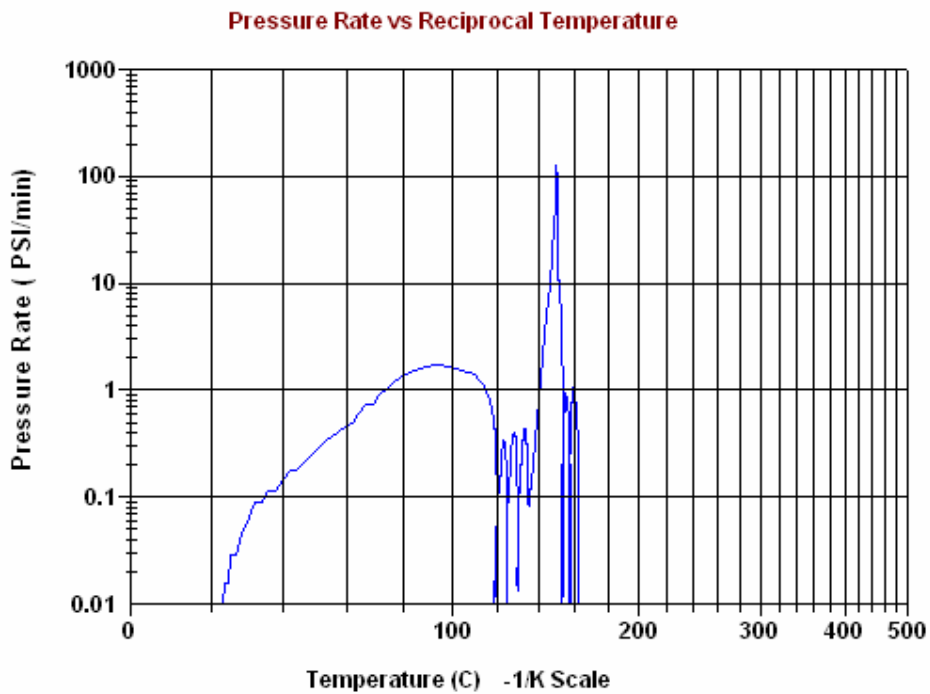


Fig.A.28. Pressure rate as a function of temperature for soak temperature of 120°C and soak time of 900 minutes

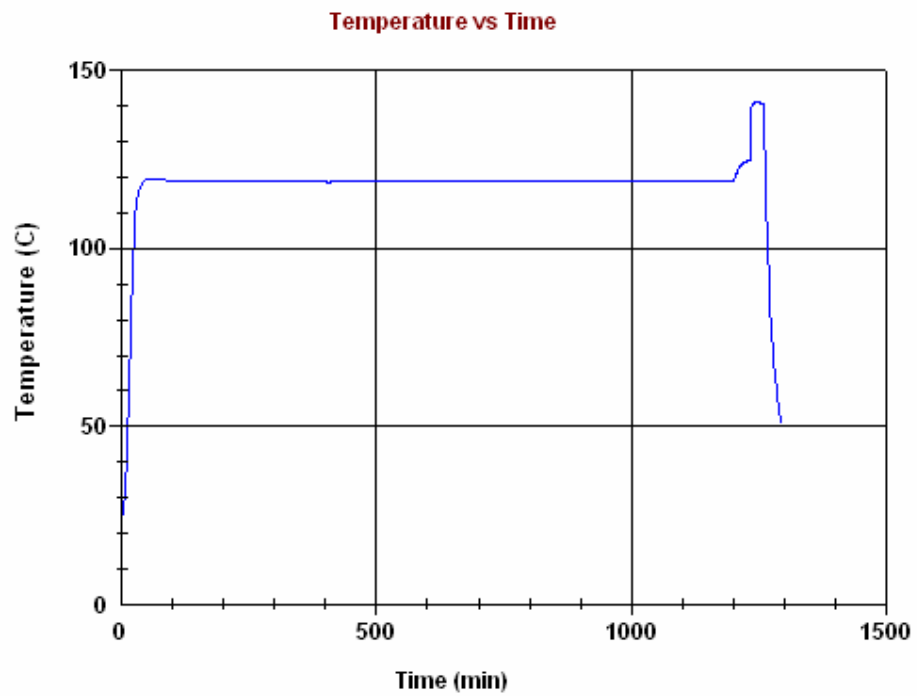


Fig.A.29. Temperature as a function of time for soak temperature of 120°C and soak time of 1,150 minutes

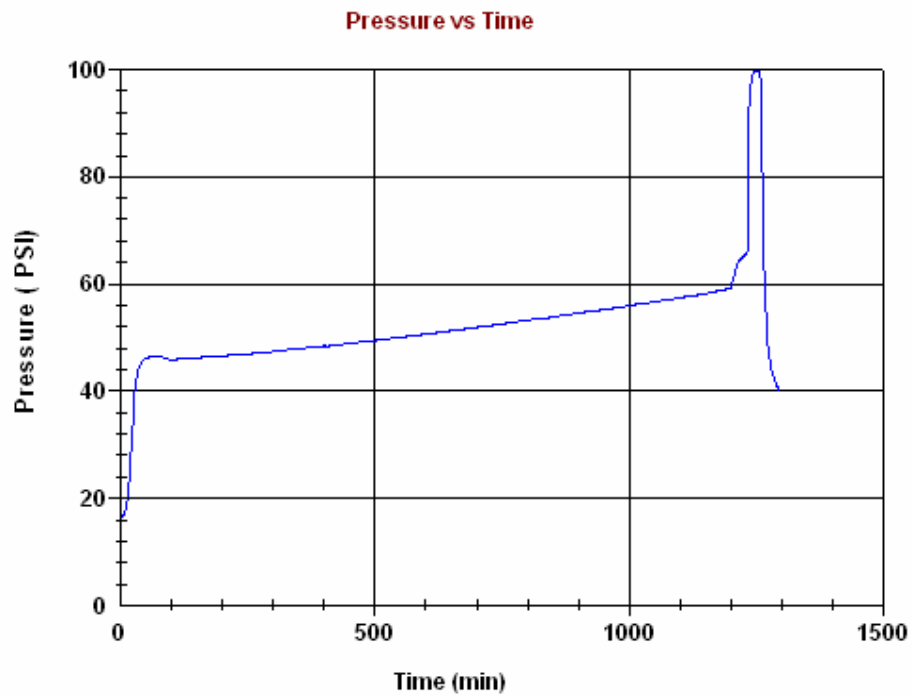


Fig.A.30. Pressure as a function of time for soak temperature of 120°C and soak time of 1,150 minutes

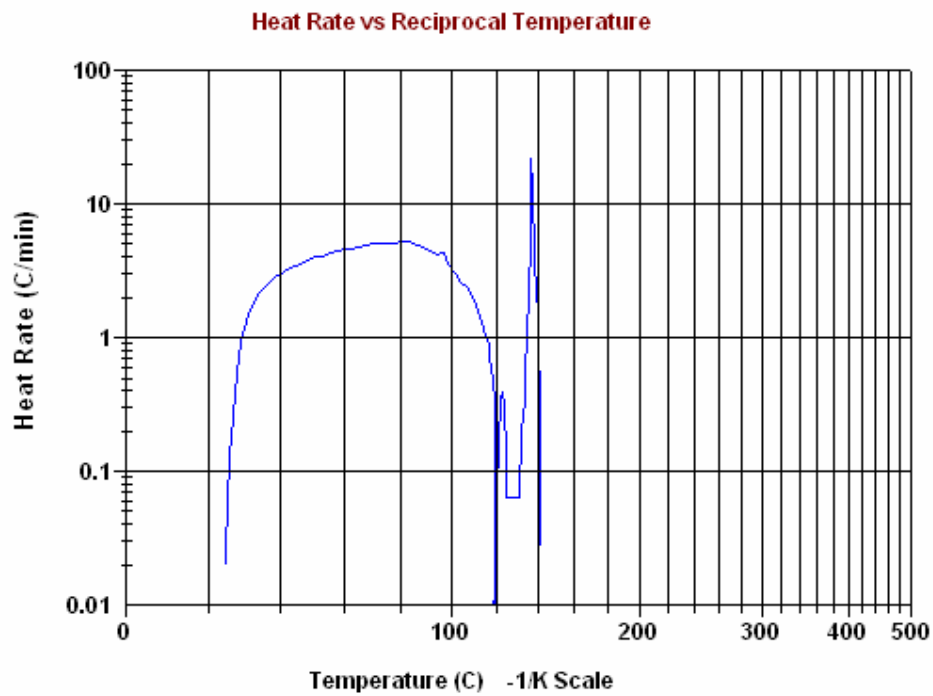


Fig.A.31. Heat rate as a function of temperature for soak temperature of 120°C and

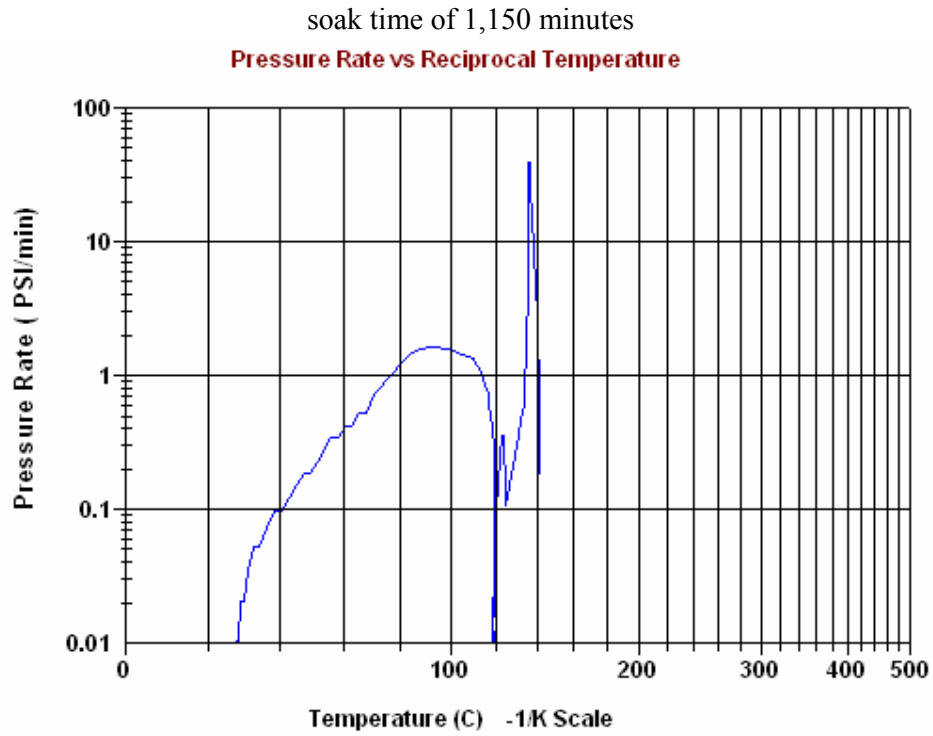


Fig.A.32. Pressure rate as a function of temperature for soak temperature of 120°C and soak time of 1,150 minutes

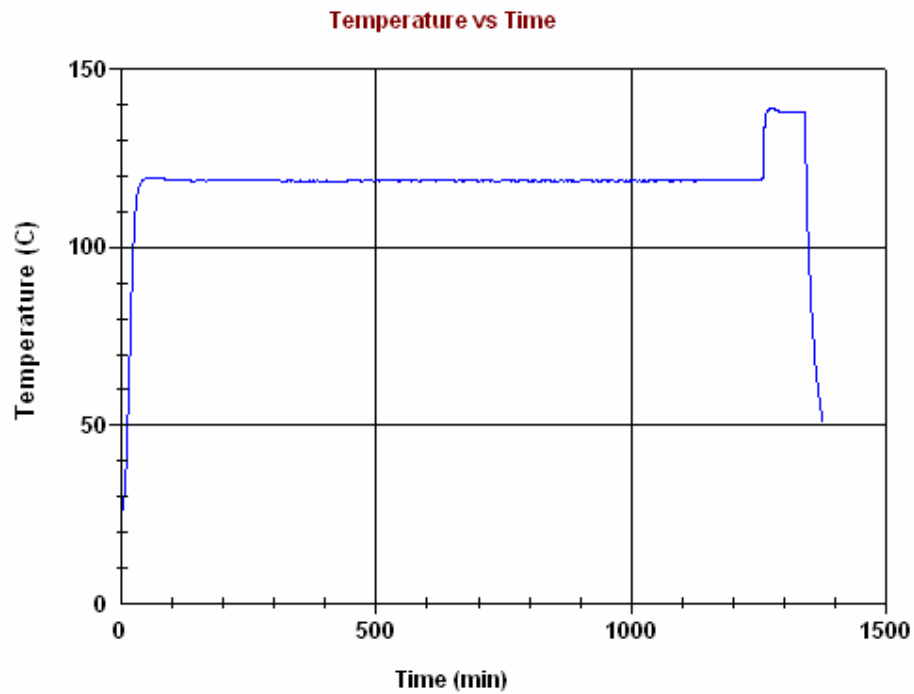


Fig.A.33. Temperature as a function of time for soak temperature of 120°C, showing

the exotherm detected in the soak stage

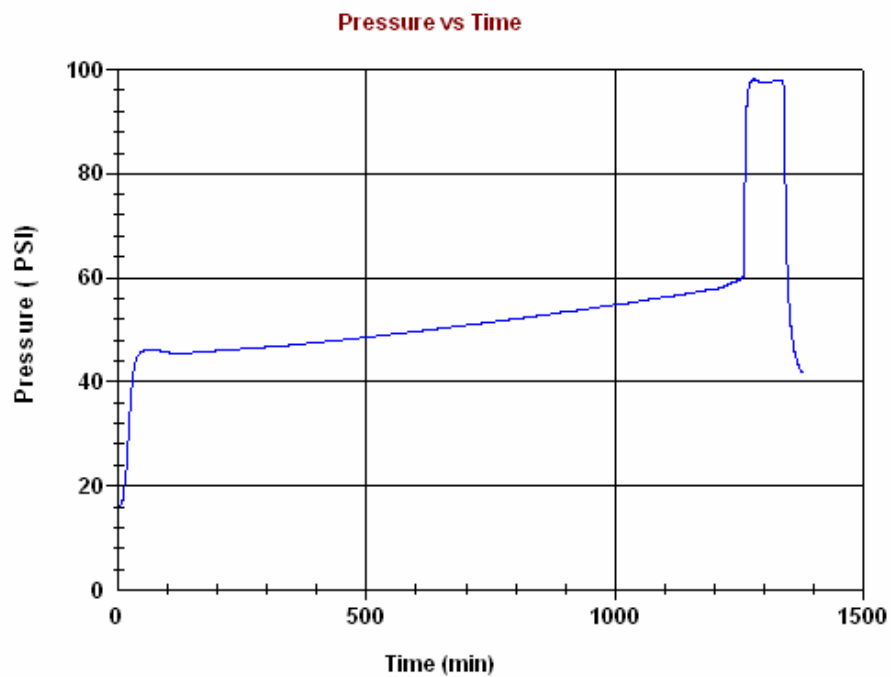


Fig.A.34. Pressure as a function of time for soak temperature of 120°C, showing the exotherm detected in the soak stage

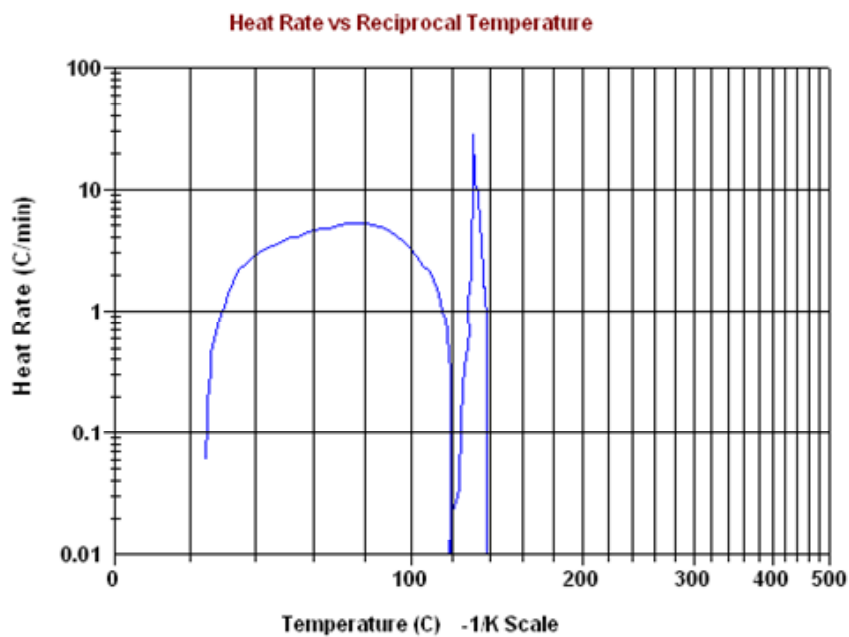


Fig.A.35. Heat rate as a function of temperature for soak temperature of 120°C, showing the exotherm detected in the soak stage

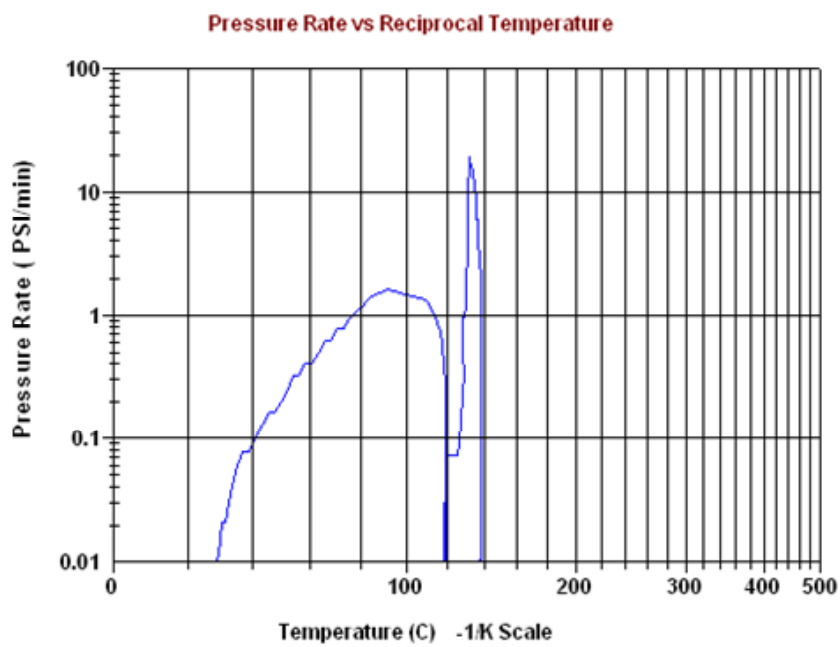


Fig.A.36. Pressure rate as a function of temperature for soak temperature of 120°C, showing the exotherm detected in the soak stage

## VITA

Chuanji Zhang was born in P. R. China in September 1978. She received her B.S. degree in chemistry from Anhui Normal University in July 2000. In January 2003, she enrolled in the Science Majors Program in the Chemical Engineering Department at Texas A&M University. In January 2004, she began work on her master's degree in the area of reactive chemicals. Her permanent address is:

Chaohu Middle Road #245, Room 502

Chaohu, Anhui

P.R. China, 238000.